FRETTING FATIGUE BEHAVIOR OF THE TITANIUM ALLOY TI-6AL-4V UNDER SEAWATER CONDITIONS

THESIS

Lewis C. Lietch, Captain, USAF

AFIT/GMS/ENY/04-M02

DEPARTMENT OF THE AIR FORCE
AIR UNIVERSITY

AIR FORCE INSTITUTE OF TECHNOLOGY

Wright-Patterson Air Force Base, Ohio

AFIT/GMS/ENY/04-M02

FRETTING FATIGUE BEHAVIOR OF THE TITANIUM ALLOY TI-6AL-4V UNDER SEAWATER CONDITIONS

THESIS

Present to the Faculty

Department of Aeronautics and Astronautics

Graduate School of Engineering and Management

Air Force Institute of Technology

Air University

Air Education and Training Command

In Partial Fulfillment of the Requirements for the

Degree of Master of Science (Material Science)

Lewis C. Lietch, BS

Captain, USAF

March 2004

AFIT/GMS/ENY/04-M02

FRETTING FATIGUE BEHAVIOR OF THE TITANIUM ALLOY TI-6AL-4V UNDER SEAWATER CONDITIONS

Lewis C. Lietch, BS
Captain, USAF

Approved:

//signed//	3/10/04
Shankar Mall (Chairman)	date
//signed//	3/10/04
Vinod K. Jain (Member)	date
//signed//	3/10/04
Theodore Nicholas (Member)	date

Abstract

The fretting fatigue behavior of the titanium alloy, Ti-6Al-4V, was investigated in laboratory air (dry) and under a controlled environment consisting of synthetic seawater. Fretting fatigue tests were performed over a wide range of axial stresses to examine both low and high cycle fretting fatigue. Finite element analysis was utilized to model and analyze the experimental data. The applied stress range and the Modified Shear Stress Range were evaluated as potential fatigue parameters.

The results found from this study can be summarized as: (1) seawater had a deleterious effect on fretting fatigue life in the low cycle fatigue regime but improved life in the high cycle fatigue regime, (2) while the Q/P ratio for both conditions increased with an increasing applied stress, the seawater Q/P ratio was slightly lower than the dry condition although the difference was negligible, (3) debris from dry samples contained titanium and oxides while the debris from seawater samples contained titanium, oxides, and seawater contaminants, (4) fretting scar volume was larger under seawater conditions than dry conditions, (5) there were more, closely spaced striations on the fracture surface of the dry samples than of the seawater samples, and (6) both the applied (far field) stress range and the Modified Shear Stress Range can potentially be used as conservative fretting fatigue parameters under high cycle fatigue conditions.

Acknowledgements

I would like to thank my thesis advisor, Dr. Shankar Mall, for his patience, guidance, and support throughout this thesis project. I would also like to thank Dr. Hyukjae Lee and Major Kisu Shin for their technical support and guidance while performing the tests and Finite Element Analysis. Finally, I would like to thank Robert Kearns from the Air Force Materials Laboratory for his instruction and assistance in using the laboratory equipment.

Table of Contents

Page

List of Figures

Page

Page

List of Tables

NOMENCLATURE

a	Contact half-width
a_{FEA}	Contact half-width determined by FEA
a_{RUIZ}	Contact half-width determined by Ruiz Solution
A	Curve fitting parameter
A`	Composite compliance
B	Curve fitting parameter
BSE	Back scatter emission
b	Half of specimen thickness
C	Curve fitting parameter
D	Curve fitting parameter
E	Modulus of elasticity
EDS	Energy dispersive spectroscopy
FEA	Finite element analysis
k	Radius of curvature
m	Material curve fitting parameter
MSSR	Modified Shear Stress Range
N_f	Number of cycles to failure
P	Normal load
Q	Tangential load
Q_{max}	Maximum tangential load
Q_{min}	Minimum tangential load

R	Axial stress ratio
R_1	Radius of fretting pad
R_2	Radius of fretting specimen
R_τ	Shear stress ratio
SEM	Scanning electron microscope
V	Lower applied axial load
W	Upper axial load
σ_{axial}	Axial stress
$\sigma_{axial,max}$	Maximum axial stress
$\sigma_{axial,min}$	Minimum axial stress
σ_{max}	Maximim applied stress
σ_{min}	Minimum applied stress
σ_{eff}	Effective stress
σ_{xx}	Normal stress in the x direction
σ_τ	Surface tangential stress
$\Delta\sigma$	Change in applied stress
τ	Shear stress in the x y plane
τ_{max}	Maximum shear stress on critical plane
$\Delta\tau_{crit,eff}$	Change in critical effective shear stress
ν	Poisson's ratio
δ	Slip at interface

FRETTING FATIGUE BEHAVIOR OF THE TITANIUM ALLOY TI-6AL-4V UNDER SEAWATER CONDITIONS

I. INTRODUCTION

Fretting is the surface damage that occurs when two contacting surfaces experience an oscillatory motion of small amplitude. The two main effects of fretting are an increased production of debris due to surface wear and initiation of fatigue cracks. When fretting occurs under cyclic loading conditions, the process is termed fretting fatigue. Fretting fatigue increases the tensile and shear stresses at the contact surface producing surface defects which can act as stress concentration sites. Fretting fatigue cracks can nucleate at these sites leading to an overall reduction in the fatigue strength of the material. The United States Air Force is interested in the process of fretting fatigue as it is frequently encountered in several aircraft structural components. Fretting fatigue decreases the structural integrity of the aircraft and engine components and eventually leads to component failure. Component failure due to fretting fatigue is characterized by four stages: crack nucleation, crack propagation due to the combination of contact and bulk stresses, crack propagation due to bulk stresses only, and fracture [1]. The blade/disc dovetail joint in turbine engines is an example of an aircraft component whose failure is frequently due to fretting fatigue (Figure 1).

The environment in which fretting occurs can greatly influence the type and amount of resultant damage. This is especially true in a corrosive environment where fretting disrupts surface films through its mechanical and chemical actions thereby exposing the

underlying metal to the corrosive agents. Corrosion and its effect on aircraft have been a concern of the United States Air Force for many years. Programs such as the Environmental Severity Index [2] have been developed to measure the corrosion severity of the environment and predict the levels of corrosion damage that may be encountered within the aircraft fleet. Many factors can influence corrosion rates at individual bases including local soil chloride content, humidity, pollutants, and coastal proximity. However, corrosion is a concern for every aircraft regardless of its home base as each can be exposed to various corrosive environments during training and operational assignments. In the Fiscal Year 2001 (FY01), the direct maintenance cost of corrosion for the United States Air Force was approximately $1.14 billion [3].

The effect of corrosion varies depending on the type of material being evaluated. Titanium alloys are common materials used in aerospace applications and are found in aircraft gas turbine engines blades, discs, inlet guide vanes, and cases. Additionally, highly stressed components, such as forged wing structures and landing gear components, are constructed from titanium alloys. Ti-6Al-4V is the most commonly used titanium alloy within the aerospace industry as it exhibits an excellent strength to weight ratio, high operational temperatures, and corrosion resistant properties. These corrosion resistant properties are due to the protective nature of the oxide film on the surface of the material. While many studies have evaluated the fretting fatigue behavior of Ti-6Al-4V under laboratory conditions, few studies have focused on the fretting fatigue behavior of Ti-6Al-4V in a corrosive environment. Yet it is well known that, when subjected to fretting conditions, the surface oxide film is damaged thereby leading to a reduction in corrosion resistance [4,5,6,7]. The titanium alloy then becomes susceptible to both the fretting

degradation mechanisms and the corrosive agents in the environment. In an effort to evaluate the effect of seawater exposure on aircraft, this study will investigate the fretting fatigue behavior of Ti-6Al-4V under seawater conditions.

Due to the complexity of aircraft and engine geometries and loading conditions, it was not possible to replicate these conditions in an experimental configuration. Therefore, simplified geometry and loading conditions were used in this study to determine the effect of seawater on fretting fatigue conditions. Figure 2 shows the simplified experimental configuration. Lateral springs were used to press the cylindrical fretting pads against the fretting specimen under a constant normal load. A servo-hydraulic test machine was used to generate an axial stress, σ_{axial}, on the fretting specimen. This stress produced a tangential load, Q, which was dependant on the lateral spring stiffness and coefficient of friction at the contact surface.

In this study, the normal load (1334 N) and the cylindrical pad radius (50.8 mm) were held constant. The applied axial loads were varied to evaluate both low and high cycle fatigue regimes. These fatigue cycle regimes were tested under laboratory air (dry) conditions and seawater conditions. The seawater condition consisted of an open air system that applied synthetic seawater onto each pad/specimen contact surface. The seawater was applied for two seconds every one minute resulting in an application rate of approximately five ml per minute to each side of the specimen.

Data from both the dry and seawater conditions were collected and compared using two fatigue parameters, the applied (far field) stress range and the Modified Shear Stress Range (MSSR) parameter [8,9]. The axial, transverse, and shear stress distributions along the contact surface used to evaluate the Modified Shear Stress Range

fatigue parameter were determined by finite element analysis. The MSSR fatigue parameter was evaluated to determine if an equivalence between the seawater fretting fatigue data and the dry fretting fatigue data could be established after including the effects of the contact conditions. If an equivalence could be established, fretting fatigue experiments under seawater conditions could be reduced thereby saving both time and money.

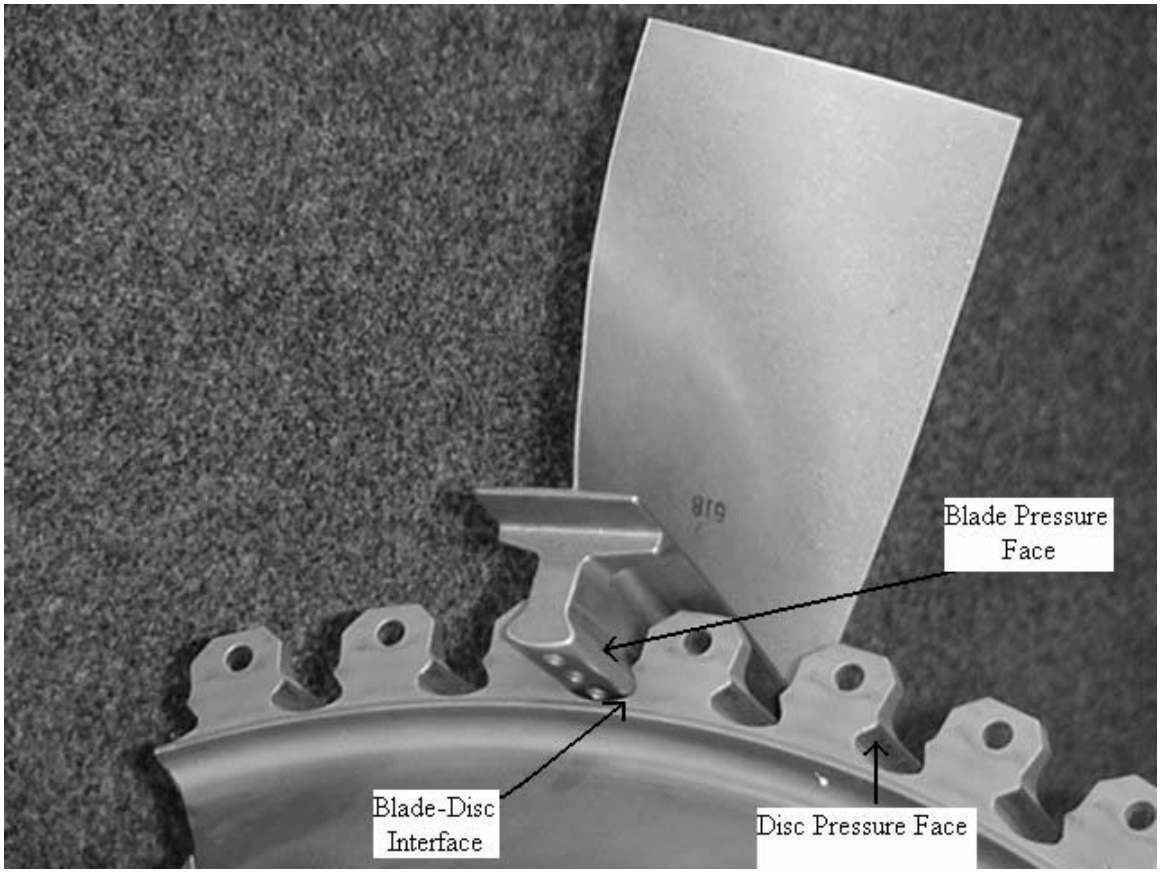

Figure 1. Blade/Disc Dovetail Joint in Turbine Engine.

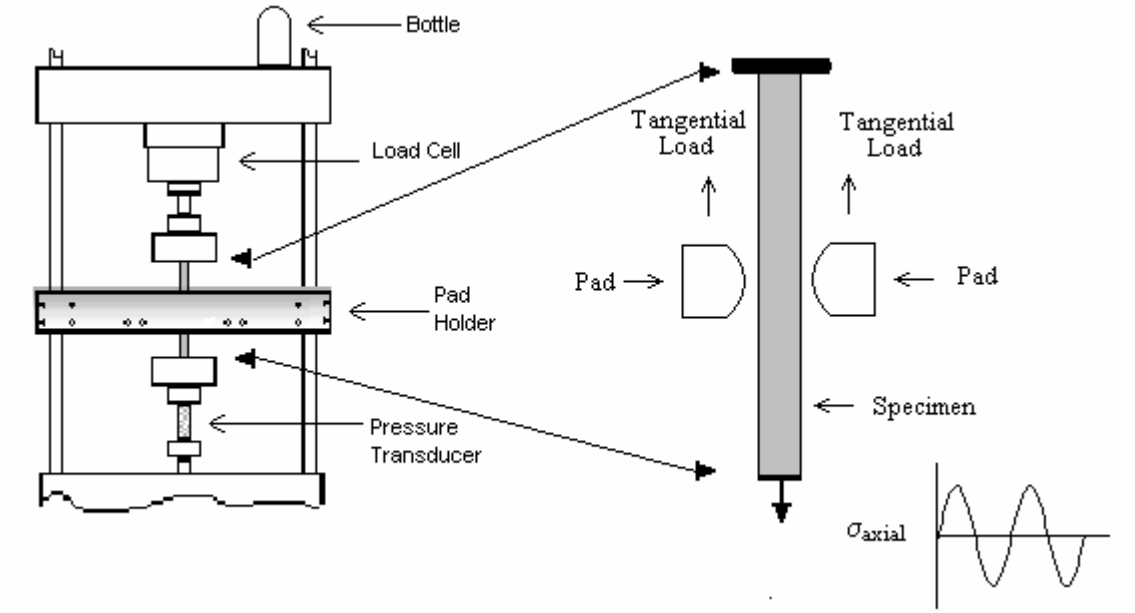

Figure 2. Fretting Fatigue Experimental Configuration.

II. BACKGROUND

In this chapter, the mechanical, chemical and electrochemical mechanisms involved in fretting fatigue will be described. Variables affecting fretting fatigue will be presented, and previous studies regarding the effect of the environment on fretting fatigue will be discussed. Finally, fatigue parameters used in this study will be mentioned.

Mechanical and Chemical Mechanisms of Fretting Fatigue

Initially, fretting damage was thought to be a result of the mechanical action of two contacting surfaces subjected to cyclic loading conditions. It is now widely accepted that both mechanical and chemical mechanisms are responsible for fretting damage. The material's surface film is disrupted by the mechanical action of fretting once cyclic loading begins. Conner et al. [1:261] described the disruption as follows: plastic deformation occurs at the surface in asperity tips as yield stresses are exceeded locally. The asperities are welded together at the area of contact, become brittle, and eventually fracture from either of the contacting bodies due to the fatiguing action. Surface damage then occurs due to an abrasive action of the metal particle as it moves between the two surfaces. This exposes the material's underlying chemically reactive sites to the chemical mechanism of fretting. Oxidation occurs on the exposed surfaces forming oxide films which are continuously broken up by the mechanical action. The oxide debris piles up and can become trapped in a valley between two contacting asperities. Pits are formed as the accumulated oxides attempt to push the contacting surfaces apart. The pits enlarge as the

mechanical and chemical mechanisms of fretting continue to produce more oxide debris. These pits form stress concentration sites where crack nucleation can originate [1,10].

Sankaran et al. [11] attempted to determine the effect of pitting corrosion on the fatigue of 7075-T6 Al. They found that pitting corrosion decreased the fatigue life by a factor of about 6-8. Additionally, they utilized the initial flaw size of the pits to measure fatigue life and found that fatigue life could be predicted using pits of average dimension.

Studies have shown that the presence of oxide debris does not necessarily result in an increase in fretting fatigue crack growth rates. An increase in the amount of oxide debris can lead to an increase in slip or displacement. As a result, the fretting fatigue condition becomes a gross slip condition thereby creating excessive wear [12] which can rub away embryonic cracks before they can propagate [1,13]. Takeuchi et al. [14] suggested that the accumulation of wear particles and corrosion products within cracks may contribute to crack closure thus retarding fretting fatigue crack growth. Conner et al. [1] made a similar observation noting that debris may fill a crack resulting in crack closure. The debris can also adhere to the surface acting as a solid lubricant thereby lowering the coefficient of friction and reducing the stresses at the surfaces [15].

Environment Assisted Crack Growth

When fatigue occurs in a corrosive environment, it is well known that electrochemical reactions occur which can accelerate crack propagation. These reactions are dependent on a number of variables including temperature, environment, material type, material microstructure, hydrogen concentration, and yield stresses [16,17]. While few studies have evaluated these electrochemical mechanisms under fretting fatigue conditions,

these mechanisms have been widely investigated in the propagation of fatigue cracks. Several atomic elements have been suggested as playing a role in these reactions. Bach et al. [18] showed that crack propagation in Ti-6Al-4V was highly sensitive to external and internal oxygen concentrations. Chlorine has also been suggested as enhancing crack growth of Ti-6Al-4V in an aqueous NaCl environment [6]. Much attention has been given to the effect of hydrogen in crack propagation. In many metals, including titanium and its alloys, hydrogen has been suggested as being at least partially responsible for increasing propagation of the crack tip [16,19,20]. When a metal comes into contact with an environment containing hydrogen, hydrogen can be absorbed by the metal. During the electrochemical reaction, hydrogen atoms dissociate from the environment and diffuse through the surface area of the metal. The hydrogen atoms then recombine into molecular hydrogen and concentrate in regions of high triaxial stress such as the region in front of the crack tip. The exact mechanisms of hydrogen induced cracking (aka hydrogen embrittlement) are not clearly understood although several mechanisms have been suggested [17,21]. The pressure expansion mechanism occurs as hydrogen collects in front of the crack tip thereby creating higher pressure and allowing cracks to spread. The decohesion mechanism occurs as hydrogen concentrates locally on internal surface cracks and voids. The surface energy is lowered and chemical bonds weaken, thus promoting hydrogen induced cracking. The hydrogen enhanced local plasticity (HELP) mechanism suggests that hydrogen enhances the localized plasticity at the crack tip. This plasticity allows dislocation motion and slip displacement to increase thereby allowing the growth and coalescence of voids. Although plastic deformation is associated with ductile fractures, due to the highly localized nature of the failure, the surface will resemble a brittle

fracture. It has been suggested that hydrogen induced cracking occurs in titanium by means of the HELP mechanism [17]. However, hydrogen related phase changes have also been suggested as the mechanism behind hydrogen induced cracking in titanium and its alloys [16,22]. Hydrides form a brittle phase thereby decreasing the overall ductility of the alloy and increasing crack growth.

A material's susceptibility to hydrogen induced cracking is dependent on its microstructure. It has been shown the hexagonal closed packed α phase and the α + β phase of titanium are more susceptible to hydrogen induced cracking than the body center cubic β phase [16,22,23]. It has also been reported that in titanium, crack initiation sites occur at the α-β interfaces when exposed to hydrogen [19,24].

Bache and Evans [25] showed that the effect of 3.5% NaCl on fatigue crack growth of Ti-6Al-4V varied based on the microstructure of the material. They found that mill annealed and bimodal microstructures were relatively insensitive to the saline environment. However, a relatively coarse lamellar microstructure was more susceptible to the saline solution and sustained increased crack growth.

Variables Affecting Fretting Fatigue

It is well known that there are many variables which can influence fatigue life under fretting conditions. In 1972, Waterhouse [26:106] classified these variables into three categories: mechanical, physical, and environmental. Mechanical variables include normal load, amplitude of slip, frequency, and number of cycles. Temperature, relative hardness of the surfaces, and surface finish are all physical variables. Atmospheric composition, humidity, and liquid lubricants are all environmental variables which can influence the

chemical process involved in fretting fatigue. Continued research has uncovered many more variables which can affect fretting fatigue including rate of oxidation, surface roughness, coefficient of friction, chloride ions, amount of oxygen and hydrogen, type of sample material, and the microstructure of the material [7,10,27,28,29,30]. Not only does each individual variable affect the fretting fatigue process, but the variables often influence one another. In fact, the fretting process itself has been shown to influence these variables.

Environmental Fretting Fatigue

Previous studies have shown that the environment can greatly affect the mechanisms of fretting by either extending the fretting fatigue life or shortening it. Poon and Hoeppner [10] evaluated the fretting fatigue of an aluminum alloy in a vacuum and in air. They reported the fretting fatigue life was 10 to 20 times longer in the vacuum than in air. Both mechanical and chemical factors were present in air whereas only mechanical factors were present in the vacuum. After investigating the specimens under a scanning electron microscope, it was noted that corrosion pits were not present in the 7075-T6 Al alloy tested under vacuum conditions. Some wear tracks were present due to the mechanical action of the work hardened metal particles, but they were shallower and less defined than in air. Additionally, the loose particles were re-welded to the surface in the vacuum. It was concluded that the chemical factor of fretting was primarily responsible for the reduced fretting fatigue life in air.

Endo and Goto [31] evaluated the effects of humidity and oxygen on fretting fatigue of a carbon steel and aluminum alloy. They found that the environmental effect on fretting fatigue was dependent on the type of material being evaluated. Oxygen had little effect on

the aluminum alloy but increased the initiation and propagation of fretting fatigue cracks in carbon steel. Water vapor, on the other hand, had little effect on the carbon steel but increased the rate of fretting fatigue crack initiation and propagation in the aluminum alloy. Additionally, they found that the environment was more influential than the mechanical action of fretting fatigue on crack growth. The fretting fatigue crack rate of the carbon steel was considerably slower in argon than in room air. Both the crack initiation and propagation of the aluminum alloys were significantly lower in dry air than in room air.

Research on the effect of seawater on the fretting fatigue life of a material has been inconsistent. The overall effect on crack nucleation and propagation depends on the scenario and conditions involved. Some investigations have shown that seawater can increase the fretting fatigue life due to its lubricating effects. Others have shown that seawater has a detrimental effect on fretting fatigue life due to its corrosive nature. Takeuchi et al. [14] measured the fretting fatigue life of stainless steel in seawater and found that at higher stress amplitudes, fretting fatigue life was longer in seawater than in air. Four possible rationales for this finding were given. First, the corrosion products and wear particles produced a lower coefficient of friction. Second, the stress concentration was reduced at the crack tip due to the formation of multiple cracks in seawater. Third, seawater provided a significant cooling effect at increased stress levels. Finally, the accumulation of debris in the cracks may have contributed to an increase in crack closure thereby lowering the fatigue crack growth rate.

Sato et al. [28] compared the effects of fretting on stainless steel in air, de-ionized water, 3.07% NaCl solution, synthetic seawater, and natural seawater. They found that the

corrosion products produced in synthetic and natural seawater served as a lubricant thereby providing protection against fretting damage at large amplitudes.

Takeuchi et al. [32] investigated the electrochemical effects of seawater on fretting fatigue crack growth of high tensile roping steel. They found that electrochemical effects have a significant influence on the fretting fatigue failure mechanism. However, if the electrochemical effects were removed through the process of cathodic protection, fretting fatigue life in seawater was improved.

Price and Taylor [33] examined corrosion fatigue and fretting fatigue of a high strength, low alloy steel in seawater. They found that corrosion fatigue decreased the fatigue life by 60% compared to air. Fretting in a seawater environment resulted in another 24% reduction in fatigue life. However, when the electrochemical factor was removed by cathodic protection, they were able to restore fretting fatigue life in seawater to a level comparable to that in air.

Taylor [27:384] reported in his overview paper that while many more cracks initiate in seawater than in air, a slower crack growth rate occurs at longer crack lengths as the crack is no longer influenced by fretting. This is because closely spaced cracks reduce the stress intensity factor for an individual crack. Antoniou and Radtke [34:238] acknowledged a similar effect calling it a shielding on propagation. They found that the crack propagation rate could be affected by the presence of debris particles within the crack, the surface friction forces between the pad and the specimen, and the presence of multiple cracks which shield each other from far field stresses.

The effect of the environment on the fretting fatigue life of titanium and its alloys has received little attention. However, titanium and its alloys are often used in applications

where they are subjected to harsh environmental conditions as they are coated with a corrosive resistant oxide surface film. Although corrosion itself does not significantly affect the fatigue life of corrosion resistant materials, fretting in a corrosive environment has been shown to reduce fatigue life as the protective oxide surface film is continuously ruptured [4].

Molinari et al. [35:105] noted that titanium and its alloys have poor wear properties and attributed this to two main factors. First, low resistance to plastic shearing and low work hardening provides weak counteraction to the mechanical properties of wear. Second, the surface oxide provides little protection since it is easily removed. Alam and Haseeb [5] observed that the poor wear properties of Ti-6Al-V4 were due to its inability to retain its protective oxide layer. They found that the oxides consisted of TiO_2 and Al_2O_3, and since these oxides are not soluble in each other, the resulting scale was not very protective.

Waterhouse and Dutta [4] investigated the effect of fretting fatigue on titanium and its alloys in a corrosive environment. They found that a 1% NaCl solution was more detrimental than air on fretting fatigue strength. However, the detriment was dominant at higher alternating stresses versus lower stresses. In fact, the 1% NaCl solution improved the fretting fatigue life at lower stresses for Ti-6Al-4V.

Wharton and Waterhouse [15] performed fretting fatigue tests on Ti-6Al-4V under various corrosive and non-corrosive environments. Plots on the typical S-N curve showed that the corrosive environments were more detrimental to the fretting fatigue life at higher stress, but they extended the fretting fatigue life at lower stresses. They suggested two possible roles the environment plays in fretting fatigue. First, it results in the formation of

corrosion products. These corrosion products can either adhere to the surface acting as a solid lubricant and lowering the coefficient of friction or not adhere and contribute to fretting wear on the surface. Second, the environment can influence crack initiation and propagation. Based on S-N curves and investigation of the specimens, it was hypothesized that at higher stresses, the main effect of the environment was to increase the crack propagation rate thus decreasing the fretting fatigue life. At the lower stresses, the protective action provided by the corrosive debris resulted in a decreased initiation of fretting fatigue cracks thus improving the fretting fatigue life.

Saritas et al. [36] reported that the coefficient of friction of Ti-6Al-4V was lower in seawater than in air. They found that the coefficient of friction alternated between high and low values during the later stages of fretting as debris was periodically washed away by the seawater. Although the coefficient of friction was lower in seawater than in air, the amount of fretting scar was three times greater in seawater than in air. They suggested that the increase in scar volume was due to the abrasive wear produced by corrosion products as well as the corrosive nature of the seawater itself. Jiang et al. [37] noted that the presence of a corrosive solution considerably accelerated wear by increasing the quantity of potential crack initiation sites and increasing the micro-crack propagation rate.

Hoeppner et al. [6] evaluated the fretting fatigue of Ti-6Al-4V in laboratory air, distilled water, and 3.5% NaCl solution. They found that regardless of the stress level, a greater reduction of fretting fatigue life was found in the 3.5% NaCl solution than in distilled water or air.

Fatigue Parameters

In order to prevent component failure, it is necessary to detect fatigue crack nucleation and propagation under fretting conditions. However, this is difficult to accomplish when components are in service. For this reason, numerous fatigue parameters have been developed to predict fatigue life under various conditions (including fretting). The majority of these parameters can be categorized into two groups: equivalent stress models and critical plane models. Equivalent stress models often necessitate the determination of the mean stress which is used with the uniaxial stress life data to predict fatigue life. The problem with this type of approach is that the mean stress is difficult to define within a multiaxial stress state. The critical plane models are based on the observation that cracks nucleate on a critical plane. These approaches consider crack nucleation to be a result of the combination of normal and shear stresses that occur on a critical plane. The normal stress is hypothesized to open the crack and reduce the friction between the crack surfaces while the shear stress causes crack nucleation and growth due to dislocation movement along slip lines. An advantage of critical plane models is that they predict the orientation of the crack and have the potential to estimate crack size [8,9].

Two fatigue parameters will be evaluated in this study. The first parameter predicts fretting fatigue life based on the applied (far field) stress and takes into consideration the stress ratio effect on fatigue life. This parameter, based on a method suggested by Walker [38] and employed by Lykins et al. [39] for Ti-6Al-4V, is expressed by the equation:

$$\sigma_{eff} = \sigma_{max}(1-R)^{m} \qquad (1)$$

where σ_{eff} is the effective stress taking into account the stress ratios, σ_{max} is the maximum applied stress, m is a curve fitting parameter determined to be 0.45 for Ti-6Al-4V by Lykins et al. [39], and R is the stress ratio:

$$R = \frac{\sigma_{axial,\min}}{\sigma_{axial,\max}} \qquad (2)$$

where $\sigma_{axial,min}$ is the minimum axial stress and $\sigma_{axial,max}$ is the maximum axial stress based on the far field loading. This parameter has been shown to be effective at predicting fretting fatigue life for certain pad geometries [8,9]. Additionally, it has been shown to be effective at estimating the fretting fatigue life of Ti-6Al-4V under elevated temperatures as well as shot peening conditions [40,41].

The second parameter that will be evaluated in this study is the Modified Shear Stress Range (MSSR) parameter. This multiaxial parameter is based on critical plane models and therefore accounts for the observation that cracks nucleate on critical planes as a result of both normal and shear stresses. The MSSR is expressed as:

$$MSSR = A*\Delta\tau^{B}_{crit,eff} + C*\sigma^{D}_{max} \qquad (3)$$

where $\Delta\tau_{crit,eff}=\tau_{max}(1-R_\tau)^m$ [8,38], τ_{max} is the maximum shear stress on the critical plane, R_τ is the shear stress ratio on the critical plane, m is a curve fitting parameter determined to be 0.45 for Ti-6Al-4V [39], σ_{max} is the maximum applied stress, and A, B, C, D are curve fitting parameters determined to be 0.75, 0.5, 0.75, and 0.5 respectively for Ti-6Al-4V by Namjoshi et al. [8]. The first term takes into account the mean shear stress ratio effect while the second term incorporates the maximum normal stress on the critical

plane. In the case of Ti-6Al-4V, the MSSR has been found to be effective at predicting fretting fatigue life from plain fatigue life data in conjunction with an analysis. Additionally, the MSSR has effectively predicted both location and orientation of fretting fatigue crack initiation in Ti-6Al-4V [8]. Similar to the applied stress range parameter, the MSSR has been proven robust enough to be used with various pad geometries and under various conditions [40,41,42].

III. Experimental Studies

The experimental setup and results are presented in this chapter. Topics include the fretting fatigue test configuration, Q/P ratio determination, fracture surface debris identification, fretting fatigue striation measurements, and scar volume estimations. Additionally, a comparison is made between seawater and dry fretting fatigue life data.

Fretting Fatigue Experimental Configuration

The fretting fatigue tests were performed under laboratory conditions at room temperature on a 22.2 kN servo-hydraulic load frame [43] mounted with a rigid fretting fixture (Figures 3 and 4). The laboratory humidity ranged from 20-65% throughout the experiments. Two cylindrical fretting pads, each with a radius of 50.8 mm, were held against each side of the fretting specimen via the fretting fixture. Both the fretting pads and specimens were machined from Ti-6Al-4V forged plates using the wire electrical discharge method. The plates were received after being preheated and solution treated at 935°C for 105 minutes, cooled under flowing air, vacuum annealed at 705°C for 120 minutes, and cooled under flowing argon. The resulting microstructure consisted of 60% hexagonal closed pack α phase and 40% body center cubic α platelets in a β matrix phase. The grain size was approximately 10μm. The dimensions of the dog bone shaped Ti-6Al-4V specimen were as follows: specimen thickness of 3.86 mm, specimen width of 6.35 mm, cross sectional area of 24.511 mm^2. The specimen and pads are shown in Figure 5. Once the pads were aligned with the specimen, the normal load was applied. Four lateral springs, two on each side of the specimen, maintained contact of the pads and specimen

under a constant normal load of 1334 N. This value was chosen in order to maintain the maximum stress in the x-direction below the yield stress of the fretting specimen. Two load cells, one on each side of the specimen, were used to measure the normal load. A load cell, attached to the servo-hydraulic load frame above the specimen, measured the axial load above the pads. A lightweight pressure transducer was used to measure the axial load at the bottom of the specimen. This system allowed the user to vary the axial load by controlling the displacement in the axial direction. The displacement was applied in the axial direction at constant amplitude of 5 Hz to allow the specimen to be adequately exposed to the environmental conditions. The tangential load was a function of the axial load and the resistance from the pads caused by the lateral springs. The control system of the test equipment maintained the frequency and the amplitude of the applied axial displacement constant during the duration of the test. The fretting fatigue tests for both dry and seawater conditions were conducted over a wide range of axial stresses from σ_{max}= 383 to 760 MPa, with stress ratios, R, ranging from 0.03 to 0.54.

A 1.59 mm inner diameter Tygon® flexible plastic tube fitted with a simple Economatic drain valve was inserted into a plastic water bottle containing ASTM D 1141 synthetic seawater. The 590 mL bottle was positioned above the servo-hydraulic load frame. The drain valve, located 1.1 meters below the bottle, allowed the user to vary and control the frequency and duration of the seawater application. Below the drain valve, a copper tee fitting was attached to the end of the plastic tubing. Two additional Tygon® flexible plastic tubes, each with a 1.59 mm inner diameter, were attached onto the tee fitting as shown in the schematic Figure 6. The plastic tubes were then attached to each side of the specimen above the fretting pads using transparent tape. Once the drain valve

was opened, seawater dripped onto each side of the specimen. Since this was not an enclosed setup, the equipment below the specimen was protected against the excess seawater that flowed over the specimen. Kimwipes, size EX-L, were wrapped around the bottom specimen grip and pressure transducer and attached with transparent tape. Plastic Wrap was then placed over the Kimwipes and secured in place with transparent tape. Additionally, 40.64 cm by 50.8 cm Pig® Universal absorption pads were layered below the bottom specimen grip and pressure transducer for additional protection. If a drip was detected away from the specimen, plastic containers were positioned to collect the excess seawater.

A total of thirteen fretting fatigue tests were conducted, seven under seawater conditions and six under dry conditions. All fretting fatigue tests were started under dry conditions to allow for adjustment of the axial load and to ensure fretting conditions were occurring. Fretting conditions were determined using the hysterises loop between tangential force and displacement. Figure 7 shows a typical hysterises loop. The initial application of seawater occurred between 2,000 and 3,000 cycles. The seawater was applied for two seconds every one minute. This resulted in an application rate of approximately five ml per minute to each side of the specimen. Figure 8 shows the effect of the various amounts of seawater applied to the specimen in terms of effective stress amplitude, σ_{eff}, versus number of cycles to failure, N_f, while Figure 9 illustrates the effect of various seawater application frequencies on the number of cycles to failure. It was determined that as long as the specimen surface was wet, regardless of frequency of application or amount applied, an environmental effect would occur as the seawater temporarily pooled at the contact surface between the pads and the specimen after

application. It was observed that once the seawater was applied, the tangential load remained constant as gross slip did not occur during seawater application.

Table 1 provides a complete summary of the experimental data for both dry and seawater fretting fatigue conditions. Figure 10 shows both the seawater and dry fretting fatigue data expressed as the effective stress amplitude, σ_{eff}, versus the number of cycles to failure, N_f. The effective stress amplitude was found using equations (1) and (2). As evident from the figure, seawater fretting fatigue conditions were more detrimental on the fretting fatigue life of Ti-6Al-4V than dry fretting fatigue conditions at the higher stress levels. However, at the lower stress levels, seawater fretting fatigue conditions slightly improved the fretting fatigue life of Ti-6Al-4V.

Load Determination

In order to perform finite element analysis (FEA) in chapter four, the axial and tangential loads must be determined as each represents input data for FEA. As previously mentioned, a load cell was attached to the servo-hydraulic load frame above the specimen to monitor the axial load. The tangential load can be determined by the equation:

$$Q = \frac{V - W}{2} \qquad (4)$$

where Q is the tangential load on each side of the specimen, V is the axial load applied in the down direction upon the specimen, and W is the upper axial load. Figure 11 shows a load illustration.

Q/P Ratio

The Q/P ratio was determined by dividing the tangential force, Q, by the normal load, P. The tangential load was found using equation (4) while the normal load remained constant at 1334 N throughout the duration of each test. The Q/P ratio was considered the lower boundary of the coefficient of friction between the fretting specimen and pads. The Q/P ratio determined from each test was used as the coefficient of friction input data for finite element analysis, FEA, in chapter four. The coefficient of friction has been shown in previous studies [14] to increase once cycling of the specimen begins. However, Namjoshi et al. [8] found that the coefficient of friction reached a constant value after approximately 1,000 to 2,000 cycles. In this study, the specimen underwent approximately 5,000 cycles before the Q/P ratio was determined (i.e., 2,000-3,000 cycles before water was added and 2,000 cycles after water was added). Figure 12 shows the seawater and fretting fatigue data expressed as effective stress amplitude, σ_{eff}, versus the Q/P ratio. In both conditions, the Q/P ratio increased with an increasing applied stress. Figure 12 suggests that the Q/P ratio, based on a least squares fit to data with a large amount of scatter, was slightly lower in seawater conditions than in dry conditions; however, the difference between the two conditions was negligible.

Fracture Surface Debris

Once the specimens fractured, they were examined under a scanning electron microscope, SEM [44]. Figure 13 shows a typical back scatter emission (BSE) SEM photograph of a specimen exposed to seawater conditions whereas Figure 14 shows a typical BSE SEM photograph of a specimen exposed to dry conditions. Appendix A

contains two additional BSE SEM photographs of specimen exposed to seawater conditions. As evident from Figure 13, large particles were densely located in the area of the crack initiation in the seawater samples. However, the dry samples showed scattered debris particles in the area of crack initiation. Energy Dispersive Spectroscopy (EDS) [45] was utilized in order to determine the debris composition in both the dry fretting fatigue and seawater fretting fatigue studies. Figure 15 shows an EDS broad scan of the surface area of a fractured specimen exposed to seawater whereas Figure 16 shows that of a specimen exposed to dry conditions. Debris particles were identified through surface magnification using SEM as shown in Figures 17 and 18, and EDS scans were performed on these debris particles. Based on these magnified scans, two primary types of debris were identified: that composed primarily of titanium and that composed primarily of salt and other elements. Figure 19 shows a magnified EDS scan of titanium debris formed under seawater conditions. Figure 20 shows a magnified EDS scan of salt and other elements, collectively termed seawater debris, from a specimen exposed to seawater conditions. A magnified EDS scan of typical debris found on a dry fracture surface, primarily titanium and oxides, is shown in Figure 21.

After the specimens were examined under the SEM and EDS, they were cleaned by way of a three-step process involving distilled water, acetone, and ethanol. A flask containing both a specimen and distilled water was placed in a sonicator [46] for five minutes. This process was repeated for both the acetone and ethanol. BSE SEM photographs were taken a second time as shown in Figures 22 and 23. EDS data was again collected from each specimen. Figure 24 shows an EDS broad scan of the surface area of a fractured specimen exposed to seawater conditions after cleaning whereas

Figure 25 shows that of a specimen exposed to dry conditions after cleaning. There was little difference noted between the dry and seawater specimens after cleaning on a broad scale. SEM was used again after cleaning to magnify the remaining debris particles as shown in Figure 26 and 27, and EDS scans were performed on these particles. Figure 28 shows a magnified EDS scan of debris found in a seawater sample after cleaning while Figure 29 shows that of a dry sample after cleaning. In the specimens exposed to seawater, trace amounts of seawater elements were noted after cleaning, but the primary debris appeared to be titanium and oxides. The debris of the specimens exposed to dry conditions was similar to the debris identified prior to cleaning, primarily titanium and oxides. While it was not possible to determine the quantity of debris present on each sample, it was determined that more elements were found in the debris of specimens exposed to seawater conditions than in those exposed to dry conditions. It should be noted that once the specimens were cleaned, there were not any significant distinguishing characteristics visible between the fracture surfaces of the two conditions. SEM photographs of the fractured surface of each specimen after cleaning can be found in Appendix B.

Scar Volume

Scar volume is the amount of surface material removed during fretting. In order to measure scar volume, eight tests, four under seawater conditions and four under dry conditions, were ran at various effective stresses, σ_{eff}, for 15,000 cycles. This allowed a scar to form without fracturing the specimen. Appendix C contains photographs of the scars. Each specimen was placed under an Ultrascan Profilometer [47] to determine the

scar volume. A profile was taken across the scar which was then plotted in two dimensions using the x and z data provided every 0.25 mm by the Ultrascan Profilameter. Figure 30 shows a typical scar profile in terms of these data points under seawater conditions while Figure 31 shows a typical scar profile under dry conditions. Since each data point was of equal length, the scar area was found using Simpson's 1/3 rule [48]. The scar area was then multiplied by the specimen width to determine the scar volume. Table 2 summarizes the experimental conditions used to determine the scar volume. Figure 32 shows both the seawater and dry fretting fatigue data expressed as the effective stress amplitude, σ_{eff}, versus the scar volume. In both conditions, the fretting scar volume increased as the applied stress increased. Figure 32 suggests that a considerably larger scar volume occurred under seawater fretting fatigue conditions than under dry conditions.

Fatigue Striations

Striations on the fracture surface were observed under the SEM. Near the fretting surface, the striations were difficult to see due to the shear stresses caused by the fretting pads. However, farther away from the crack, striations were more visible. The number of fatigue striations found in the seawater samples was compared to those found in the dry samples. A distance of two millimeters away from the contact surface and perpendicular to the crack initiation site was chosen to identify, count, and measure the number of striations per μm. The striations in a specimen exposed to seawater at σ_{eff} =449.9 MPa is shown in Figure 33 while Figure 34 shows striations found in a dry sample at σ_{eff} =431.4 MPa. There were more closely spaced striations in the dry samples

than in the seawater samples. Figure 35 presents the seawater and dry fretting fatigue data expressed as effective stress amplitude, σ_{eff}, versus the estimated number of striations per μm for each specimen. The data suggests that crack propagation is faster under seawater conditions than dry conditions at this distance. However, the difference in growth rates between the two conditions appears to be less than a factor of two. It should be noted that, due to the surface damage shown in these figures, the measurements are approximations. Appendix D contains each SEM photograph, at various stress levels, used to measure striations.

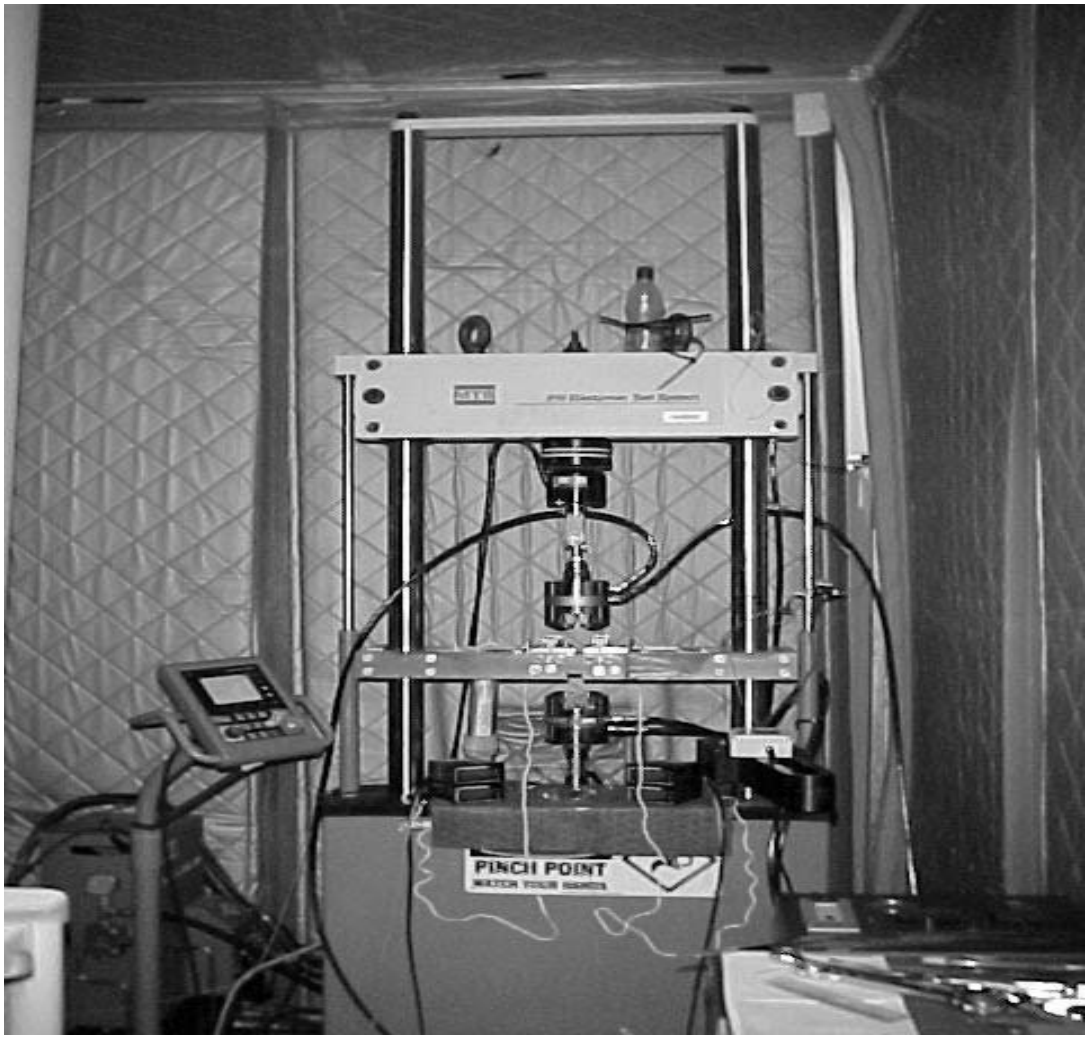

Figure 3. Servo-hydraulic uniaxial test machine with fretting fatigue apparatus.

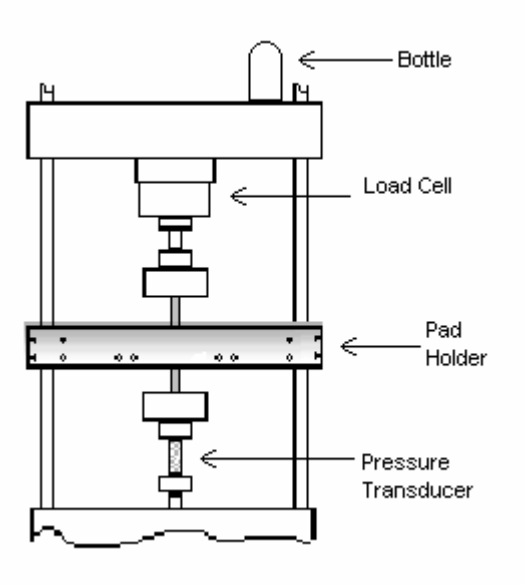

Figure 4. Fretting fatigue experimental configuration.

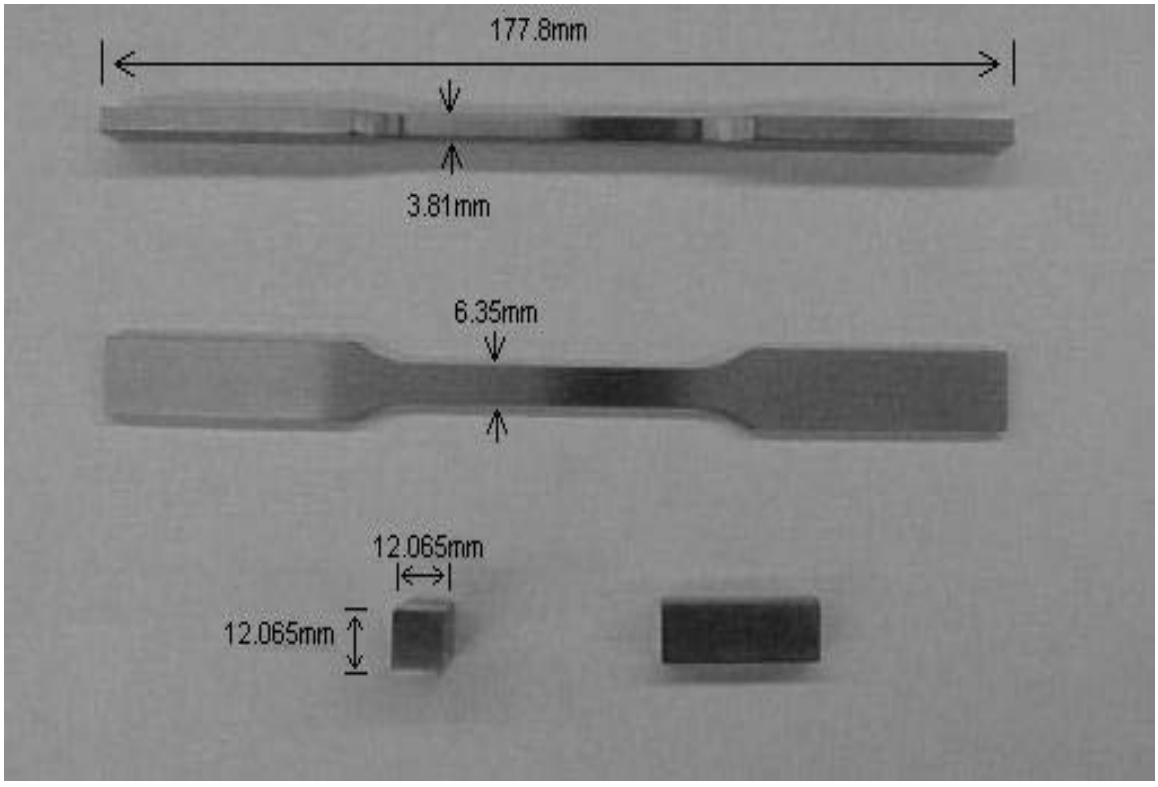

Figure 5. Fretting specimen and pad with dimensions.

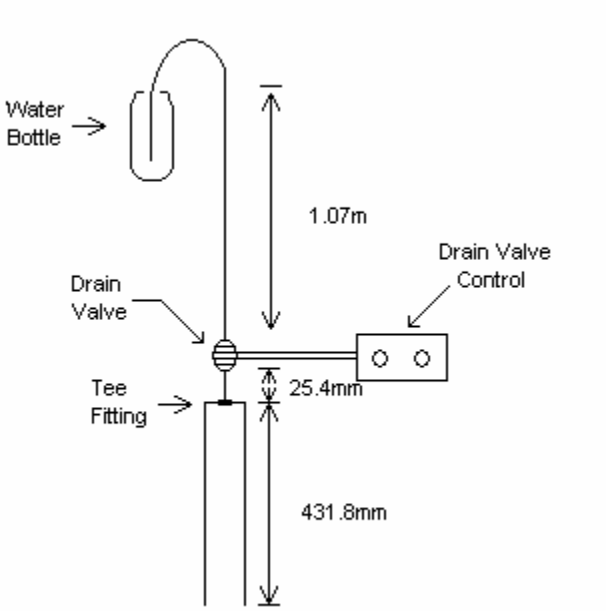

Figure 6. Schematic experimental configuration of seawater application apparatus.

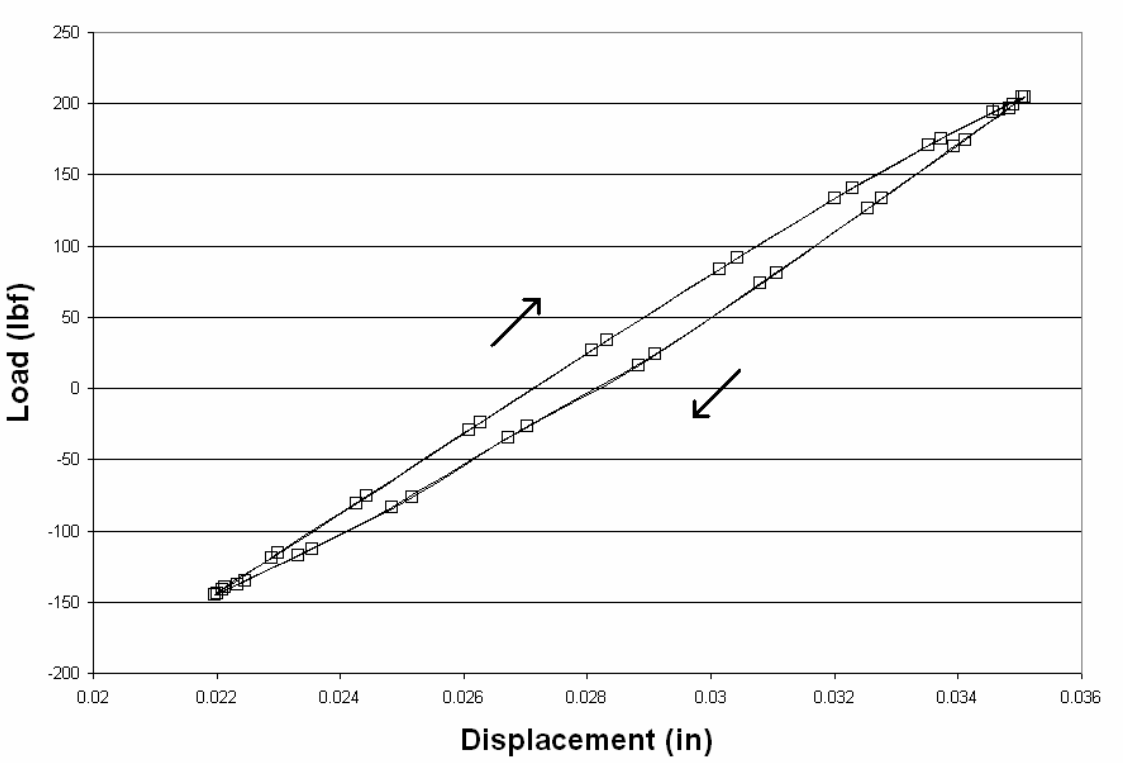

Figure 7. Typical hystersis loop of Tangential Load vs. Displacement.

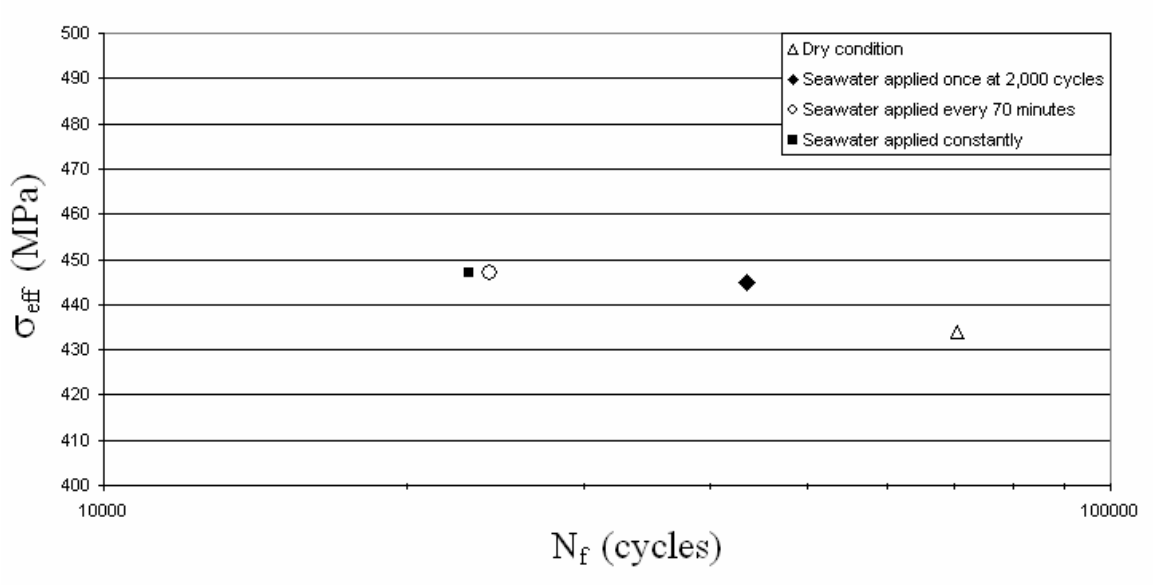

Figure 8. Effective Stress (σ_{eff}) vs. Number of Cycles to Failure (N_f) of various seawater application frequencies.

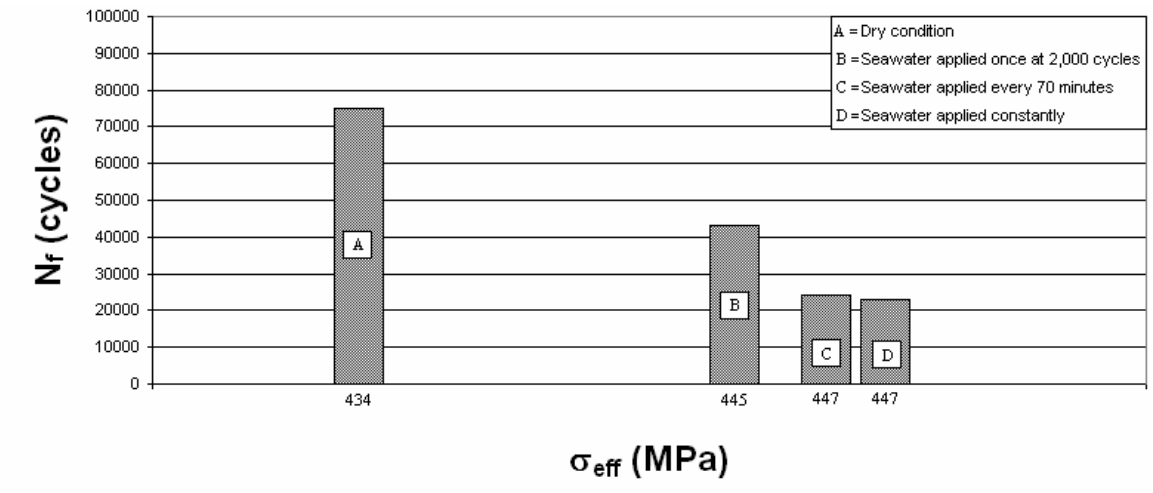

Figure 9. Effect of various seawater application frequencies on Number of Cycles to Failure (N_f).

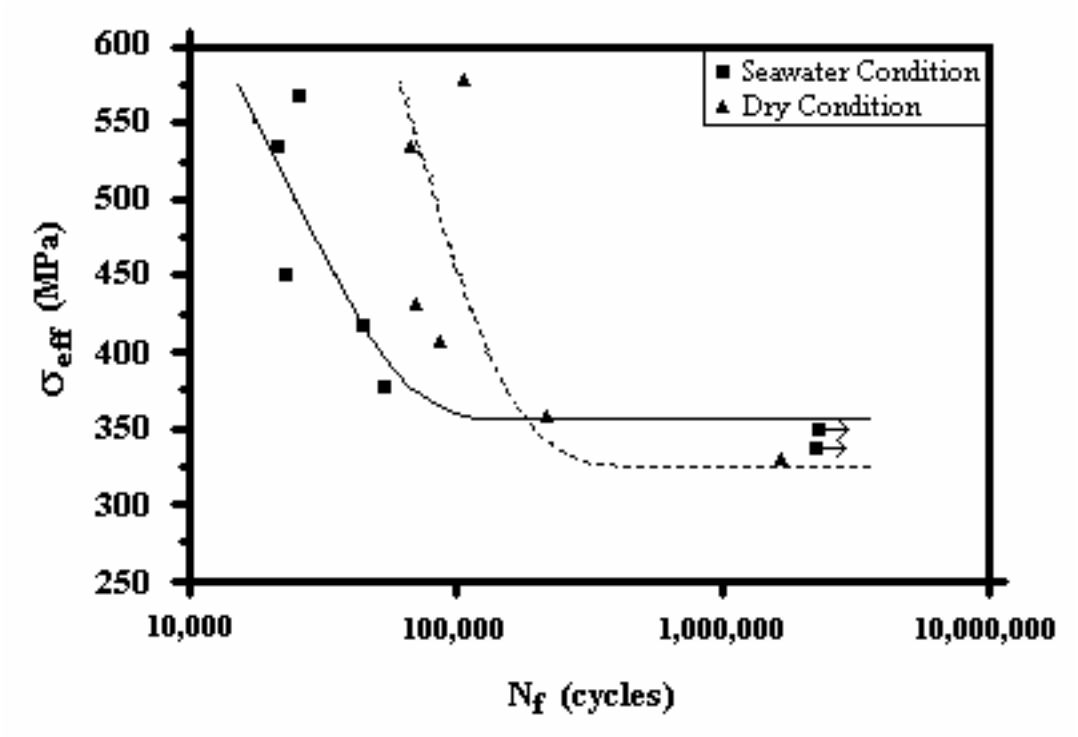

Figure 10. Effective Stress (σ_{eff}) vs. Number of Cycles to Failure (N_f) for seawater and dry conditions. An arrow indicates the test was discontinued before fracture.

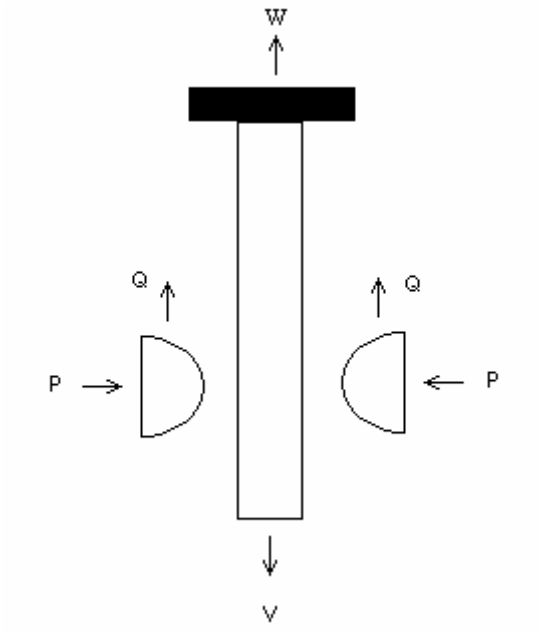

Figure 11. Load illustration.

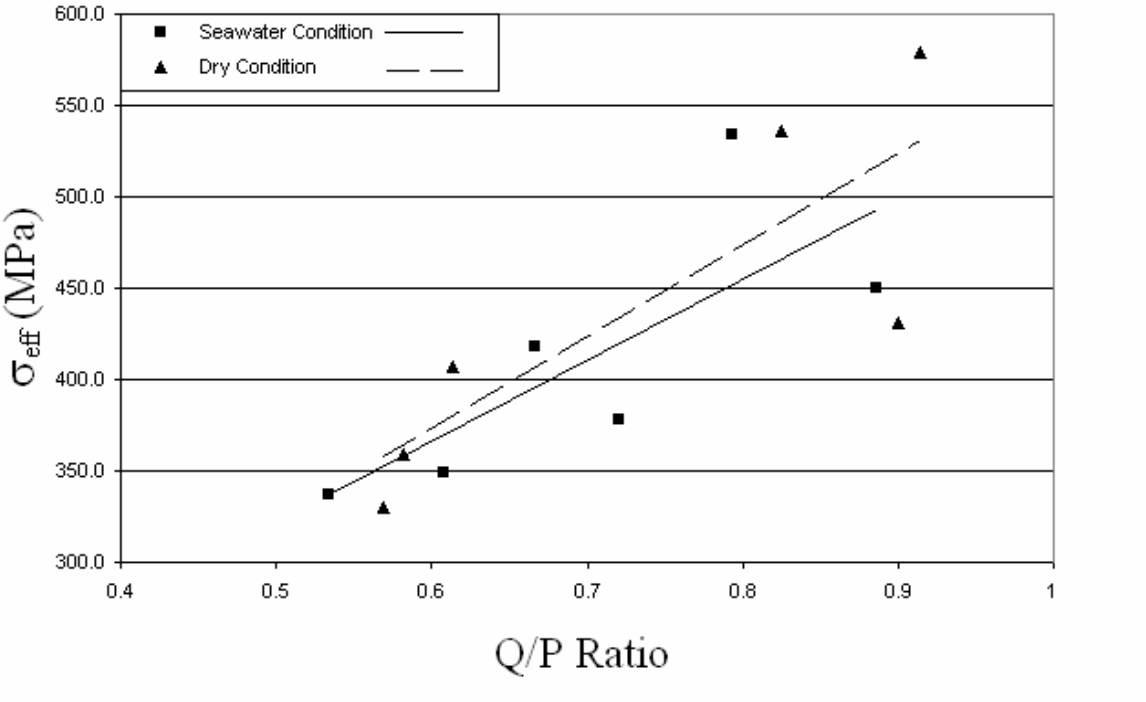

Figure 12. Effective Stress (σ_{eff}) vs. Q/P ratio for seawater and dry conditions.

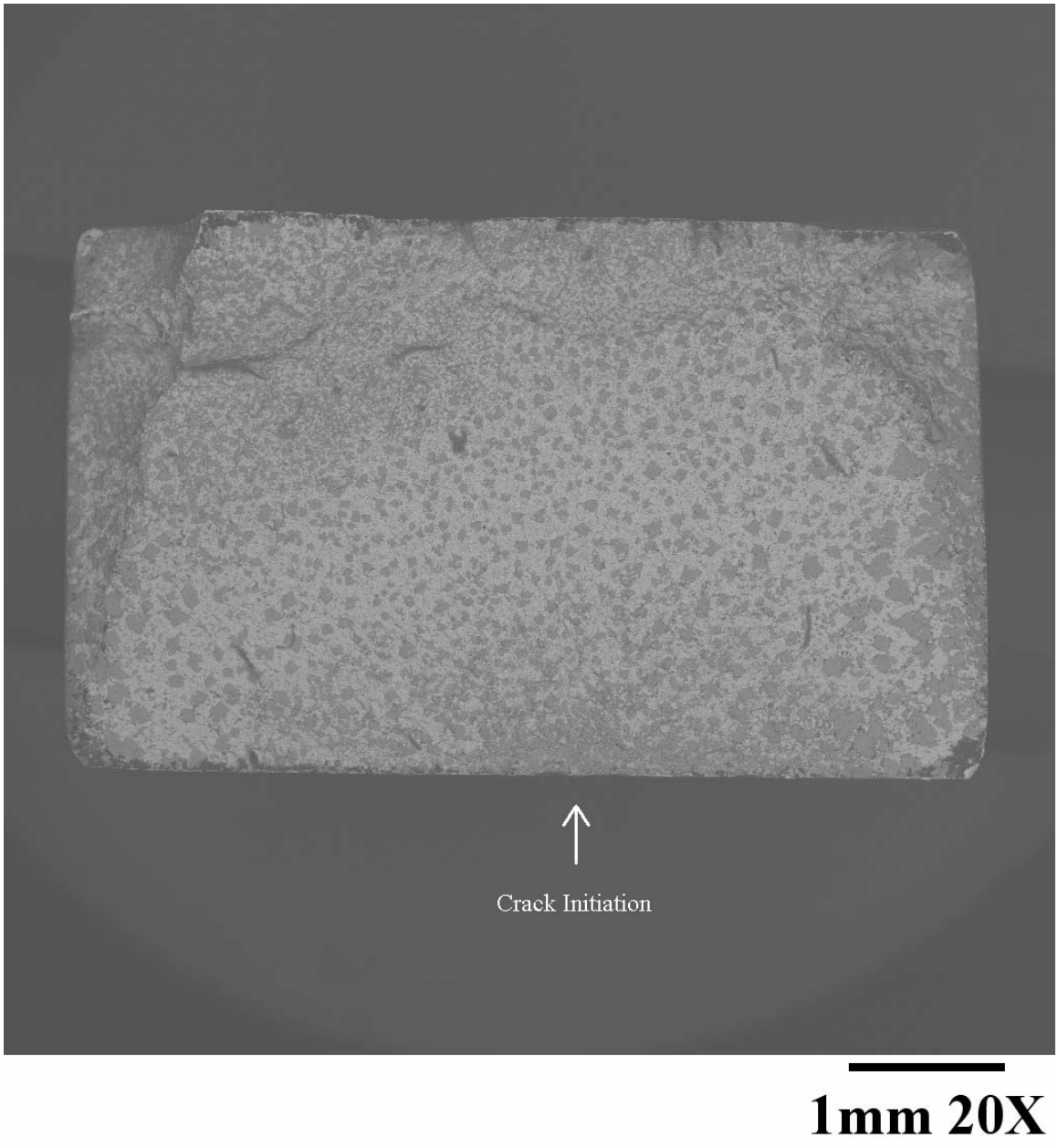

Figure 13. BSE SEM photograph of fracture surface exposed to seawater at σ_{eff}=418.0 MPa before cleaning.

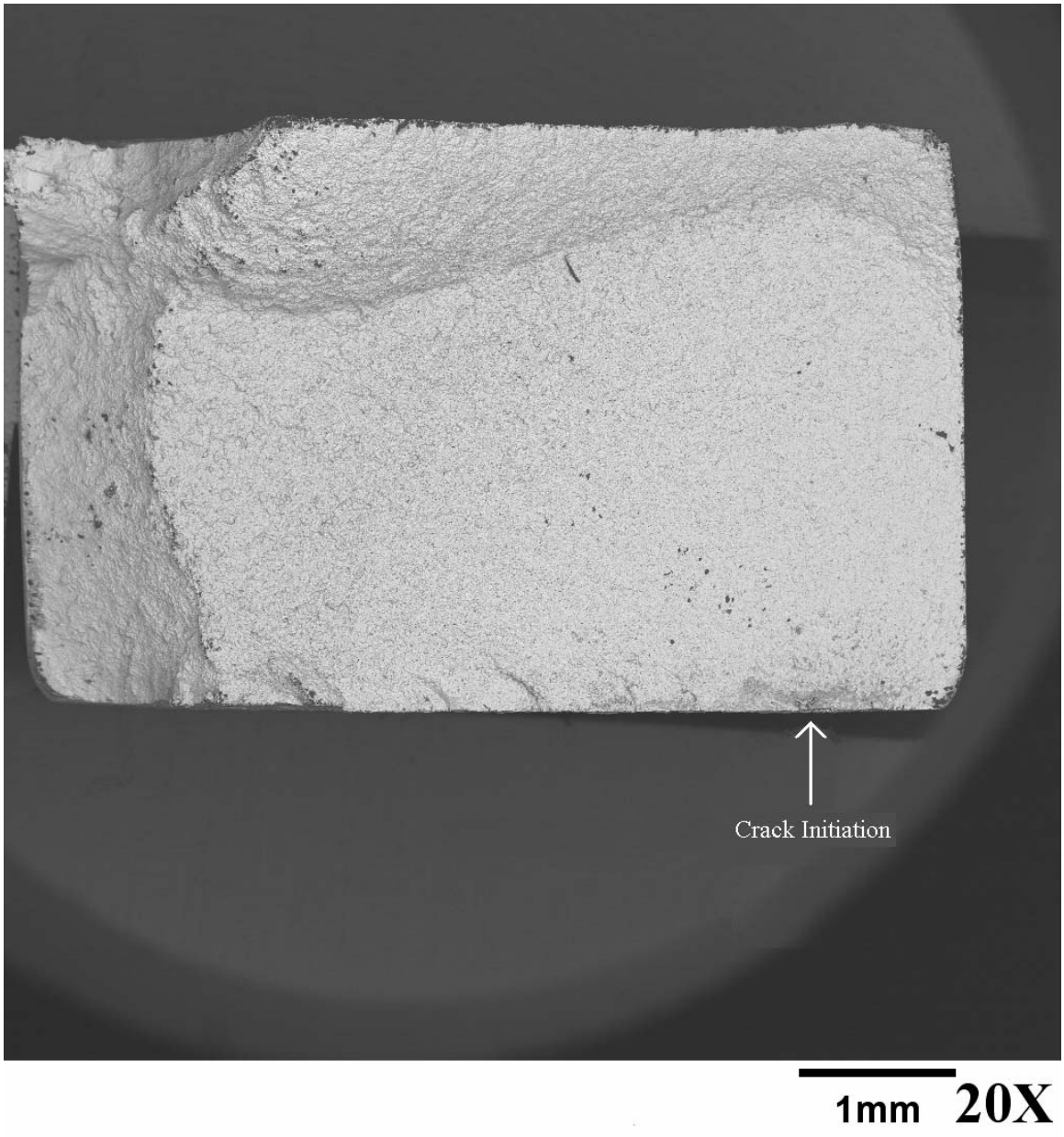

Figure 14. BSE SEM photograph of fracture surface exposed to dry conditions at σ_{eff}=535.5 MPa before cleaning.

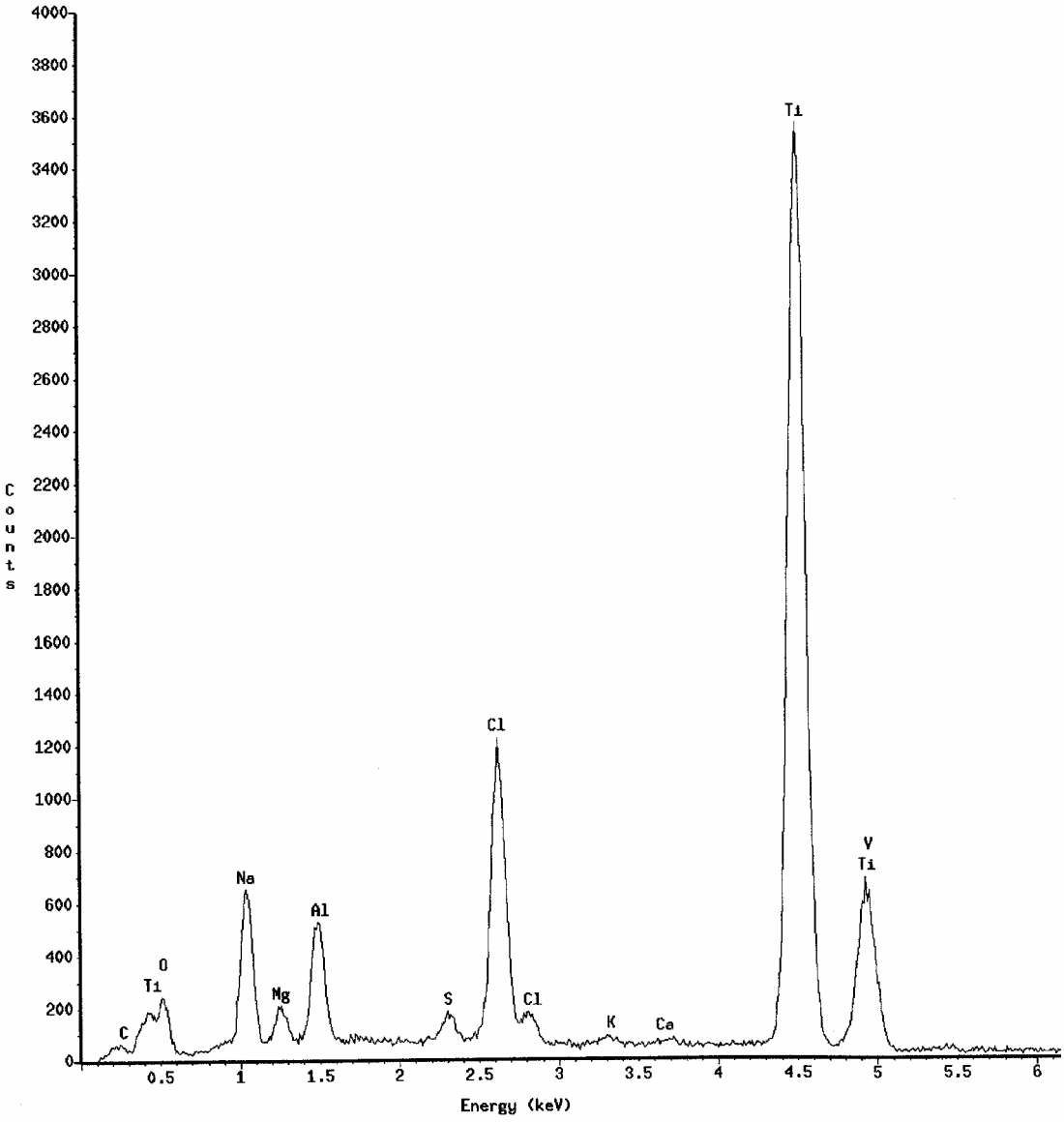

Figure 15. EDS broad scan of the fracture surface of a specimen exposed to seawater before cleaning.

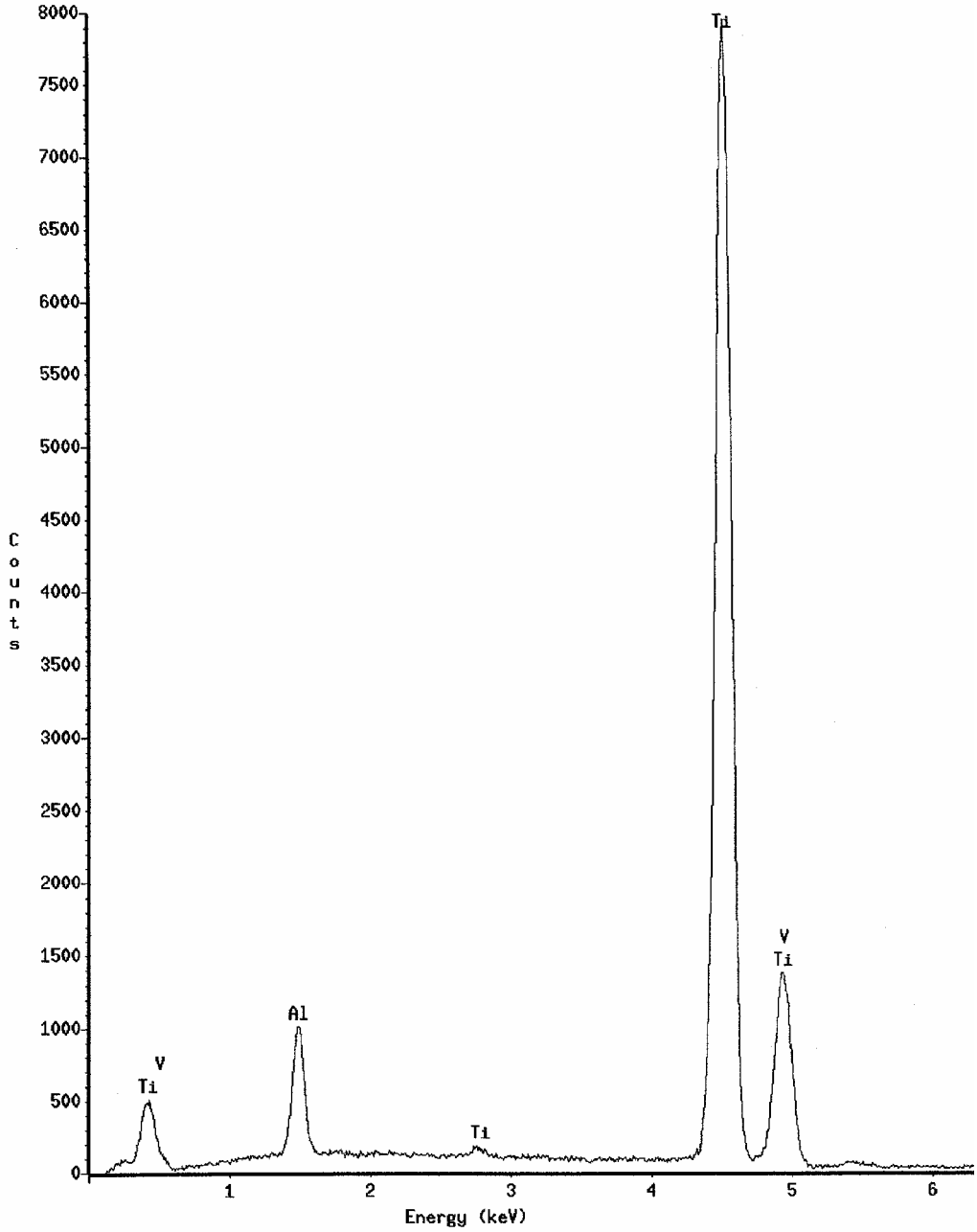

Figure 16. EDS broad scan of the fracture surface of a specimen exposed to dry conditions before cleaning.

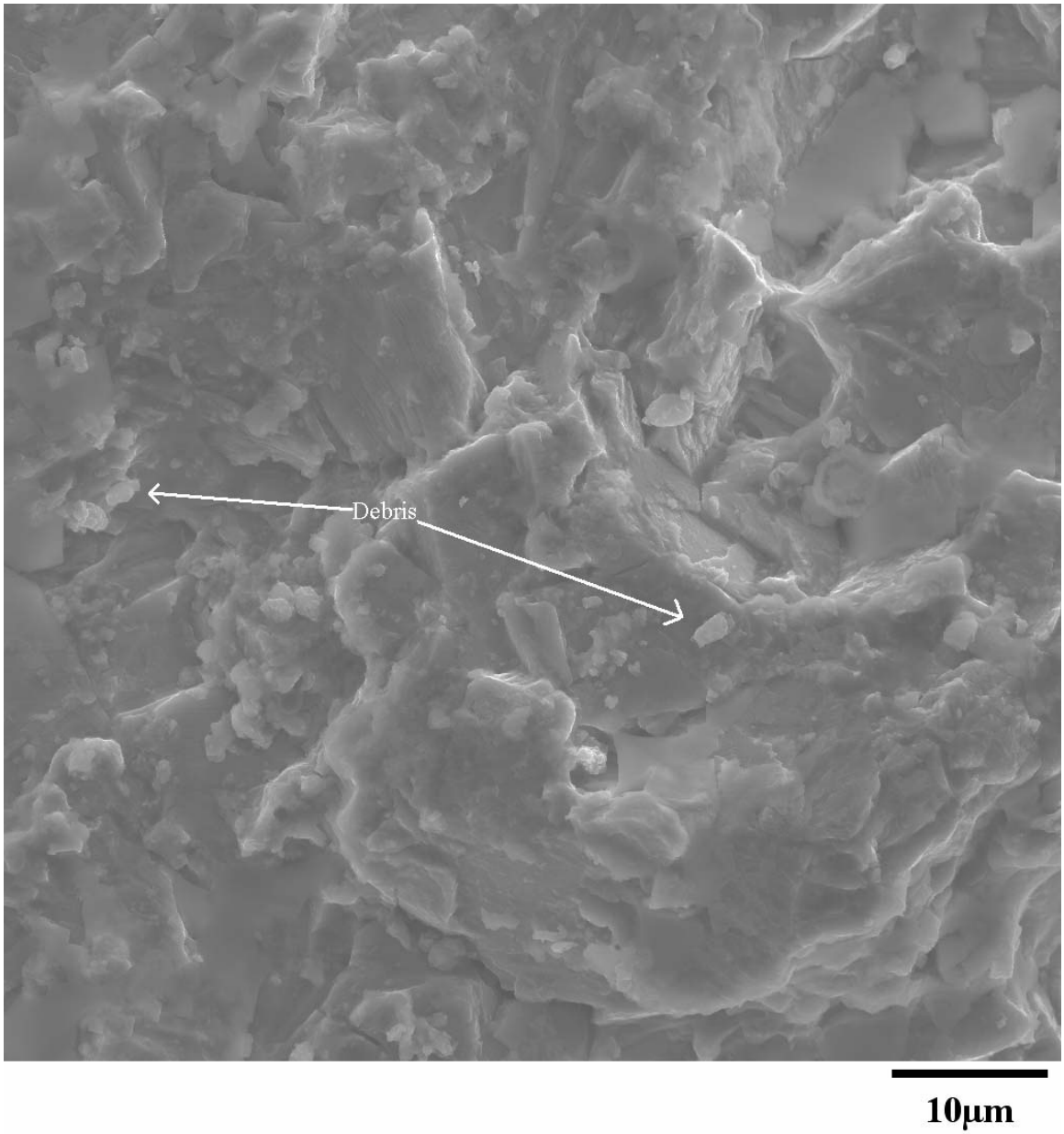

Figure 17. SEM photograph of magnified debris from specimen exposed to seawater conditions before cleaning.

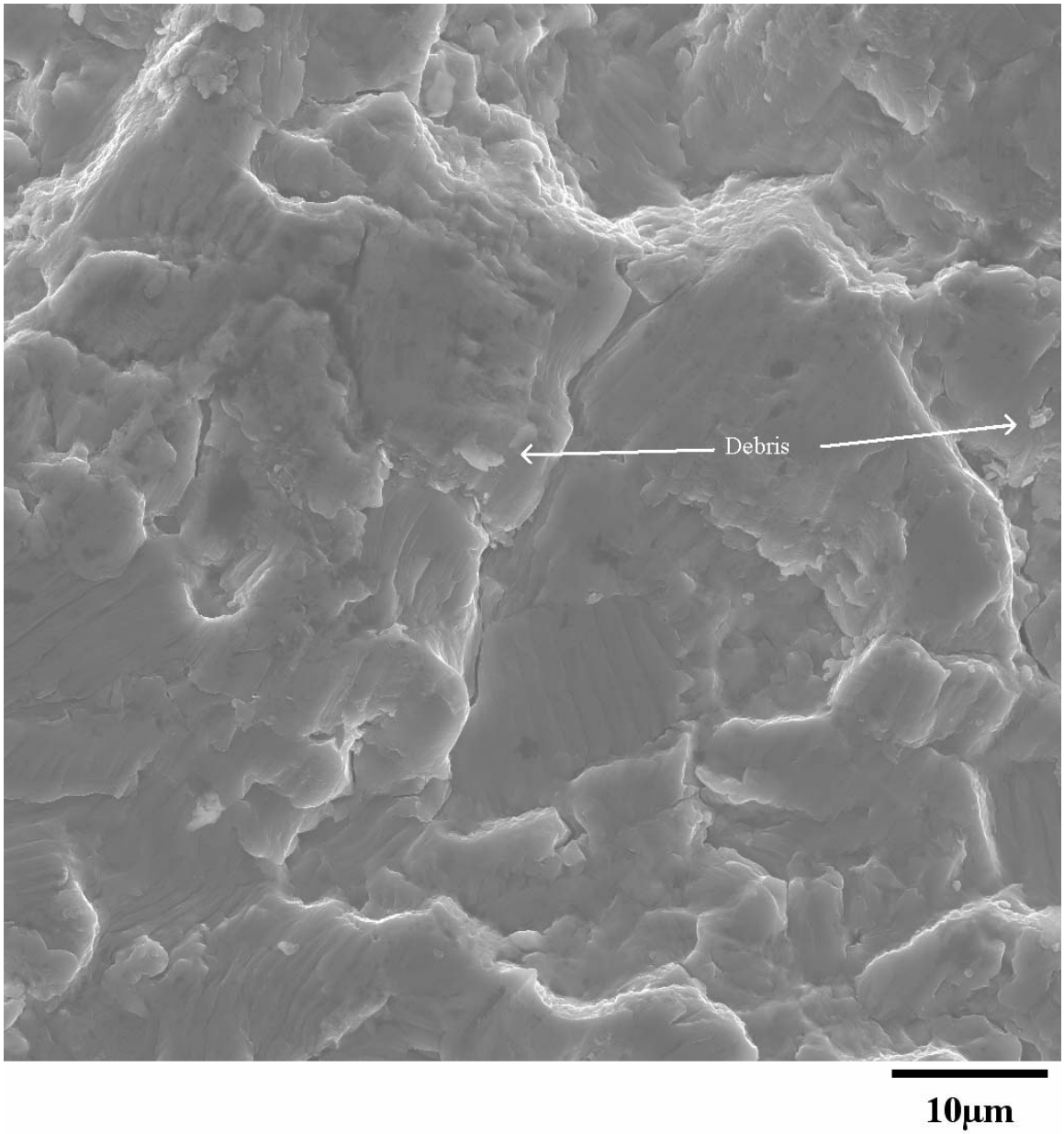

Figure 18. SEM photograph of magnified debris from specimen exposed to dry conditions before cleaning.

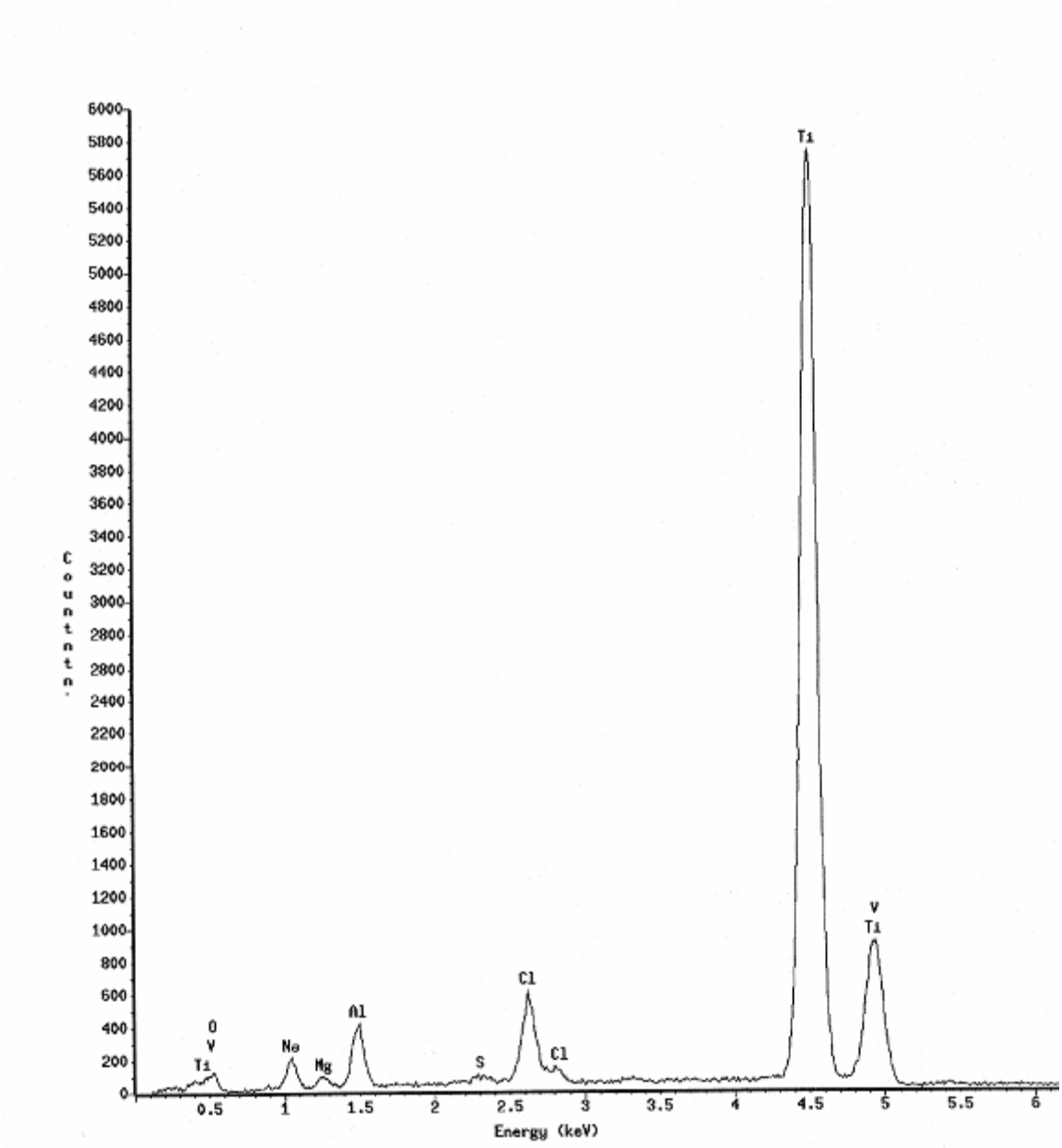

Figure 19. Magnified EDS scan of titanium debris formed under seawater conditions before cleaning.

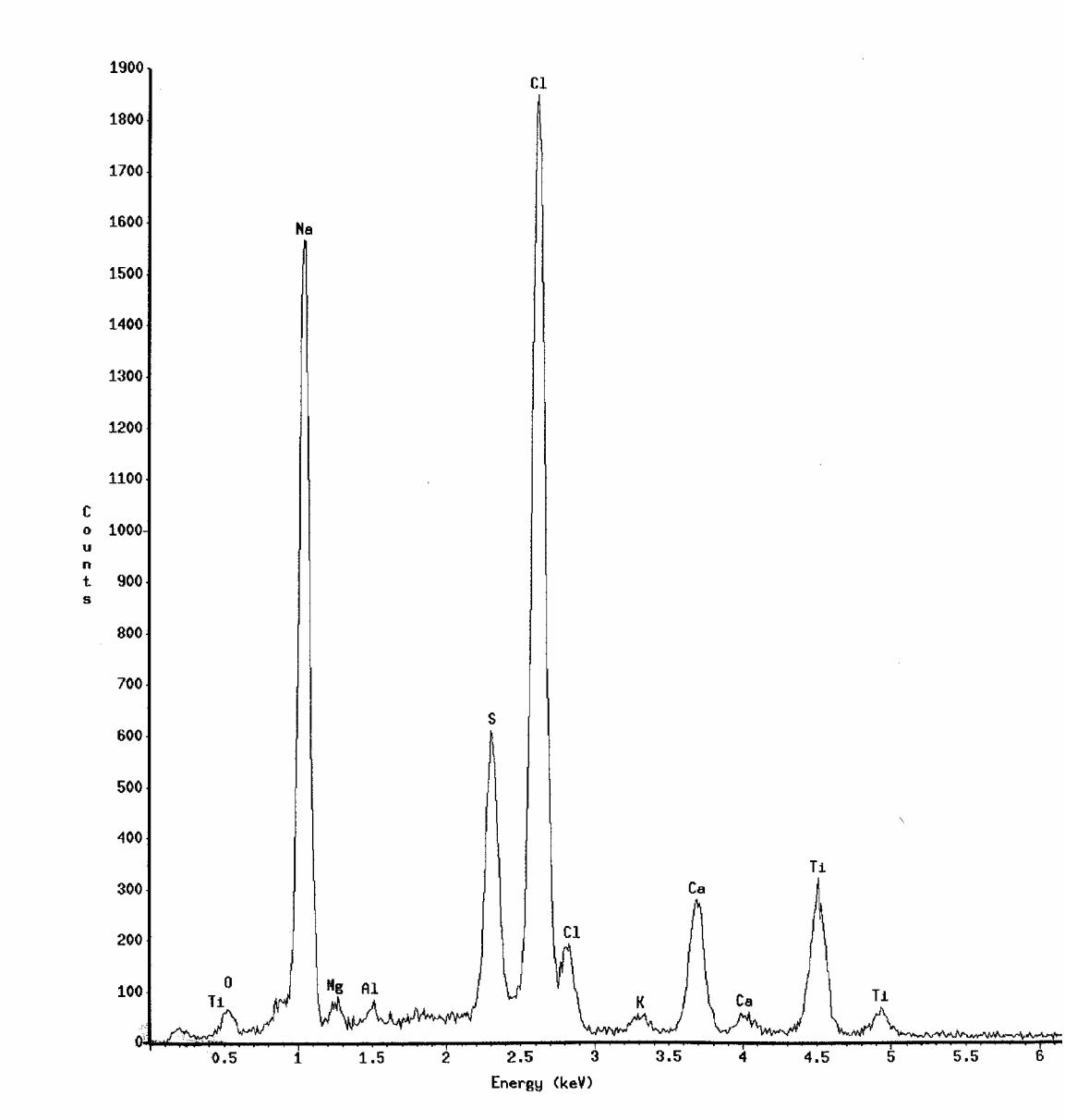

Figure 20. Magnified EDS scan of "seawater" debris formed under seawater conditions before cleaning.

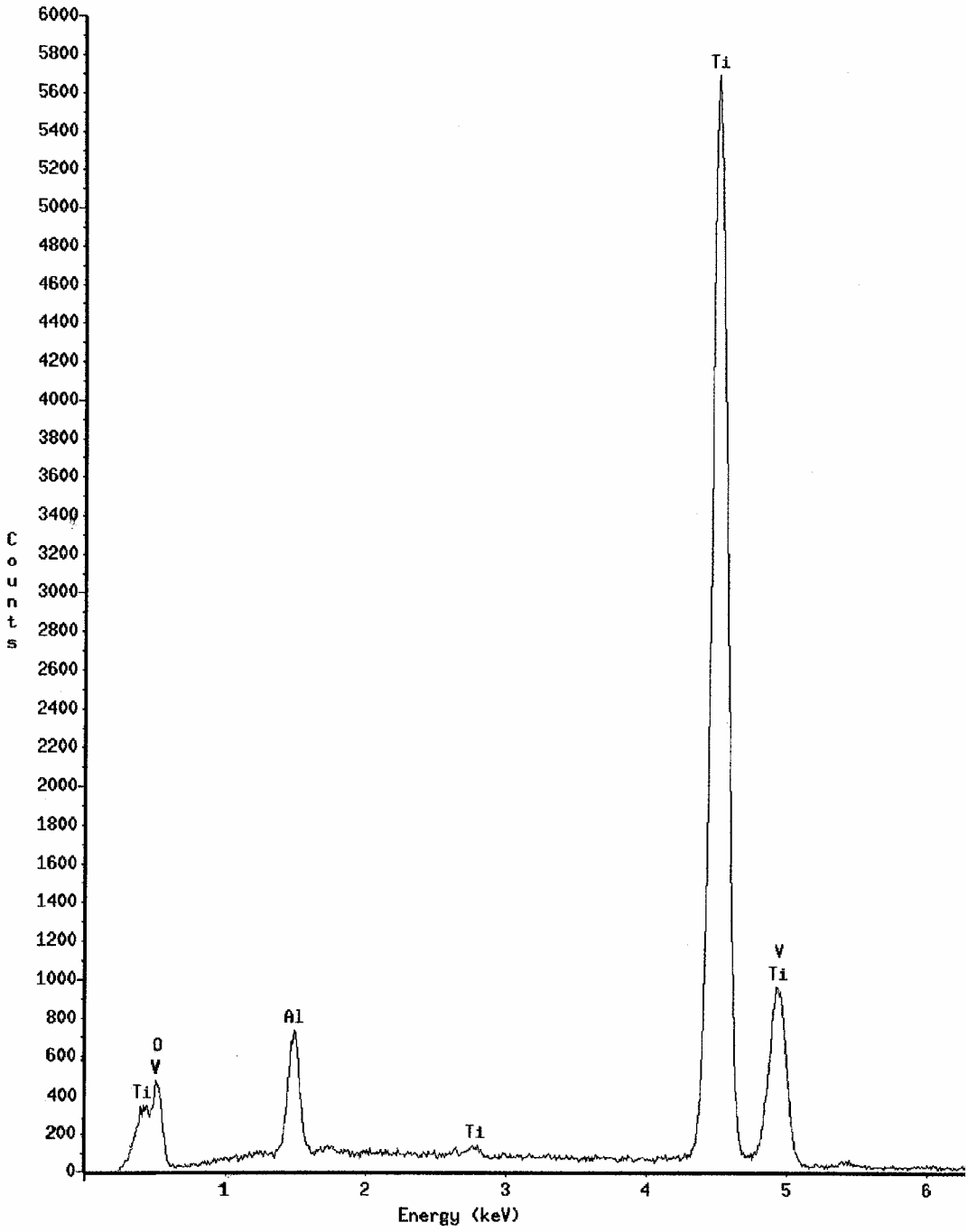

Figure 21. Magnified EDS scan of debris formed under dry conditions before cleaning.

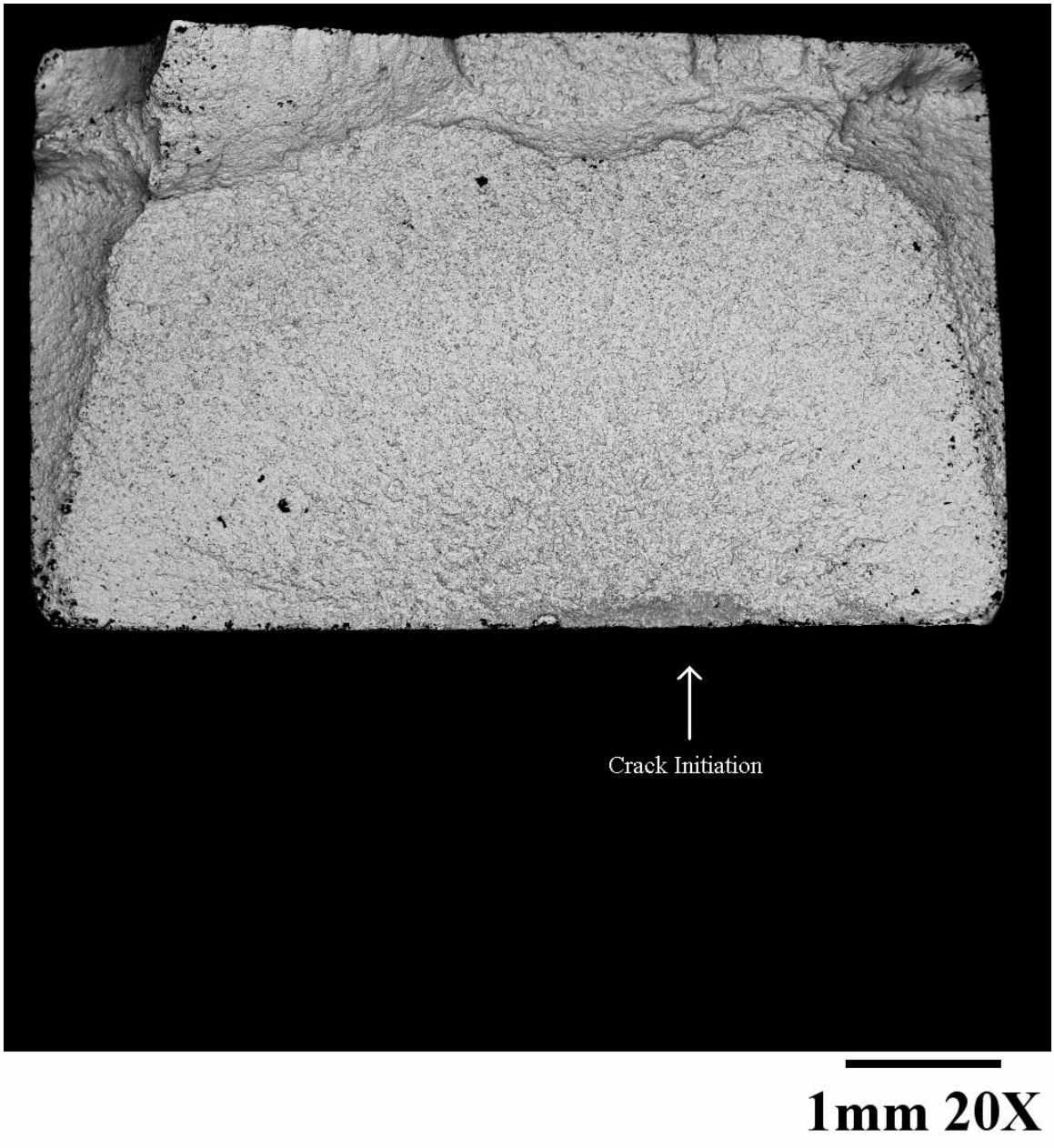

Figure 22. BSE SEM photograph of fracture surface exposed to seawater conditions at σ_{eff}=418.0 MPa after cleaning.

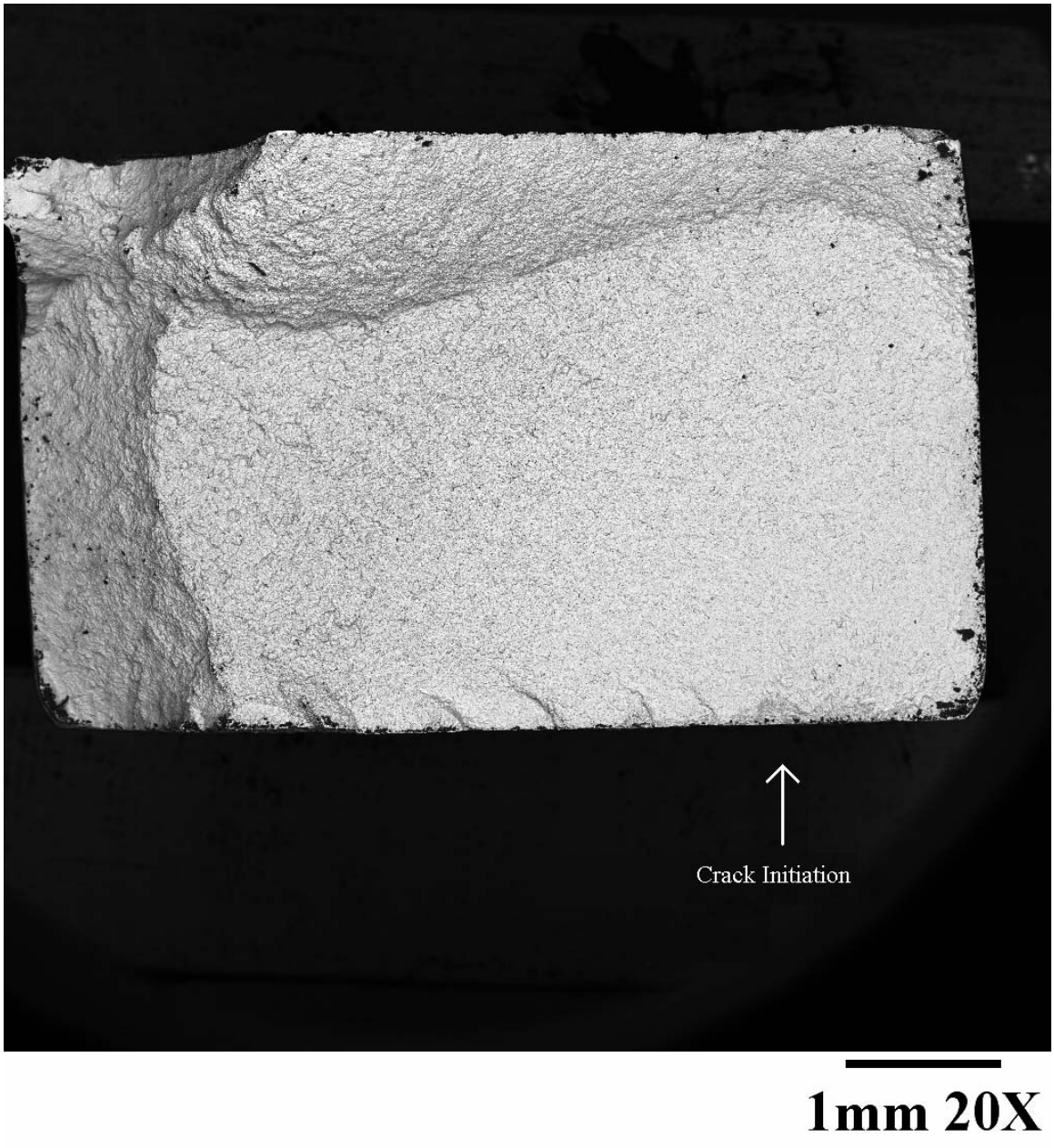

Figure 23. BSE SEM photograph of fracture surface exposed to dry conditions at σ_{eff}=535.5 MPa after cleaning.

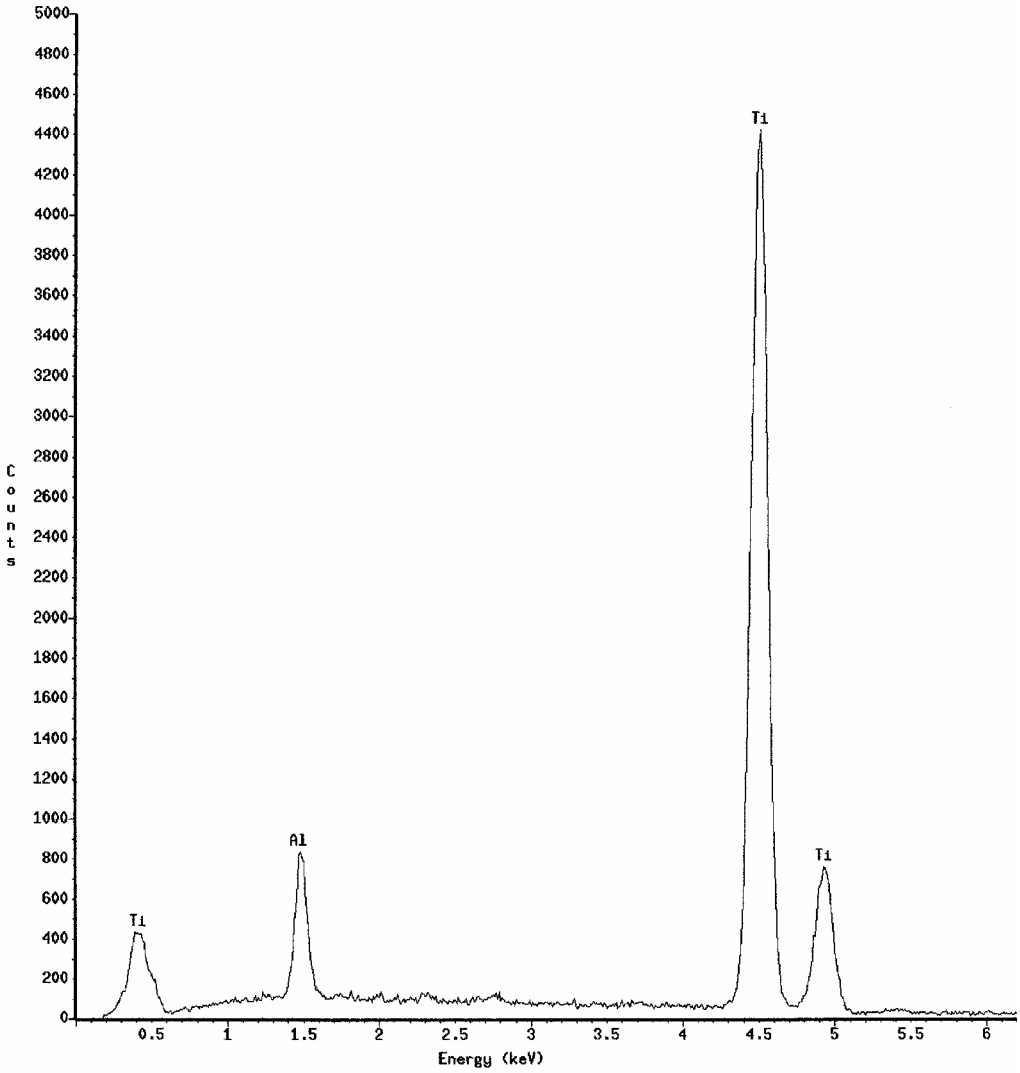

Figure 24. EDS broad scan of the fracture surface of a specimen exposed to seawater conditions after cleaning.

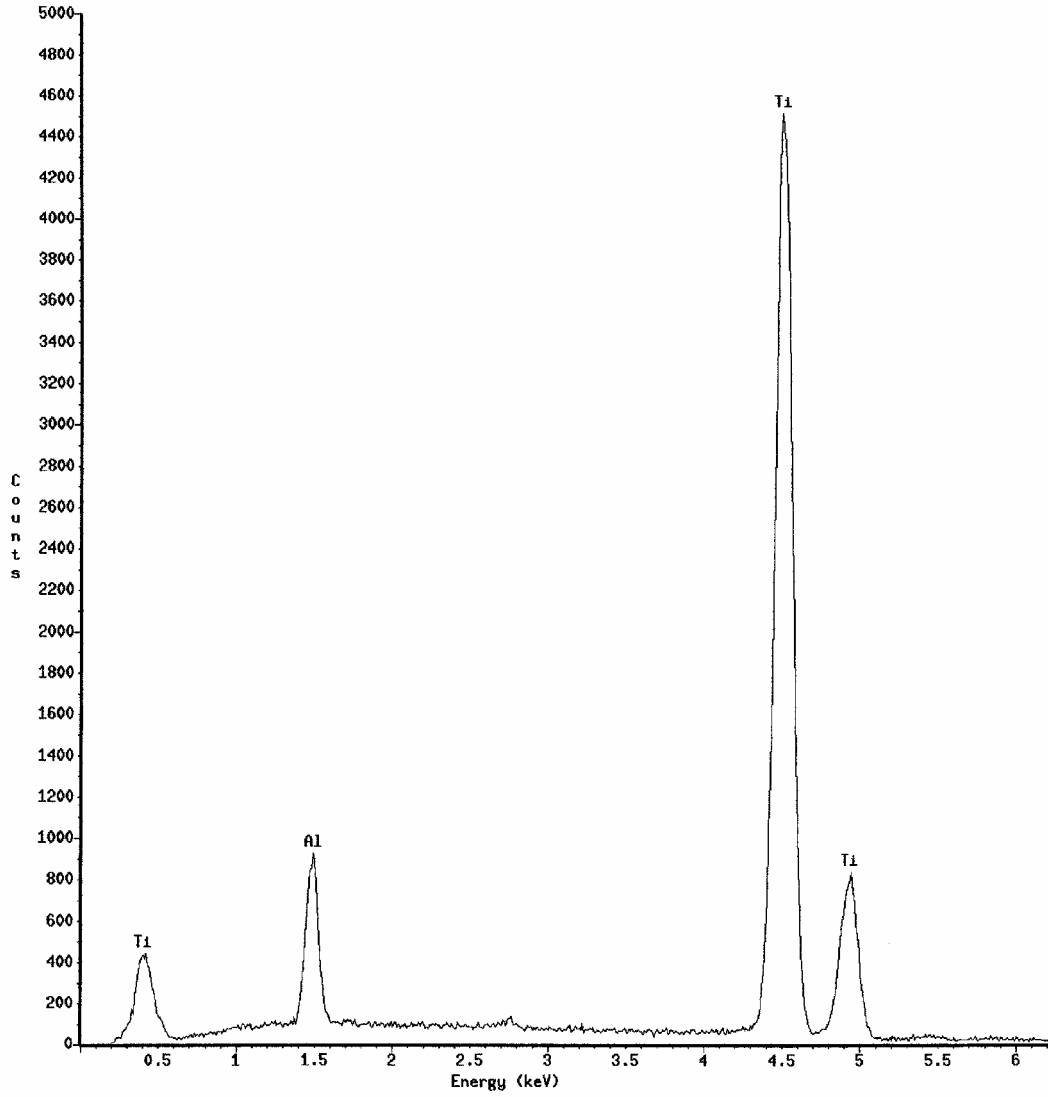

Figure 25. EDS broad scan of the fracture surface of a specimen exposed to dry conditions after cleaning.

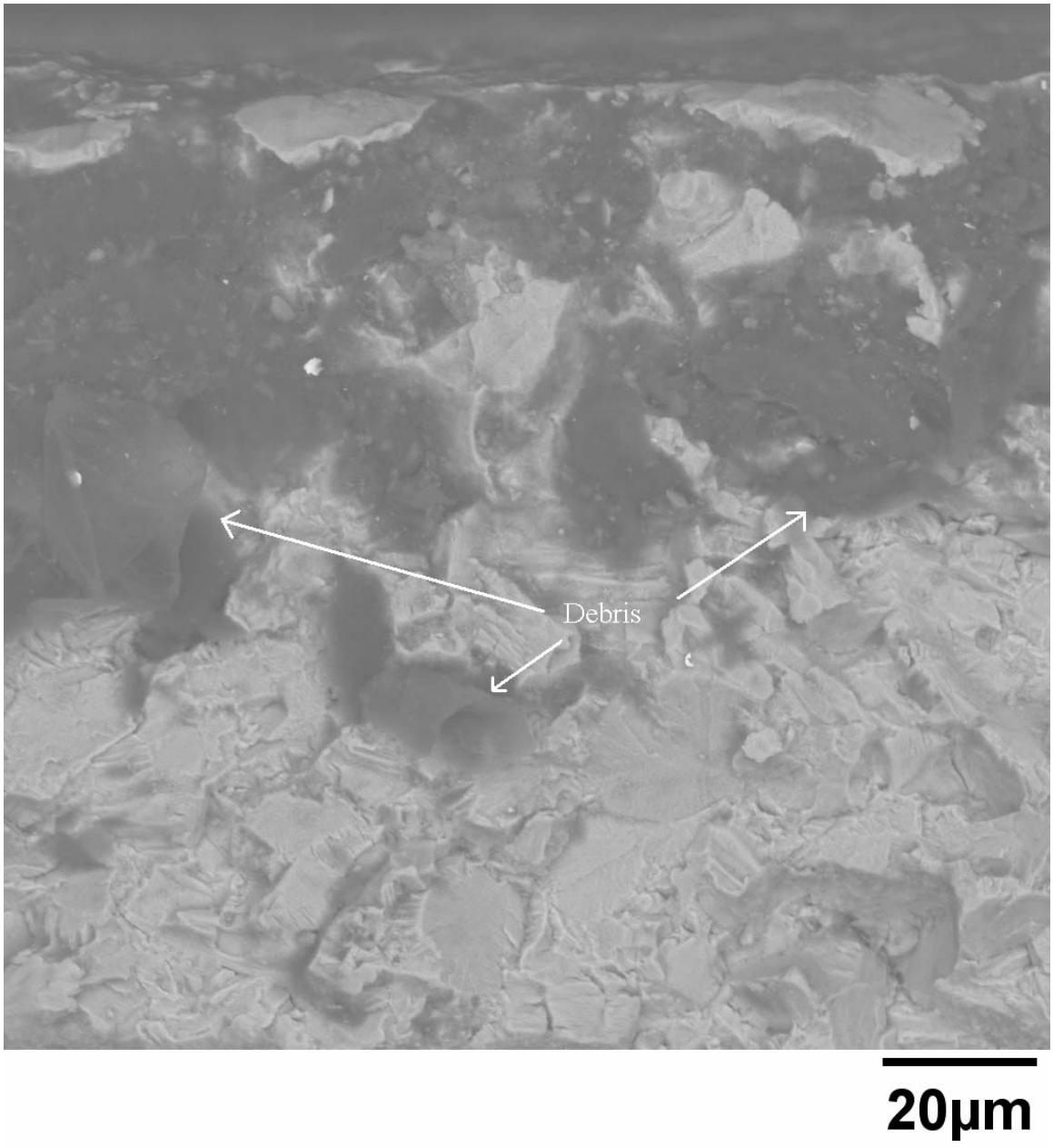

Figure 26. Magnified BSE SEM photograph of debris formed under seawater conditions after cleaning.

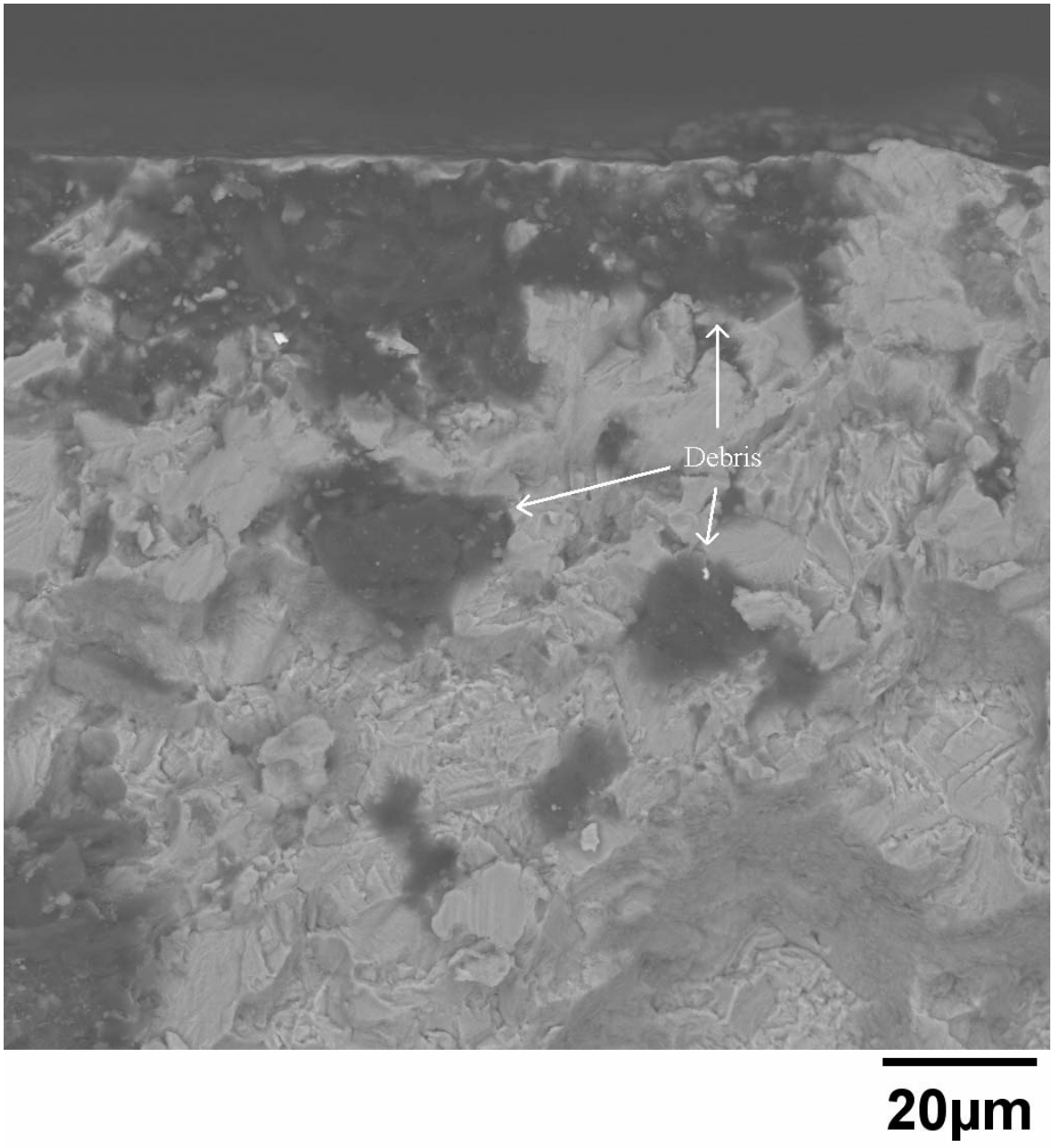

Figure 27. Magnified BSE SEM photograph of debris formed under dry conditions after cleaning.

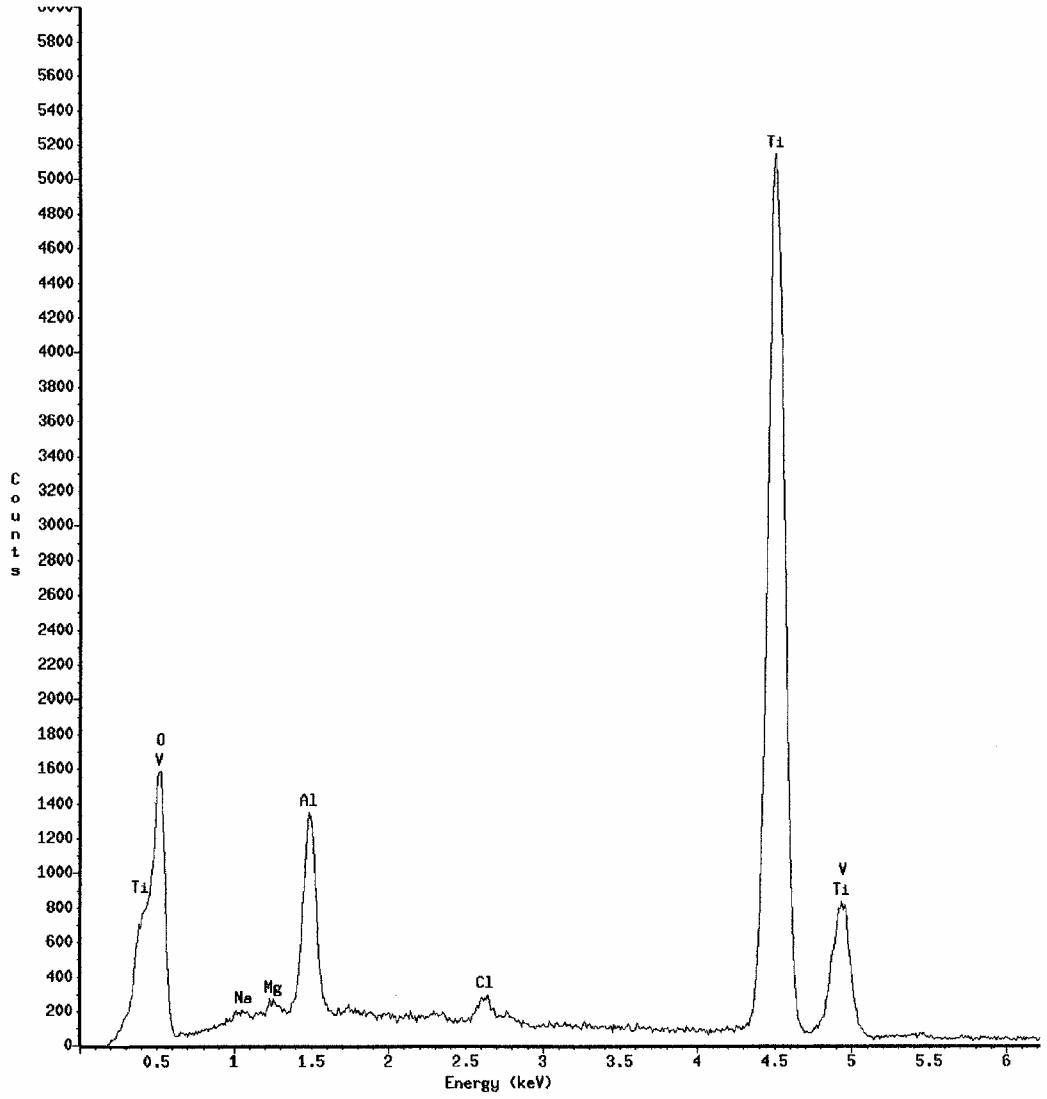

Figure 28. Magnified EDS scan of debris formed under seawater conditions after cleaning.

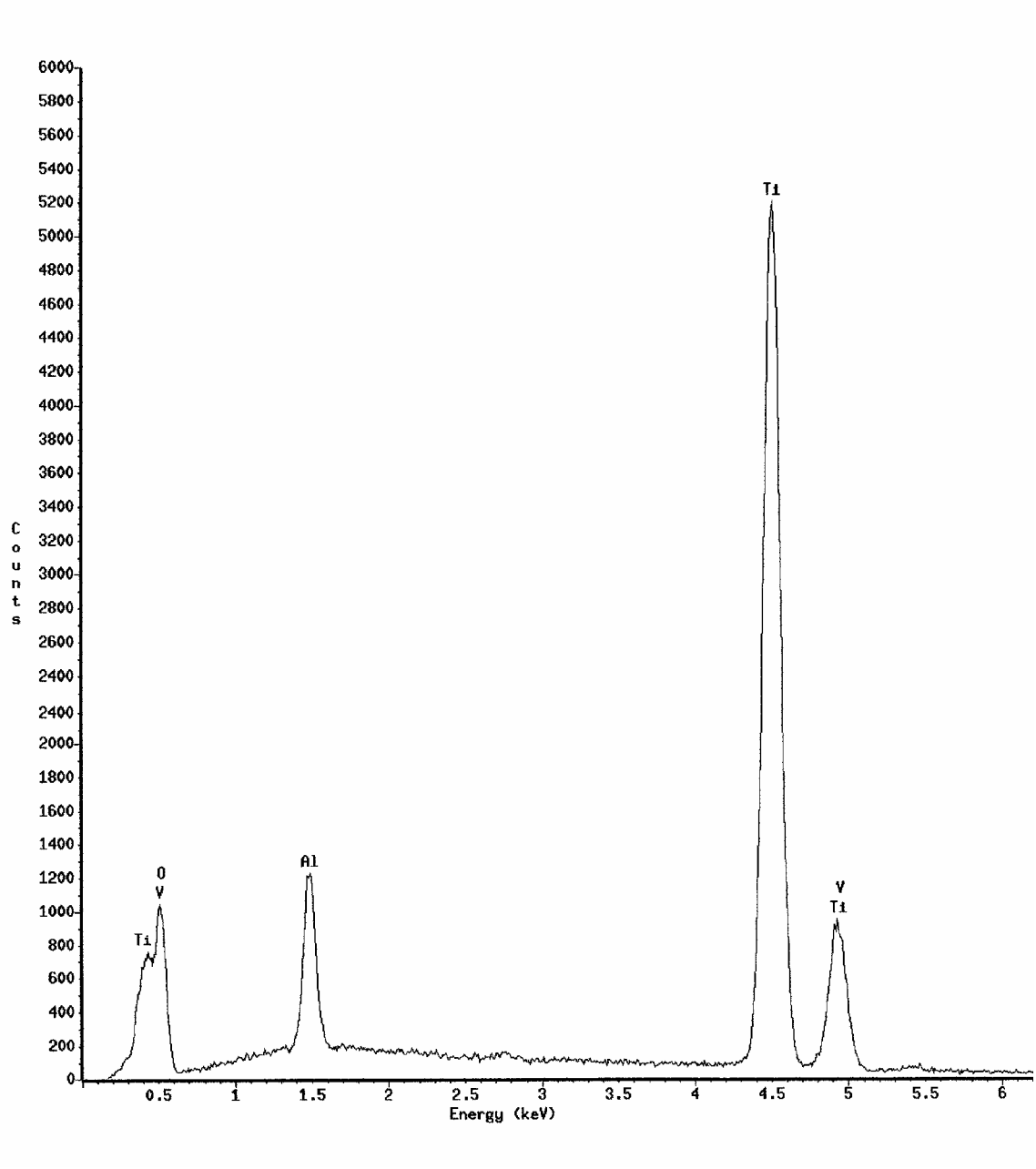

Figure 29. Magnified EDS scan of debris formed under dry conditions after cleaning.

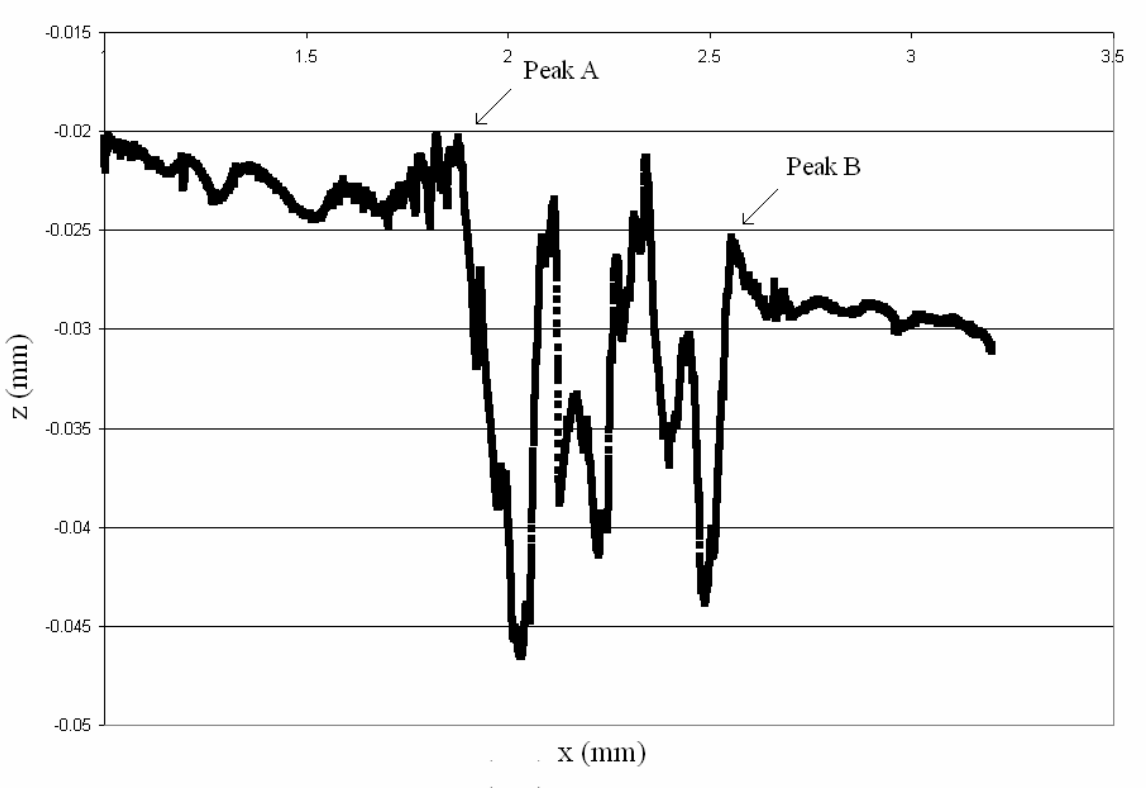

Figure 30. Scar profile with area measured from Peak A to Peak B for σ_{eff}=409 MPa under seawater conditions.

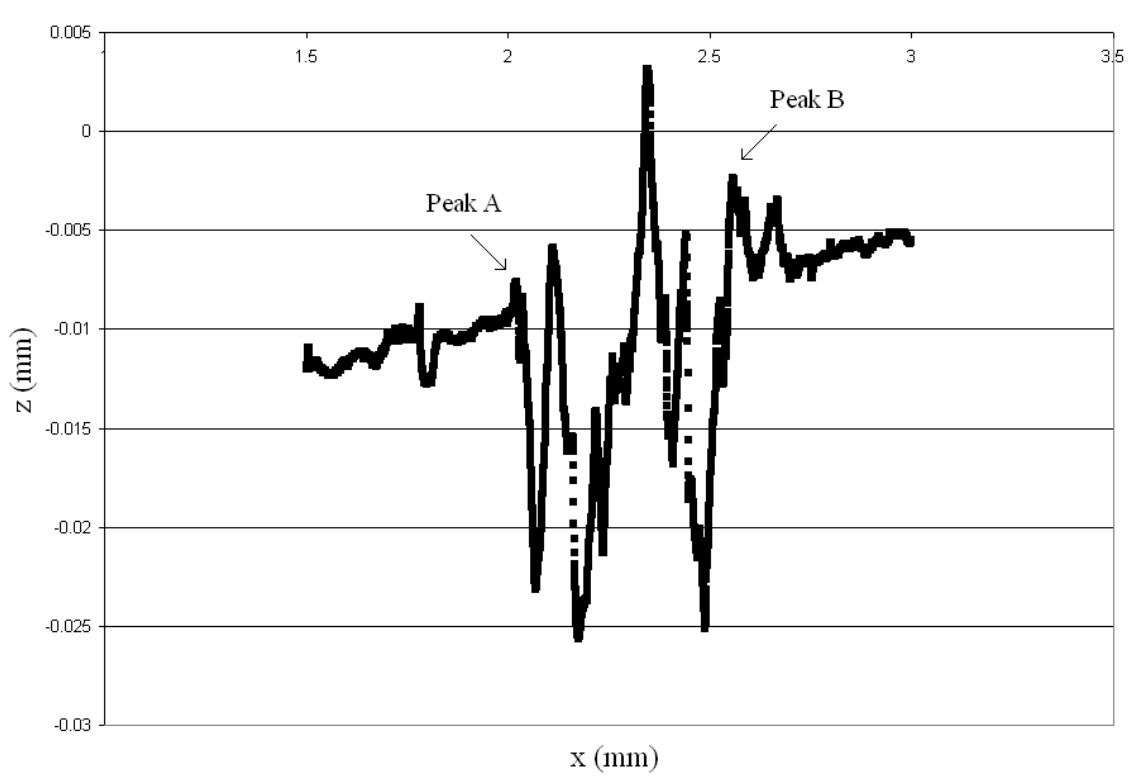

Figure 31. Scar profile with area measured from Peak A to Peak B for σ_{eff}=411 MPa under dry conditions.

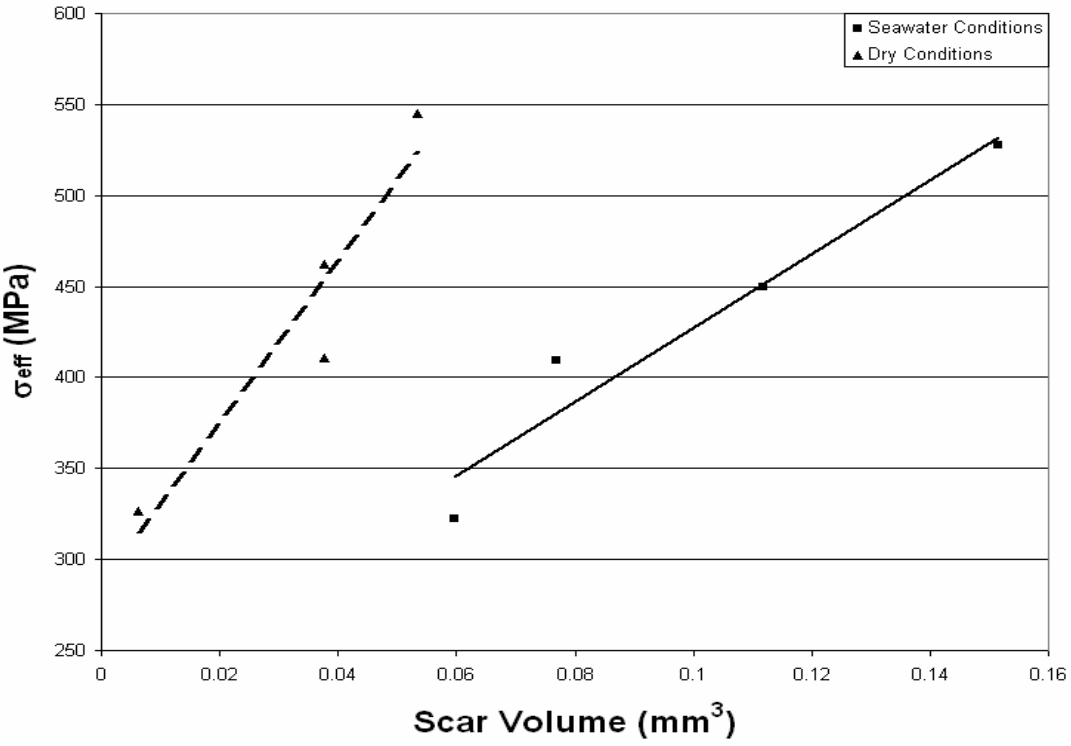

Figure 32. Effective Stress (σ_{eff}) vs. Scar Volume Estimates for seawater and dry conditions.

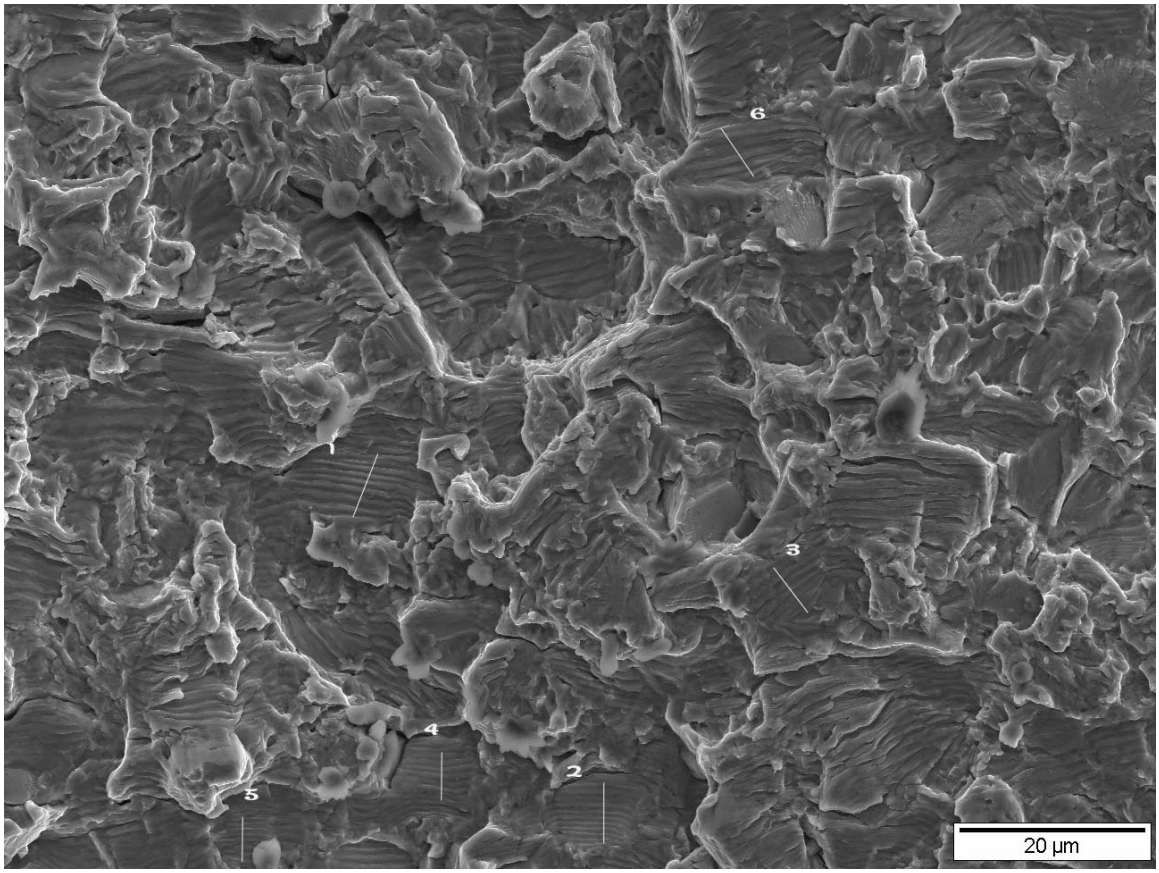

Figure 33. SEM photograph of fatigue striations in specimen exposed to seawater conditions at σ_{eff}=449.9 MPa.

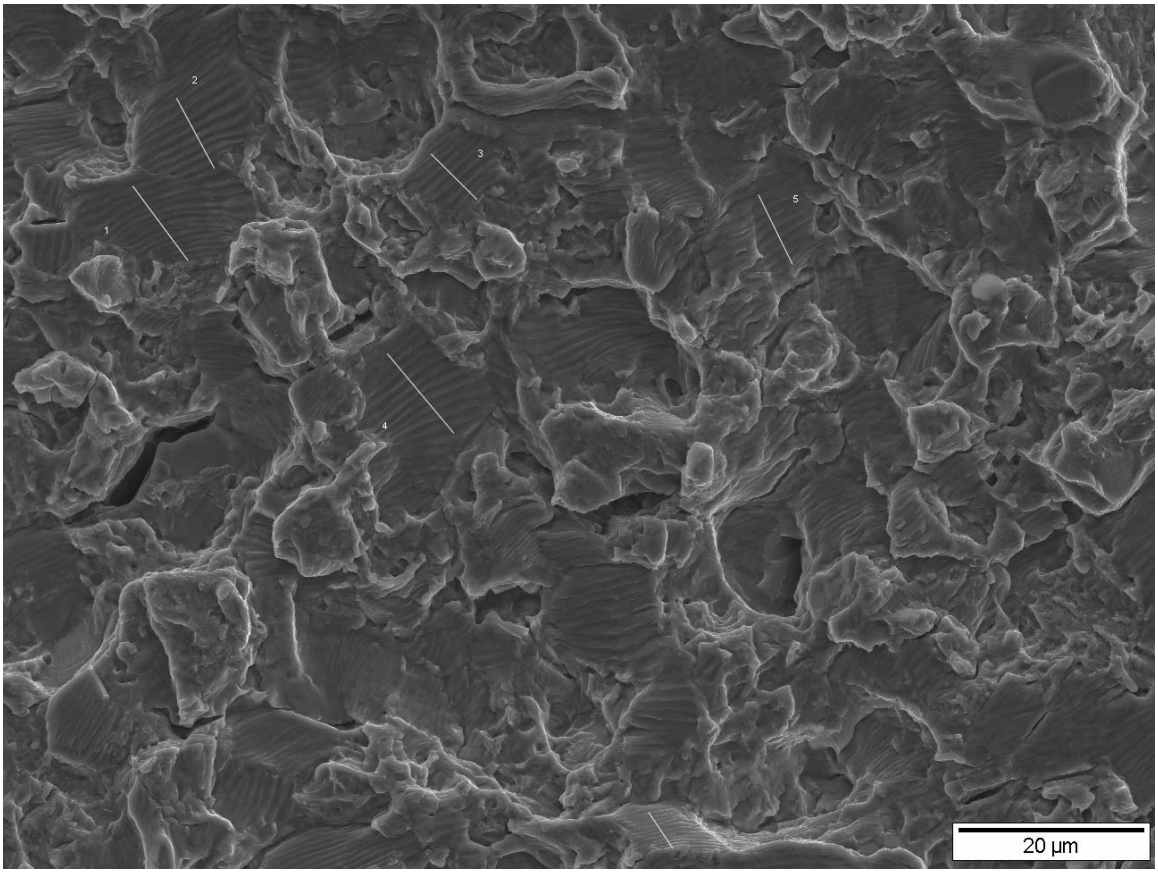

Figure 34. SEM photograph of fatigue striations in specimen exposed to dry conditions at σ_{eff}=431.4 MPa.

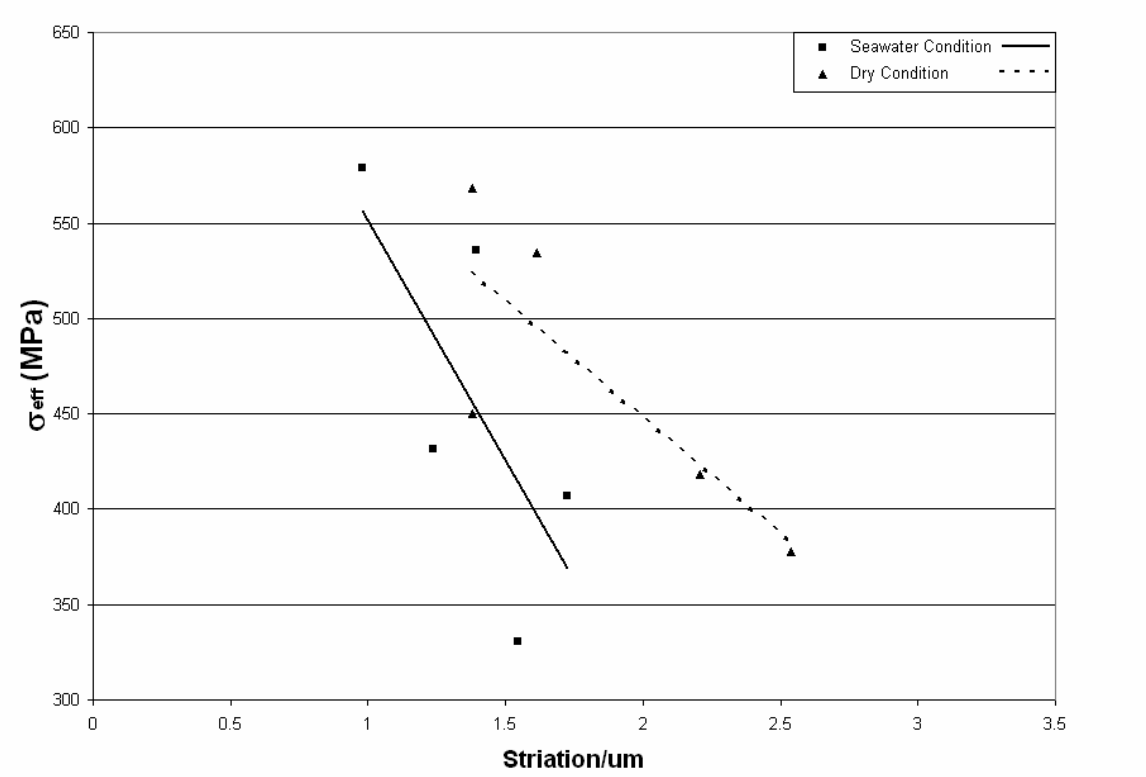

Figure 35. Effective Stress (σ_{eff}) vs. striation estimates for seawater and dry conditions.

Table 1. Experimental Data

Condition	Nf	σ_{max}	σ_{min}	$\Delta\sigma$	σ_{eff}	Q_{max}	Q_{min}	R	Q/P
	Cycles	MPa	MPa	MPa	MPa	N	N		
Dry	70500	465.5	72.5	393.0	431.4	1201.02	-983.06	0.156	0.9000
Dry	66840	546.25	23.52	522.7	535.5	1100.53	-1138.83	0.043	0.8247
Dry	106687	586.92	18.08	568.8	578.7	1219.88	-1292.3	0.031	0.9141
Dry	87846	444.15	77.95	366.2	407.2	818.74	-740.23	0.176	0.6135
Dry	1659959	383.36	107.77	275.6	330.4	759.44	-722.48	0.281	0.5691
Dry	218329	424.77	133.2	291.6	358.6	776.75	-718.7	0.314	0.5821
Seawater	23100	484.47	73.54	410.9	449.9	1183.23	-671.68	0.152	0.8867
Seawater	54280	478.04	194.89	283.2	377.7	960.82	-528	0.408	0.7200
Seawater	2221760	424.46	170.11	254.4	337.1	711.72	-622.75	0.401	0.5333
Seawater	25892	760.08	361.29	398.8	568.6	346.96	-1205.47	0.475	0.2600
Seawater	21332	687.64	295.09	392.6	534.3	1058.68	-876.3	0.429	0.7933
Seawater	44474	551.58	253.73	297.9	418.0	889.64	-705.93	0.460	0.6667
Seawater	2282108	493.77	265.65	228.1	348.8	810.46	-430.45	0.538	0.6073

Table 2. Data used to determine scar volume at 15,000 cycles.

Condition	σ_{max}	σ_{min}	$\Delta\sigma$	σ_{eff}	Q_{max}	Q_{min}	**R**	**Q/P**
	MPa	MPa	MPa	MPa	N	N		
Dry	372.7	94.1	278.6	326.9	974.34	-643.26	0.253	0.730133
Dry	435.884	53.88377	382.0	410.8	1220.725	-993.466	0.124	0.914767
Dry	501.62	83.51	418.1	462.2	1426.634	-845.598	0.166	1.069067
Dry	567.353	48.637	518.7	544.9	1617.418	-1082.52	0.086	1.212034
Seawater	486.435	77.585	408.85	449.8497	1133.638	-857.553	0.159497	0.849507
Seawater	446.93	79.375	367.555	409.2859	1092.74	790.83	0.177601	0.818859
Seawater	544.393	36.416	507.977	527.6935	1181.584	-1188.45	0.066893	0.885436
Seawater	391.5678	136.7771	254.7907	322.7204	935.3487	-464.403	0.349306	0.700916

IV. Analytical Results

Finite element analysis (FEA) and fretting fatigue parameters are discussed in this chapter. The requirement of FEA will be explained and a description of the model configuration will be provided. Finite element analysis results will be validated through a comparison with results obtained from an analytical solution. Finally, the applied (far field) stress range and the Modified Shear Stress Range parameter will be evaluated as potential fatigue parameters of Ti-6Al-4V under seawater fretting fatigue conditions.

Requirement of Finite Element Analysis

This study utilized a cylindrical fretting pad on a flat fretting specimen, a cylindrical on flat configuration, as shown in Figure 36. It has been noted that in this type of contact, the size of the contact area between the fretting pad and fretting specimen is dependent on the applied load. Hills and Nowell [49] defined an analytical solution for two parallel, infinitely long cylinders such that the radii of curvature are large compared to the contact width, a cylindrical on cylindrical configuration. The analytical solution can be modified and applied to the cylindrical on flat configuration used in this study.

The fretting pads and specimens used in this study were both machined from Ti-6Al-4V. According to the Hertz solution, when two elastically similar contacting bodies are subjected to a normal load, a pressure distribution occurs. It is assumed that the radii of both the pad and specimen are large in comparison to the contact dimensions and the contacting bodies have infinite boundaries. It has been shown that infinite boundaries can be assumed if one half of the specimen thickness, b, is ten times the contact half

width, a, or b/a>10. However, if b/a<10, then a discrepancy will exist between the numerical and analytical solutions as confirmed by Fellows et al. [50], and finite element analysis is required to validate the experimental results. Hills and Nowell derived equations to solve for the contact half-width [49]. The contact half-width can be determined from:

$$a^2 = \frac{2P\mathrm{A}`}{\pi k} \tag{5}$$

where a is the contact half-width, and P is the normal load distributed over the width of the specimen. The composite compliance, A`, for two bodies of the same material is given as:

$$\mathrm{A}` = \frac{4(1-\upsilon^2)}{E} \tag{6}$$

where ν is poisson's ratio (0.3 for Ti-6Al-4V) and E is the Modulus of Elasticity (126 GPa for Ti-6Al-4V). The radius of curvature, k, is found from:

$$k = \frac{1}{R_1} + \frac{1}{R_2} \tag{7}$$

where R_1 is the radius of the fretting pad and R_2 is the radius of the fretting specimen. In this study, the fretting pad had a constant radius while the fretting specimen was assumed to be flat (i.e. to have infinite boundaries in the cross sectional plane). Using the above equations, the contact half-width, a, was calculated to be 0.4431 mm while the specimen half thickness, b, was 1.905 mm. In this study, b/a was 4.3, thereby violating the infinite boundary assumption and necessitating the use of finite element analysis.

Finite Element Model of Fretting Fatigue Configuration

The finite element analysis used in this study was similar to the one utilized by Lykins [42] and Yuksel [40]. A commercially available finite element code, ABAQUS [51], was used to model the experimental conditions. The finite element mesh was developed using four noded, plane strain quadrilateral elements and incorporated a master-slave contact algorithm on the contacting surface between the fretting pad and specimen. The finite element model is shown in Figure 37. The model consisted of three bodies: the fretting specimen, the fretting pad, and a rigid body constraint which constrained the fretting pad in the x and y directions. A multipoint constraint was applied to the top of the fretting pad to prevent rotation as a result of the applied loads.

Loads were applied to the finite element model in three steps. During the first step, the normal load, P, was applied to the top of the fretting pad. The second step applied the minimum experimental load, Q_{min}, and the minimum experimental axial stress, $\sigma_{axial,min}$, to replicate the experimental minimum cyclic loading. The maximum experimental tangential load, Q_{max}, and the maximum experimental axial stress, $\sigma_{axial,max}$, were applied during the third step to duplicate the experimental maximum cyclic loading. The tangential loads were applied to the left side of the fretting pad while the axial loads were applied to the right side of the fretting specimen. The normal load was held constant at 1334 N while the tangential load, axial stress, and coefficient of friction varied during each test. The tangential load and axial stress values were direct measurements while the coefficient of friction values were based on the Q/P ratio as mentioned in chapter three. The experimental data used for FEA is shown in Table 1. Finite element analysis computations were performed on one complete load cycle since

Lykins [42] found that multiple cycles do not change the model output. Finite element analysis was conducted for each of the experimental conditions found in this study.

Finite Element Analysis Validation via Comparison with an Analytical Solution

The data collected from the finite element analysis was validated by comparing it to an analytical solution, which is available as a Fortran program developed by Chan and Lee, known as the Ruiz solution [52]. The Ruiz solution evaluates the combined effects of the surface tangential stress, σ_τ, the surface shear stress, τ, and the slip at the interface, δ. Figure 38 shows a comparison of stress in the x-direction along the contact surface for finite element analysis results and the Ruiz solution results. There is good comparison between the predicted results of the two analytical solutions. The FEA provided a maximum stress of 864.8 MPa compared to the Ruiz solution of 891.1 MPa, a variation of 3%. Hertzian peak pressure was determined to be 303.6 MPa from FEA and 302.1 MPa from Ruiz, a difference of 0.5%. Half contact width varied by only 0.4%, a_{FEA} =0.441mm versus a_{RUIZ} =0.443mm. Based on these results, finite element analysis models used in this study can be considered accurate, and the axial, transverse, and shear stress distributions along the contact surface will be used to evaluate the Modified Shear Stress Range fatigue parameter.

Fatigue Parameters

The applied (far field) stress range was evaluated to determine its potential as a fretting fatigue parameter in the environmental studies of Ti-6Al-4V. Figure 10 shows that seawater fretting fatigue conditions appeared to be more detrimental on the fretting fatigue life of Ti-6Al-4V than dry fretting conditions at the higher stress levels.

However, seawater fretting fatigue conditions appeared to improve the fretting fatigue life at the lower stress levels. Under high cycle fatigue conditions, the data from the two conditions may lie within a narrow scatter range. This suggests that dry fretting fatigue life data can be used to provide a conservative estimate of seawater fretting fatigue life under high cycle regimes. However, this is a very simplified approach in determining fatigue life as it does not account for the stresses and stress gradients encountered in the fretting contact region nor does it consider the multiaxial stress state in the contact region. For the latter reason, a multiaxial parameter, the Modified Shear Stress Range (MSSR), will be evaluated.

Of the many multiaxial parameters available, Mall et al. [9] have shown the MSSR to be effective at predicting the fretting fatigue life of Ti-6Al-4V from plain fatigue life data. The MSSR incorporates a combination of shear and normal stresses that are encountered in multiaxial fatigue loading and emphasizes the high stress concentration that occurs at the trailing edge of contact. Figures 39 and 40 show that the fretting fatigue crack initiates near the trailing edge of contact in both the seawater and dry conditions. In this study, the MSSR was evaluated to determine if it could predict seawater fretting fatigue life from dry fretting fatigue life data.

Output data collected from the FEA was inputted into an in-house Fortran program to calculate the MSSR parameter for both dry and seawater fretting fatigue conditions. The MSSR was calculated using the surface stresses determined from FEA. Once calculated, the MSSR was plotted against the number of cycles to failure, N_f, as shown in Figure 41. This figure suggests that seawater reduces the fretting fatigue life at higher stresses and improves it at lower stresses. In order for the MSSR to be used as a fretting fatigue

parameter in the environmental studies of Ti-6Al-4V, an equivalence must be established between the seawater and dry conditions. Under the low cycle fatigue regime, the data from the two conditions did not appear to collapse into a narrow scatter band thus indicating that an equivalence was not established. However, in high cycle fatigue conditions, the data did appear to lie in a narrow scatter band thus suggesting that the MSSR could be used to predict sweater fretting fatigue life from dry fretting fatigue life data. Table 3 contains data from both fatigue parameters.

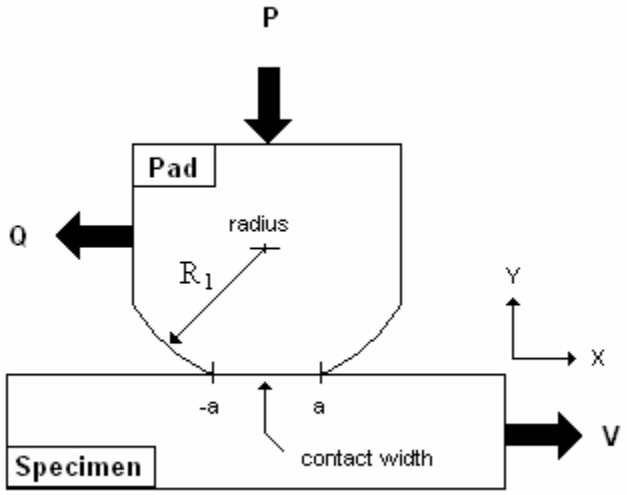

Figure 36. Cylindrical on flat configuration.

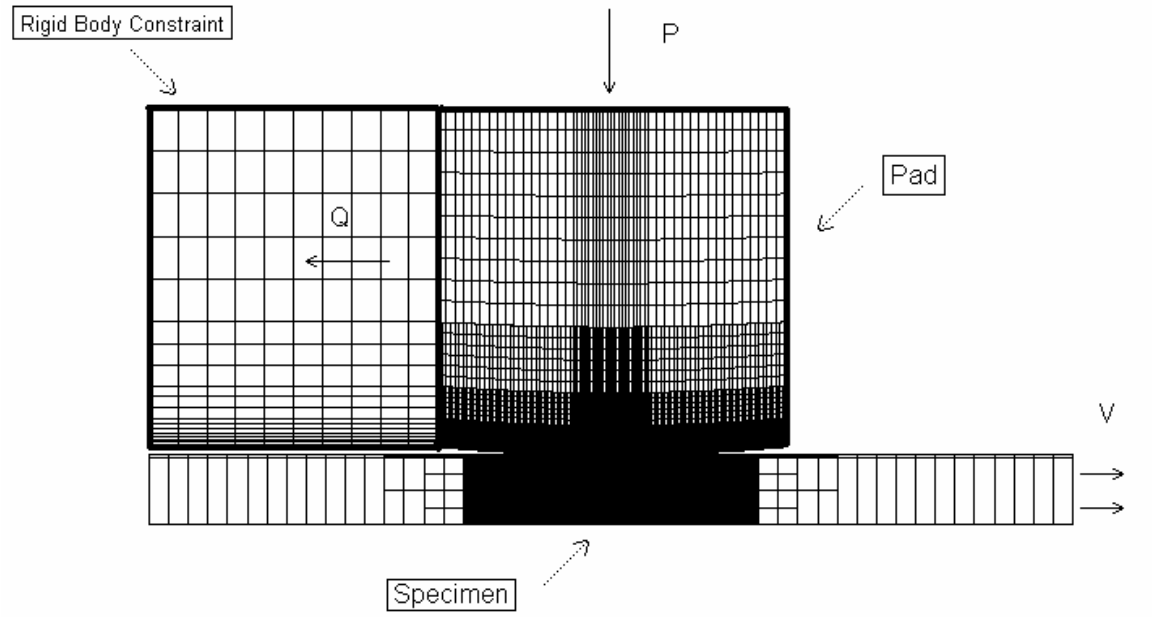

Figure 37. FEA mesh of specimen, pad, and rigid body constraint.

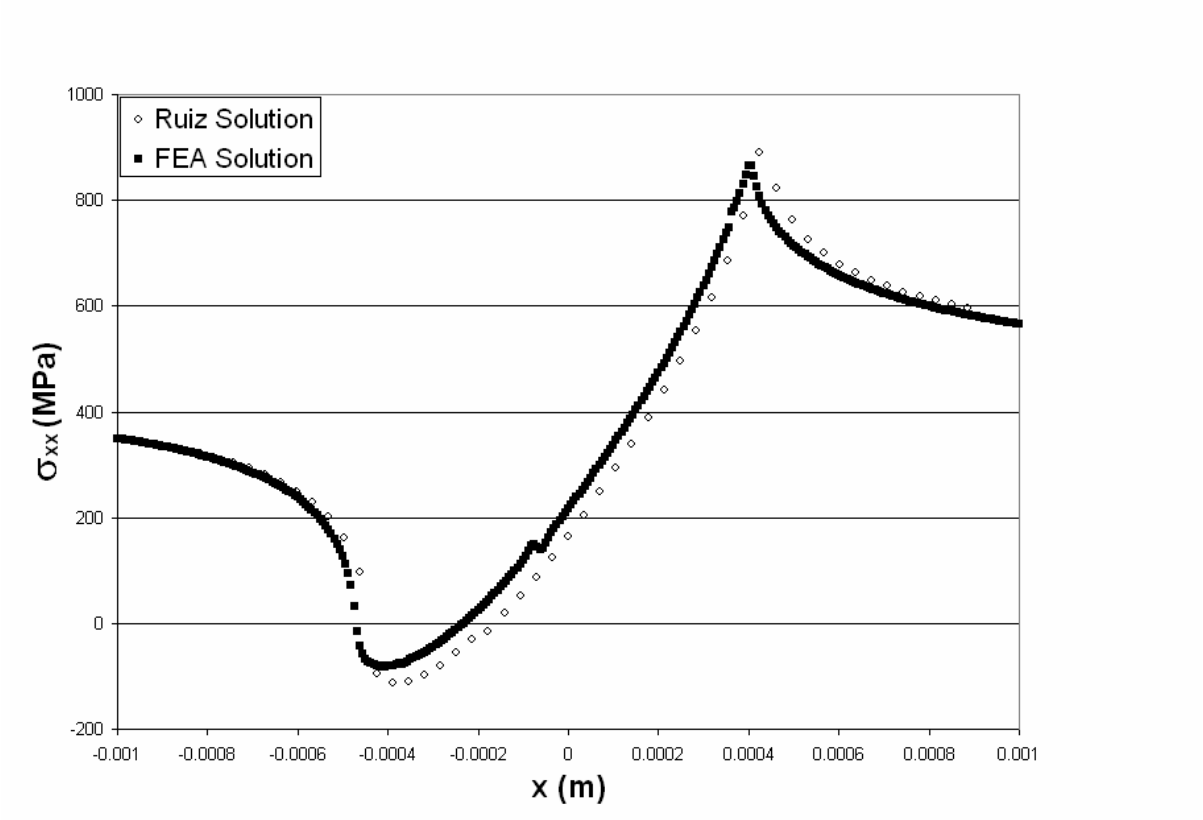

Figure 38. Normal stress in the x direction (σ_{xx}) along x-axis at the contact surface.

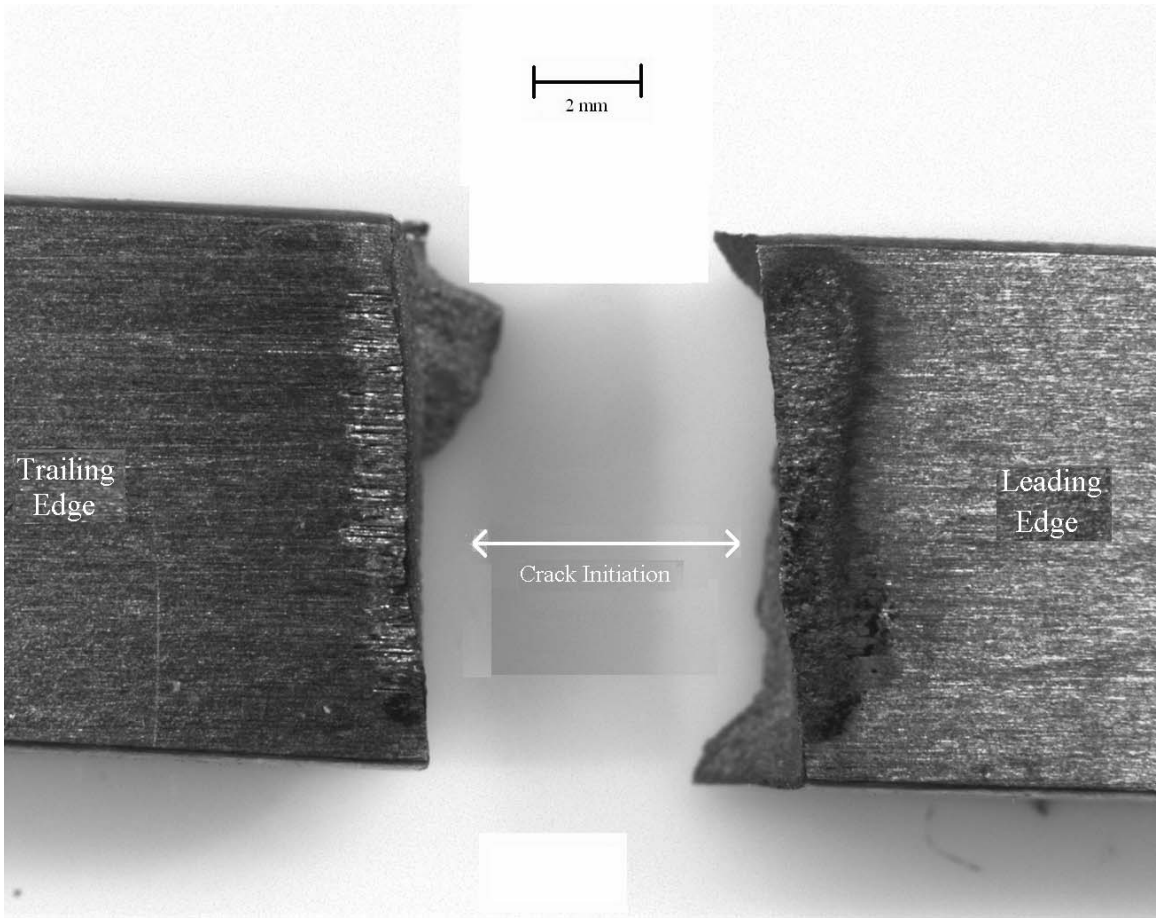

Figure 39. Fretting fatigue crack initiation at trailing edge of contact in specimen exposed to seawater conditions at σ_{eff} = 449.9 MPa.

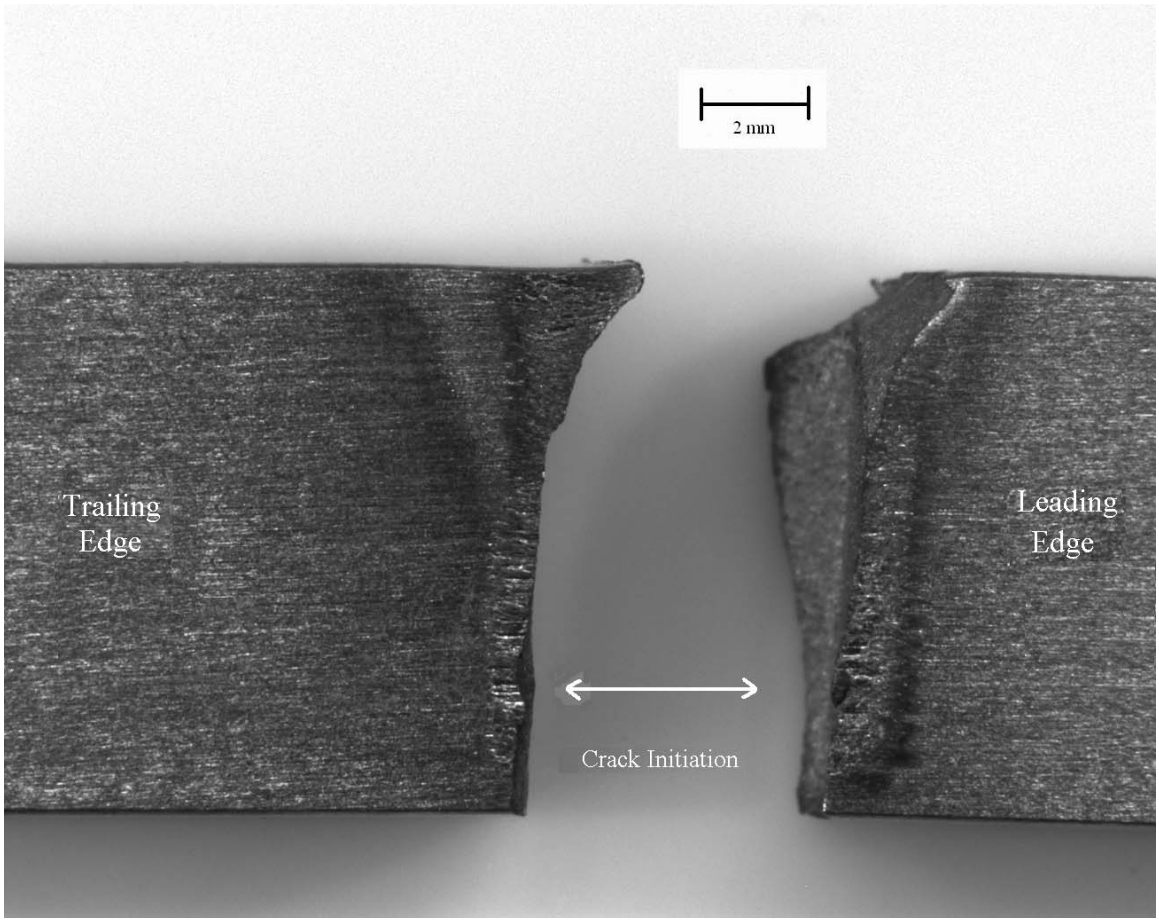

Figure 40. Fretting fatigue crack initiation at trailing edge of contact in specimen exposed to dry conditions at σ_{eff} = 431.4 MPa.

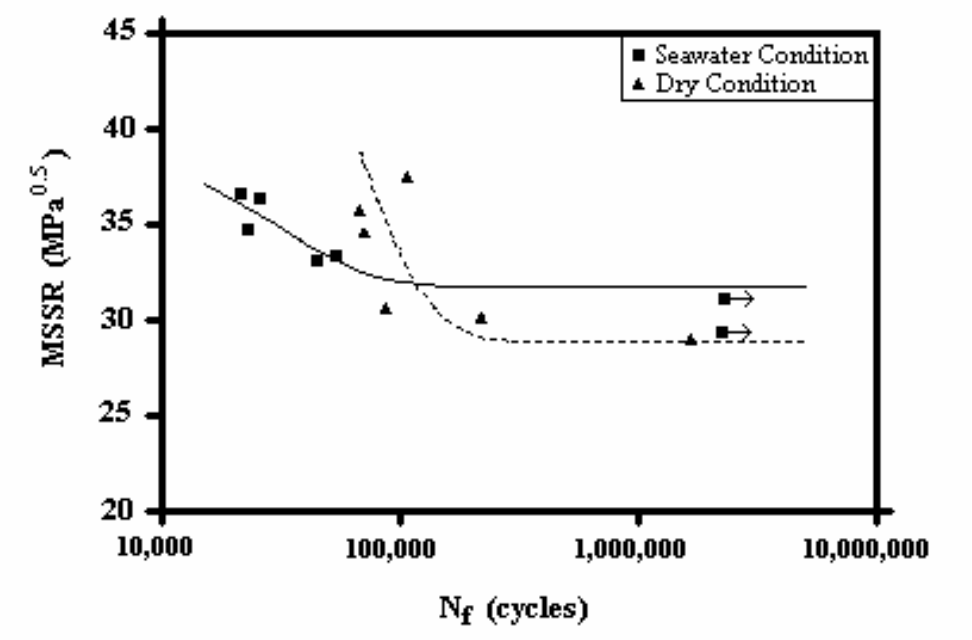

Figure 41. MSSR vs. Number of Cycles to Failure (N_f) for seawater and dry conditions. An arrow indicates the test was discontinued before fracture.

Table 3. Analytical Data.

Condition	Nf	σ_{eff}	MSSR
	Cycles	MPa	MPa^.5
Dry	70500	431.4	34.58
Dry	66840	535.5	35.7
Dry	106687	578.7	37.45
Dry	87846	407.2	30.59
Dry	1659959	330.4	28.9
Dry	218329	358.6	30.11
Seawater	23100	449.9	34.68
Seawater	54280	377.7	33.29
Seawater	2221760	337.1	29.3
Seawater	25892	568.6	36.39
Seawater	21332	534.3	36.64
Seawater	44474	418.0	33.05
Seawater	2282108	348.8	31.09

V. CONCLUSIONS

This chapter provides a summary of the work performed in this thesis. The experimental results will be discussed, and suggestions will be made for future work.

Experimental Summary

The purpose of this thesis was to investigate the fretting fatigue behavior of Ti-6Al-4V in a corrosive environment. Seawater was chosen as the test environment due to its highly corrosive nature and frequent exposure to aircraft. A simplified geometry and loading configuration was utilized to represent the complex geometry and loading conditions encountered in aircraft engines. Lateral springs in the fretting fixture applied a constant normal load while holding the fretting pads against the fretting specimen. An axial stress, σ_{axial}, was imposed on the fretting specimen by the servo-hydraulic test machine. This stress produced a tangential load, Q, which was dependent on the lateral spring stiffness and coefficient of friction at the contact surface. The normal load (1334 N) and the pad radius (50.8 mm) were held constant throughout each test. Both low and high cycle fatigue regimes were evaluated by varying the applied axial loads. Six tests were conducted under laboratory air (dry) conditions, and seven tests were performed under seawater conditions. The seawater condition consisted of an open air system which applied synthetic seawater onto each pad/specimen contact surface for two seconds every one minute. This resulted in an application rate of approximately five ml per minute on each side of the specimen.

Dry and seawater fretting fatigue life data of Ti-6Al-4V was collected and compared. Q/P ratio, fracture surface debris, scar volume, and fatigue striations were also evaluated. Finite Element Analysis (FEA) was used to model the experimental configuration and analyze the experimental data. The results of the FEA were then used to evaluate a critical plane based fatigue parameter, Modified Shear Stress Range (MSSR). The applied (far field) stress range was also evaluated to determine its potential as a fretting fatigue parameter in the environmental studies of Ti-6Al-4V.

Discussion of Experimental Results

Fretting Fatigue Life Data.

Dry and seawater fretting fatigue life data were collected and expressed as a fatigue life diagram, i.e. effective stress amplitude, σ_{eff}, versus the number of cycles to failure, N_f. Under low cycle fatigue, the fretting fatigue life appeared to be reduced in the seawater environment. However, the fretting fatigue life appeared to increase in the seawater environment under high cycle fatigue. This is in agreement with a previous study [15]. Several factors may have contributed to this behavior. First, microcrack formation may have played a role in these findings. More microcracks were formed on the contact surface under seawater conditions at all stress levels. It is hypothesized that an increase in microcrack formation correlates with an increase in debris production which in turn equates to larger scar volumes. During crack initiation and short crack growth, the increased number of microcracks could provide a shielding effect thereby slowing the overall crack growth rate. This could account for the improved fretting fatigue life under high cycle fatigue conditions as it has been suggested that high cycle

fatigue is dominated by crack initiation [15]. However, this shielding effect would be negated under low cycle fatigue conditions where crack propagation has been proposed as dictating the fretting fatigue process. Second, the environment may have assisted the crack propagation rate under low cycle fatigue conditions thus resulting in a diminished fretting fatigue life. Some environmental embrittlement mechanisms, such as strain induced hydrides, are stress dependent. Under low cycle fatigue, these embrittlement mechanisms may have contributed to the observed reduction in life. However, the stresses used under high cycle fatigue may not have been sufficient to foster these embrittlement mechanisms. Therefore, the environment may have a significant effect on crack growth rate in low cycle fatigue conditions but not in high cycle fatigue conditions. This could account for the improved fretting fatigue life observed at the lower stresses.

Q/P Ratio.

As shown in Figure 12, the Q/P ratio in both the dry and seawater conditions increased with an increasing applied stress. It was anticipated that the Q/P ratio would be lower in the seawater samples than in the dry samples as previous studies have found seawater to act as a lubricant thereby lowering the coefficient of friction [14,28]. In this study, the Q/P ratio was slightly lower in seawater conditions than in dry conditions; however, the difference between the two conditions was negligible. There are three possible explanations for this result. First, since each fretting fatigue test was started under the dry condition, the samples were not exposed to seawater until approximately 2,000-3,000 cycles. Second, only a small amount of seawater was added during the experiments as it was noted that adding a large amount of seawater would occasionally result in a gross slip scenario. Finally, previous studies may have utilized a different test

configuration where the sample specimens were completely submerged in seawater throughout the duration of the tests.

Fracture Surface Debris.

Fracture surface debris was identified under the Scanning Electron Microscope (SEM) and analyzed using Energy Dispersive Spectroscopy (EDS). As anticipated, the debris on the fracture surface of the samples exposed to seawater contained more elements than that of debris exposed to the dry condition. Prior to specimen cleaning, the debris found on dry samples was mostly oxide in nature while that of the seawater samples contained large amounts of both oxides and seawater contaminants. Debris on dry samples after specimen cleaning was similar to that found before cleaning. However, after cleaning the seawater samples, the debris appeared to mostly be oxides with a small amount of seawater contaminants noted. The presence of large amounts of oxide debris in both the dry and seawater post-cleaning specimens may be due to the oxides being less soluble than the seawater debris in the cleaning solution. Additionally, the oxide debris may have been embedded in the fracture surface while the seawater debris was more superficial. It is important to note that after cleaning, the fracture surfaces appeared very similar for both conditions. If the environmental influence on the fracture surface is not easily detected, investigators who evaluate the appearance of an aircraft component after failure may conclude that dry fretting fatigue is the sole cause of failure thereby discounting the environmental influence.

Scar Volume.

It has been noted that an increase in surface debris correlates to an increase in scar volume [35]. In order to evaluate the mechanical and chemical effects of fretting in both

dry and seawater conditions, eight tests, four under dry conditions and four under wet conditions, were ran at various effective stresses, σ_{eff}, for 15,000 cycles. This allowed a scar to form without fracturing the specimen. Scar volume was then measured using an Ultrascan Profilameter. As shown in Figure 32, the data shows that the scar volume is larger at all stress levels in the samples exposed to seawater than those exposed to dry conditions. The larger scar volume in seawater samples supports the theory that the seawater environment creates more microcracks and therefore more debris on the fretting surface.

Fatigue Striations.

Striations on the fracture surface were measured in order to compare crack growth rates in the dry and seawater environments. The striations were evaluated under a Scanning Electron Microscope (SEM) at a distance of two millimeters away from the contact surface and perpendicular to the crack initiation site. Figure 35 suggests that the seawater environment promotes an increase in crack propagation rate at this distance. However, further studies are needed to verify this theory.

Finite Element Analysis.

Due to the nature of the fretting fatigue configuration used in this study, Finite Element Analysis (FEA) was utilized to verify the experimental results. The FEA model was compared to the Ruiz analytical method in order to validate the FEA results. There was good agreement between the two solutions. The maximum stress varied by 3%, the Hertzian peak pressure by 0.5%, and the half contact width by 0.4%. Results from the FEA were thus considered accurate and were used to evaluate the Modified Shear Stress Range (MSSR) fatigue parameter.

Fatigue Parameters.

The applied (far field) stress range was evaluated to determine its potential as a fretting fatigue parameter in the environmental studies of Ti-6Al-4V. Figure 10 shows both the seawater and dry fretting fatigue data expressed as the effective stress amplitude, σ_{eff}, versus the number of cycles to failure, N_f. It appears that, under the high cycle fatigue regime, the data falls within a narrow scatter range. This suggests that the applied (far field) stress range can be used to conservatively predict seawater fretting fatigue life from dry fretting fatigue life data. However, it is important to remember that this approach does not take into consideration the contact stresses in the contact region nor does it account for the stress state in the contact region.

The MSSR was also evaluated as a potential fretting fatigue parameter in the environmental studies of Ti-6Al-4V as it incorporates the stress/strain state of the localized contact region as well as the effects of multiaxial loading. The MSSR calculations were plotted against the number of cycles to failure, N_f, for both the dry and seawater environments as shown in Figure 41. The data from the two conditions do not appear to collapse into a narrow scatter range under low cycle fatigue conditions. However, the data do appear to lie in a small scatter band under high cycle fatigue conditions. This suggests that the MSSR can be used to conservatively predict seawater fretting fatigue life from dry fretting fatigue life data under high cycle fatigue conditions. However, more tests should be conducted under both the high cycle fatigue regime and the transitional phase between low and high cycle fatigue to verify this finding.

Future Work

In this study, samples were tested under dry and seawater conditions only. Future studies should also compare the effects of distilled water and humidity on the fretting fatigue behavior of Ti-6Al-4V. This would allow a comparison of the hydrogen found in distilled water and humidity with the combined effects of hydrogen and other elements found in seawater to determine which, if any, elements contribute to the reduced fretting fatigue life found in low cycle fatigue. Temperature should be evaluated to understand its effect on the mechanical and chemical mechanisms of fretting fatigue under seawater conditions. The various microstructures of Ti-6Al-4V should be evaluated under fretting fatigue seawater conditions to determine if the microstructures respond differently to the seawater environment. Fretting fatigue studies should also be performed on Ti-6Al-4V under seawater conditions with the electrochemical effects of seawater reduced through the process of cathodic protection. This would determine whether electrochemical effects are involved in reducing the fretting fatigue life of Ti-6Al-4V in low cycle fatigue regimes. Additional studies could investigate the effects of surface treatments, such as shot-peening, on the fretting fatigue behavior of Ti-6Al-4V under seawater conditions since surface treatments have been shown to improve fretting fatigue life [40]. Since this study utilized only one pad size and a constant normal load, future tests should be conducted with various pad geometries and normal loads to determine if the fretting fatigue crack initiation mechanism is altered by the various combinations of shear and normal stresses at the contact surface. Plain fatigue tests under seawater conditions should also be performed to develop a baseline for further comparison. Tests should be conducted at higher frequencies to simulate operational environments. Finally, future

work should examine the initiation, location, and orientation of fretting fatigue cracks in seawater conditions to determine if the MSSR fatigue parameter is able to predict these results.

Appendix A. Back Scatter Emission Scanning Electron Microscope (BSE SEM) Photographs of Fracture Surfaces of Specimens Exposed to Seawater Conditions.

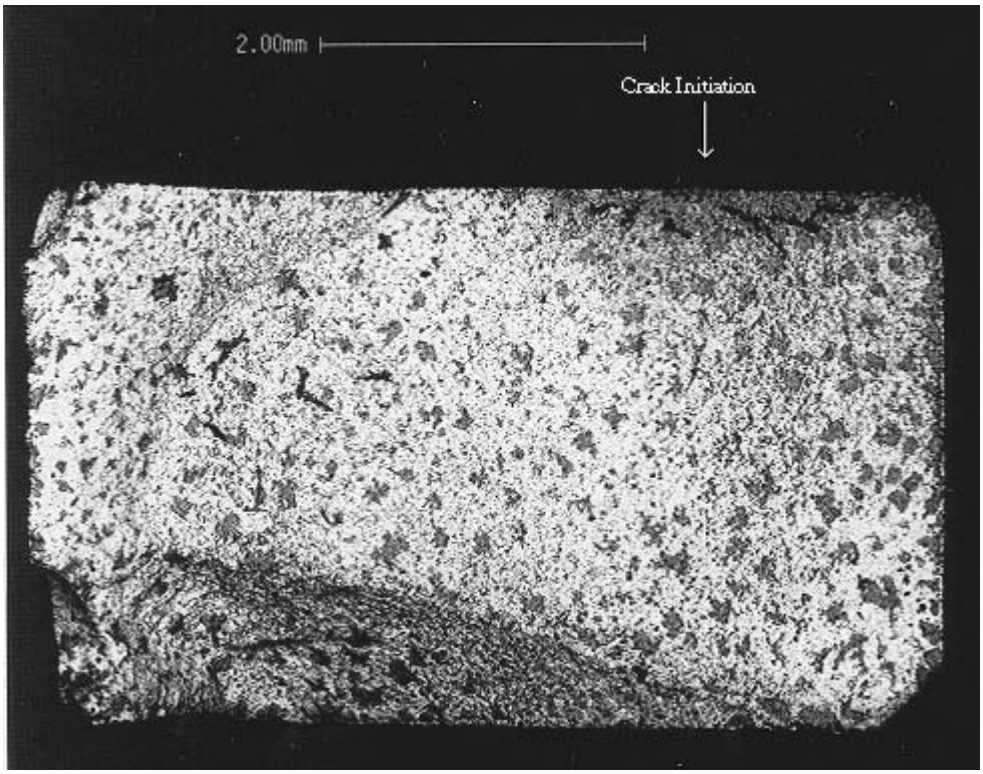

BSE SEM of fracture surface exposed to seawater conditions at σ_{eff}=377 MPa before cleaning.

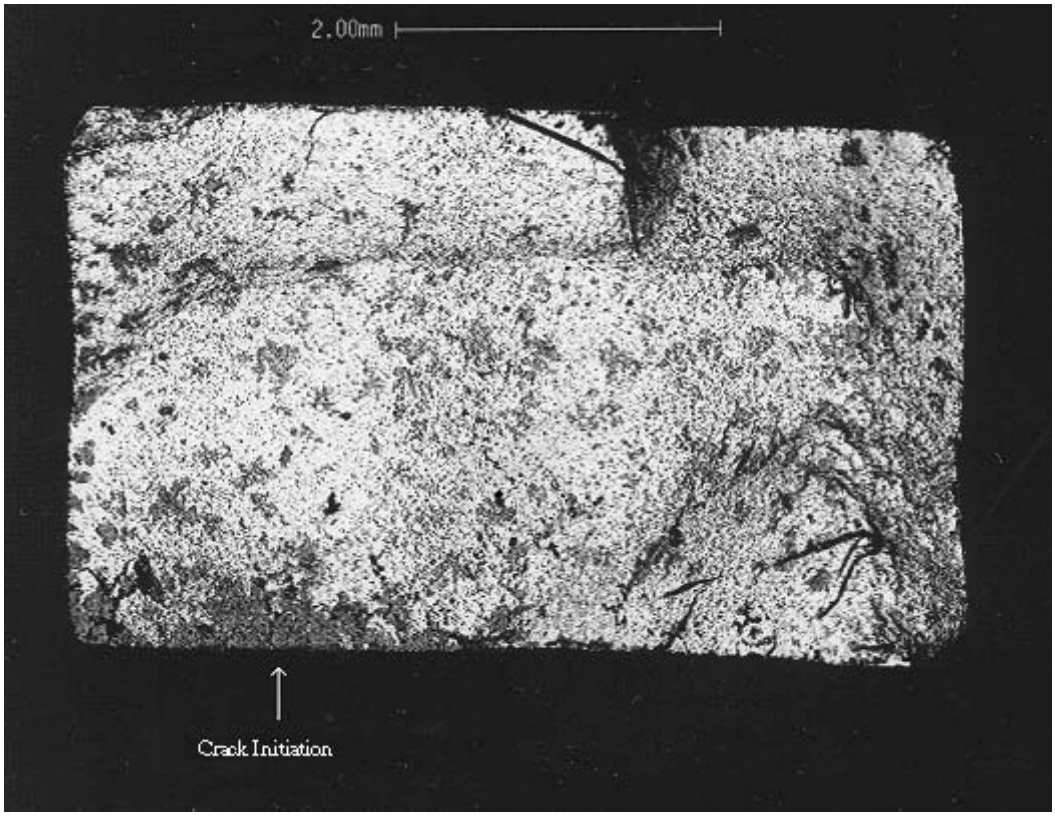

BSE SEM of fracture surface exposed to seawater conditions at σ_{eff}=570 MPa before cleaning.

Appendix B. Scanning Electron Microscope (SEM) Photographs of the Fractured Surfaces of Each Specimen after cleaning.

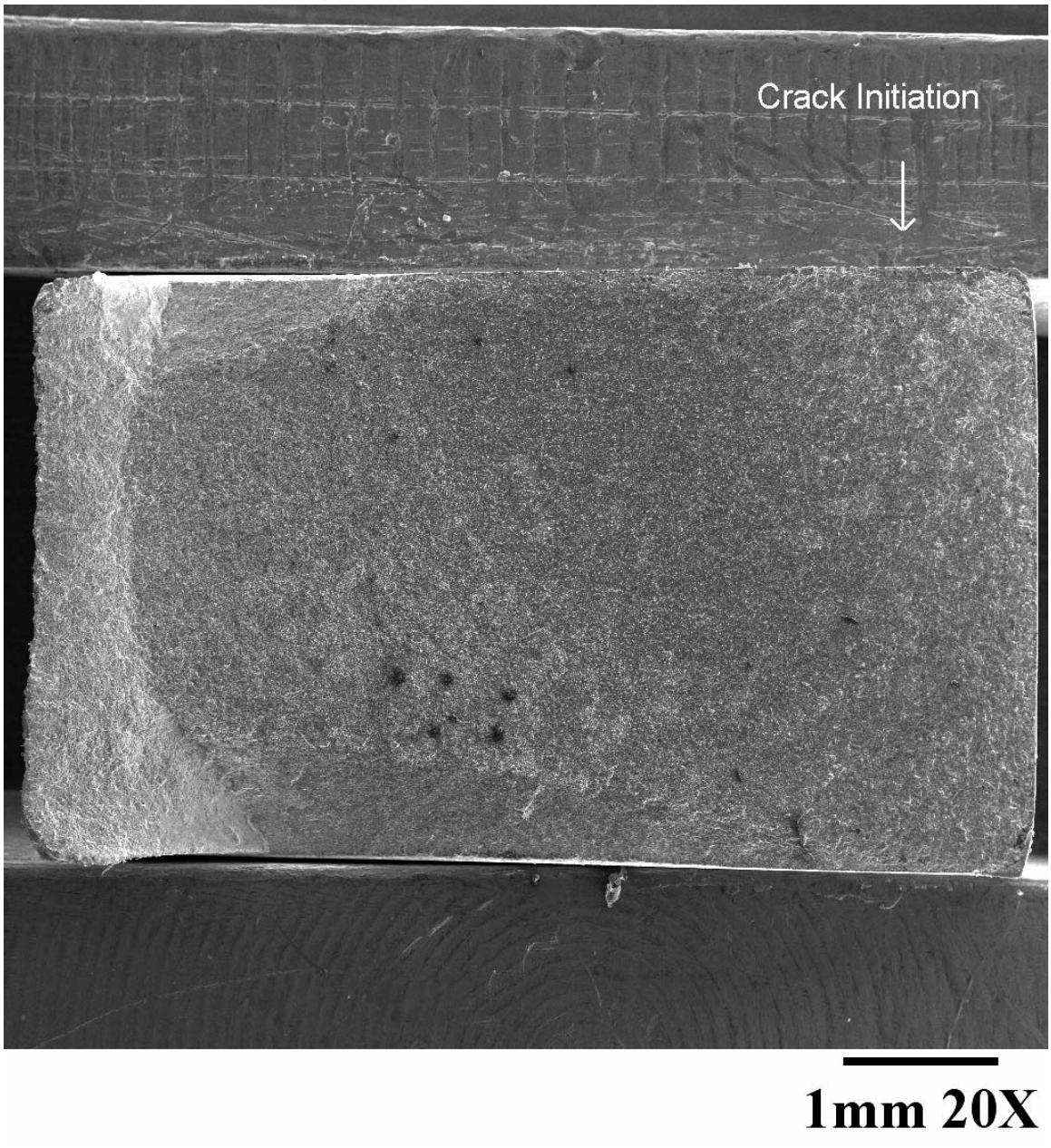

Specimen exposed to dry conditions at σ_{eff}=330.4 MPa.

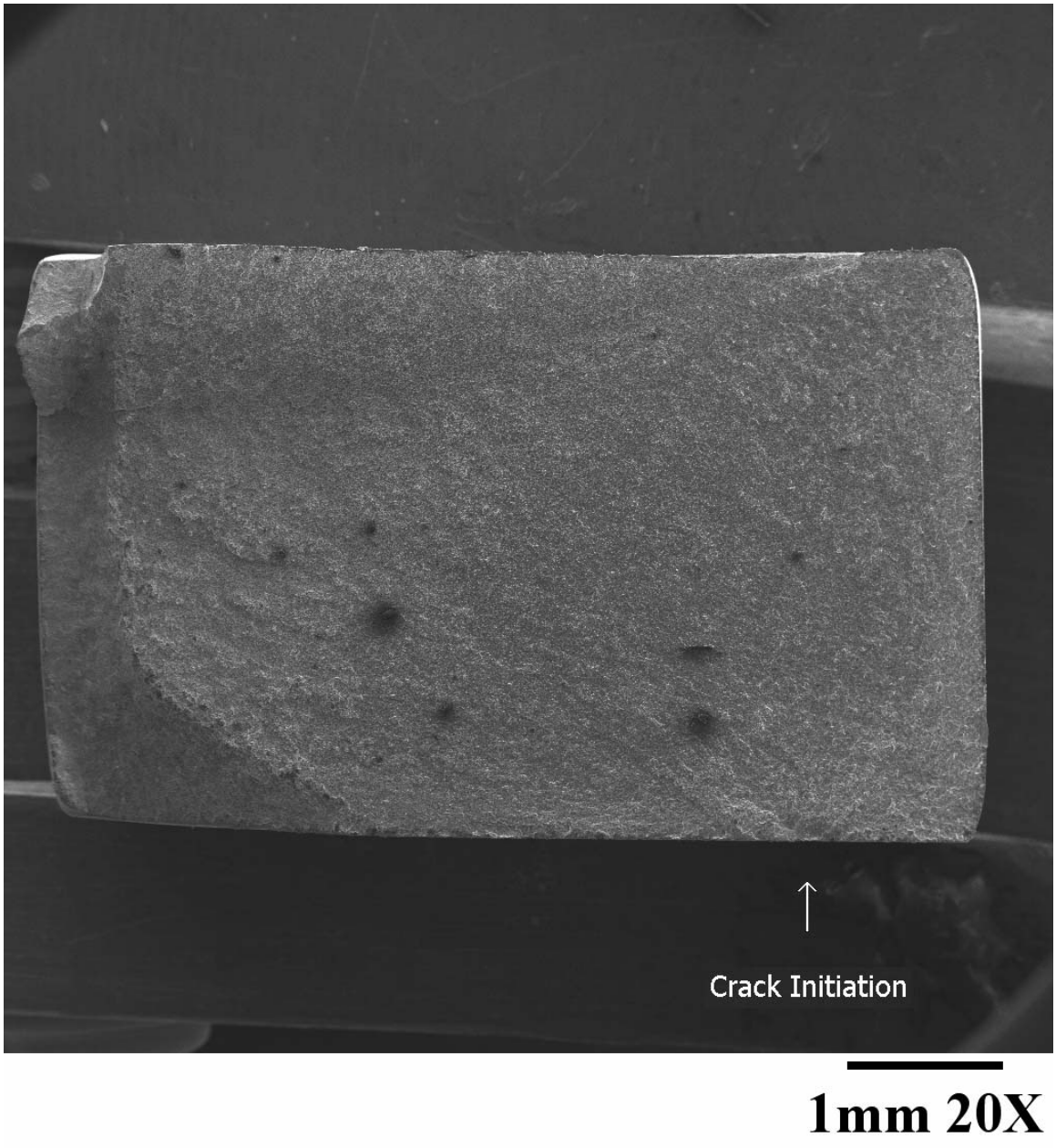

Specimen exposed to dry conditions at σ_{eff}=358.6 MPa.

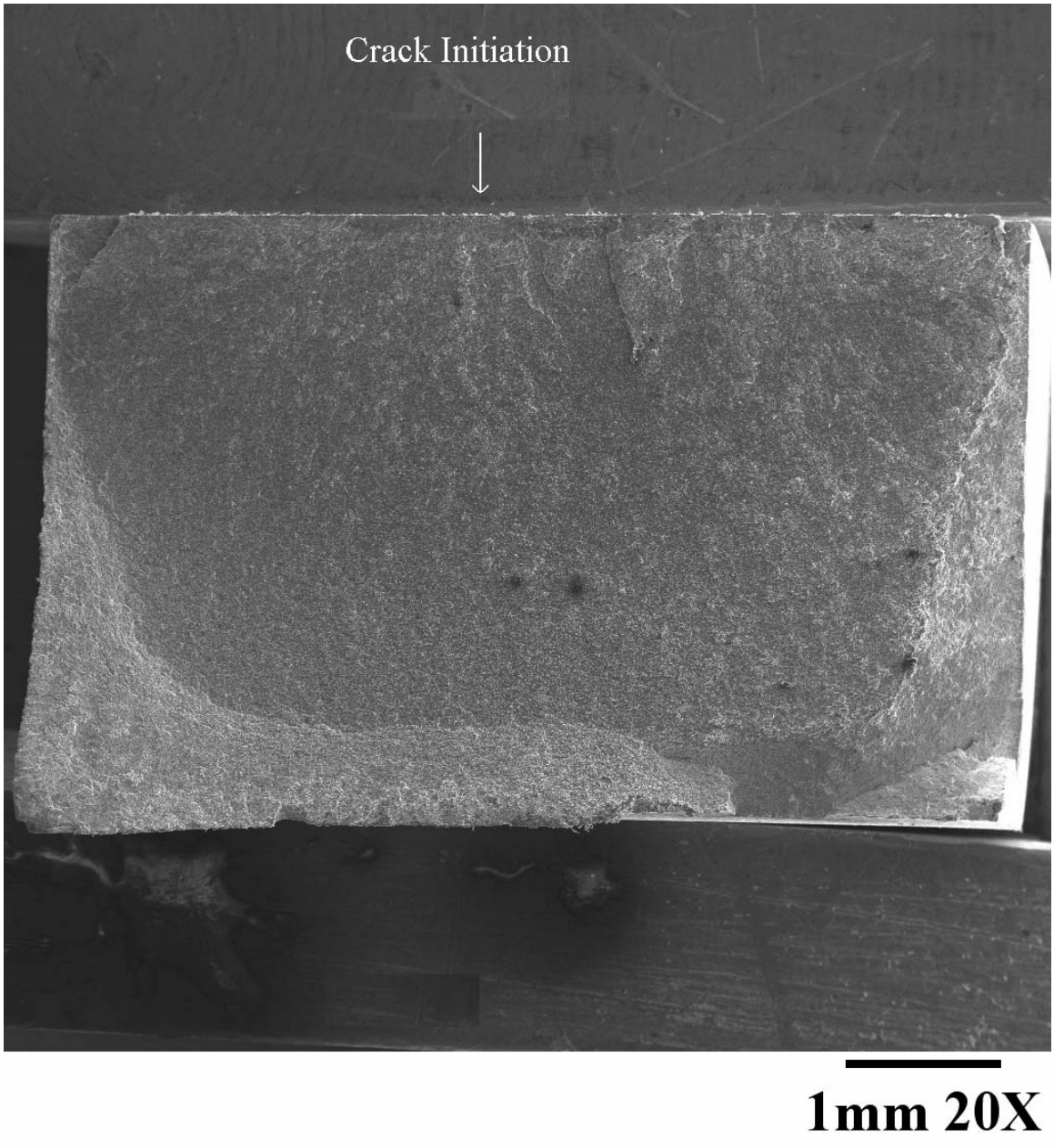

Specimen exposed to dry conditions at σ_{eff}=407.2 MPa.

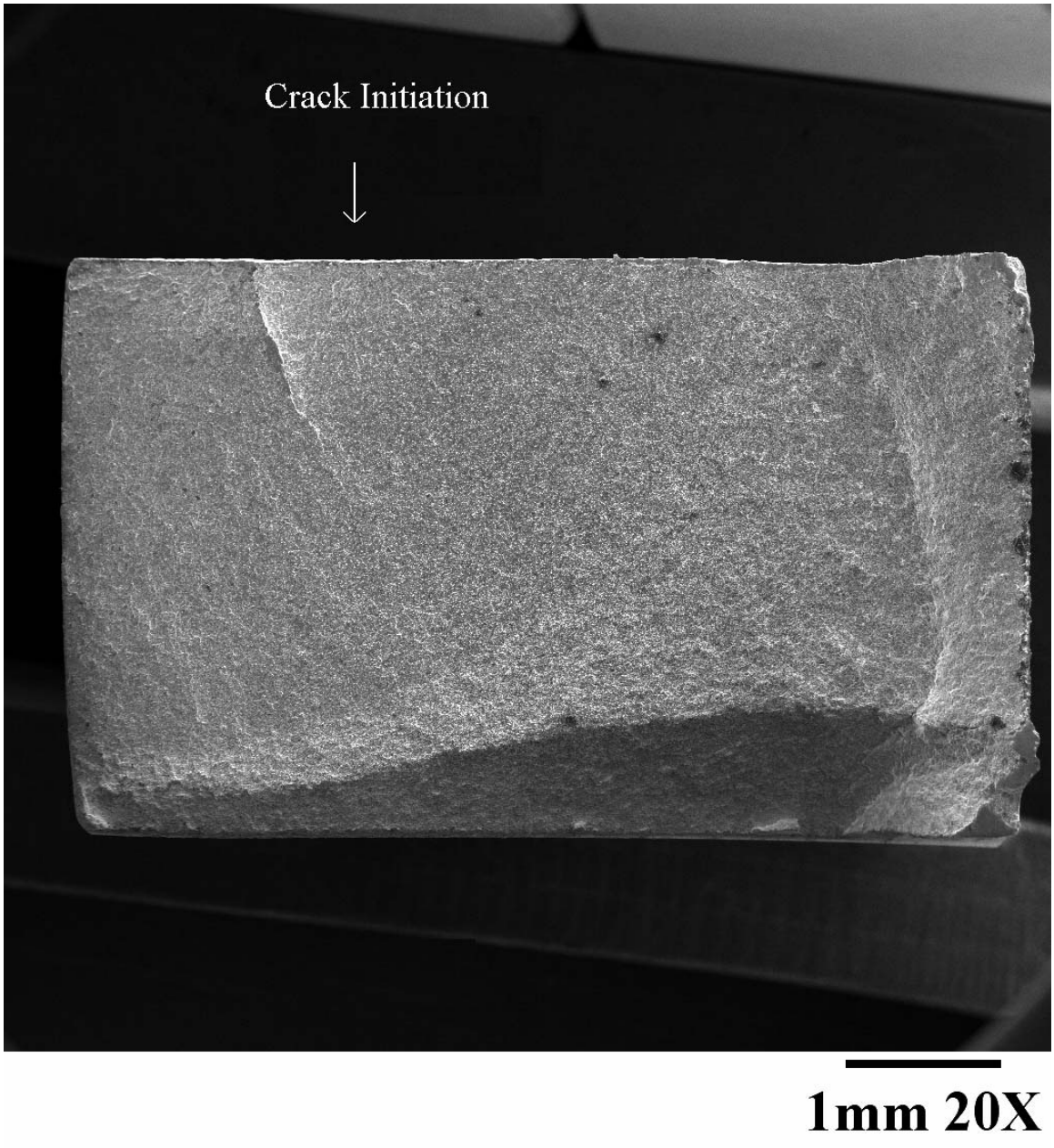

Specimen exposed to dry conditions at σ_{eff}=431.4 MPa.

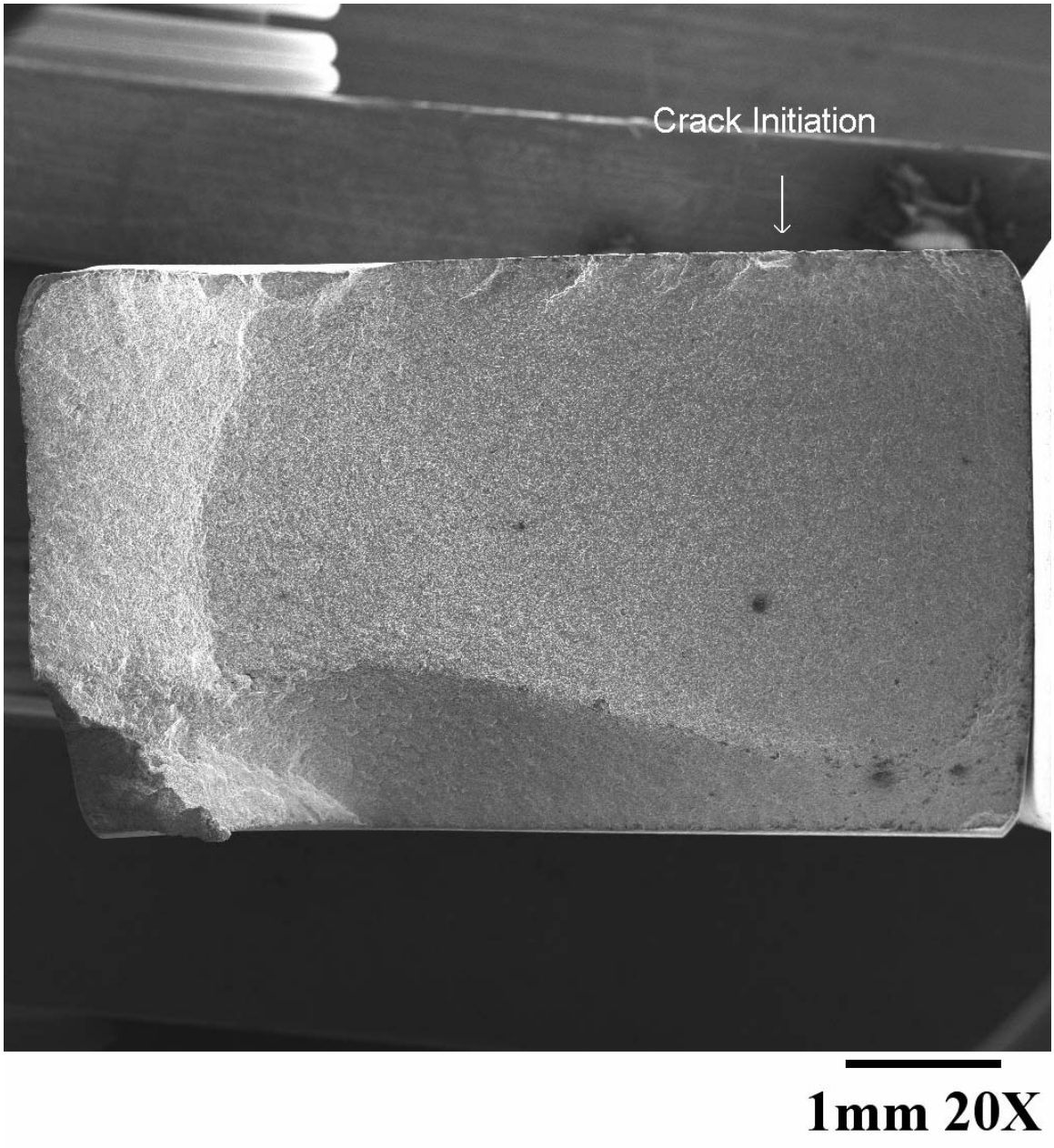

Specimen exposed to dry conditions at σ_{eff}=535.5 MPa.

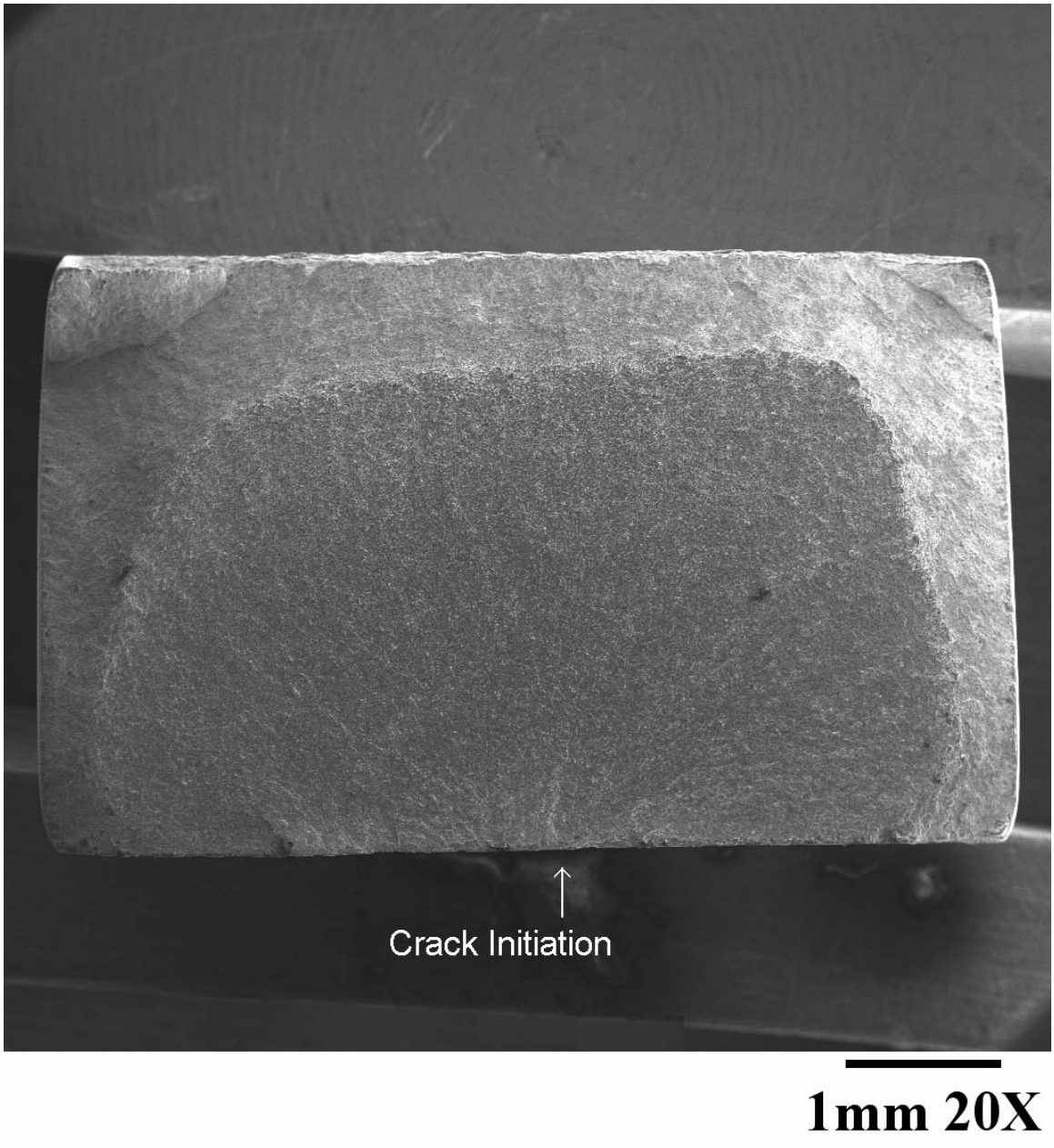

Specimen exposed to dry conditions at σ_{eff}=578.7 MPa.

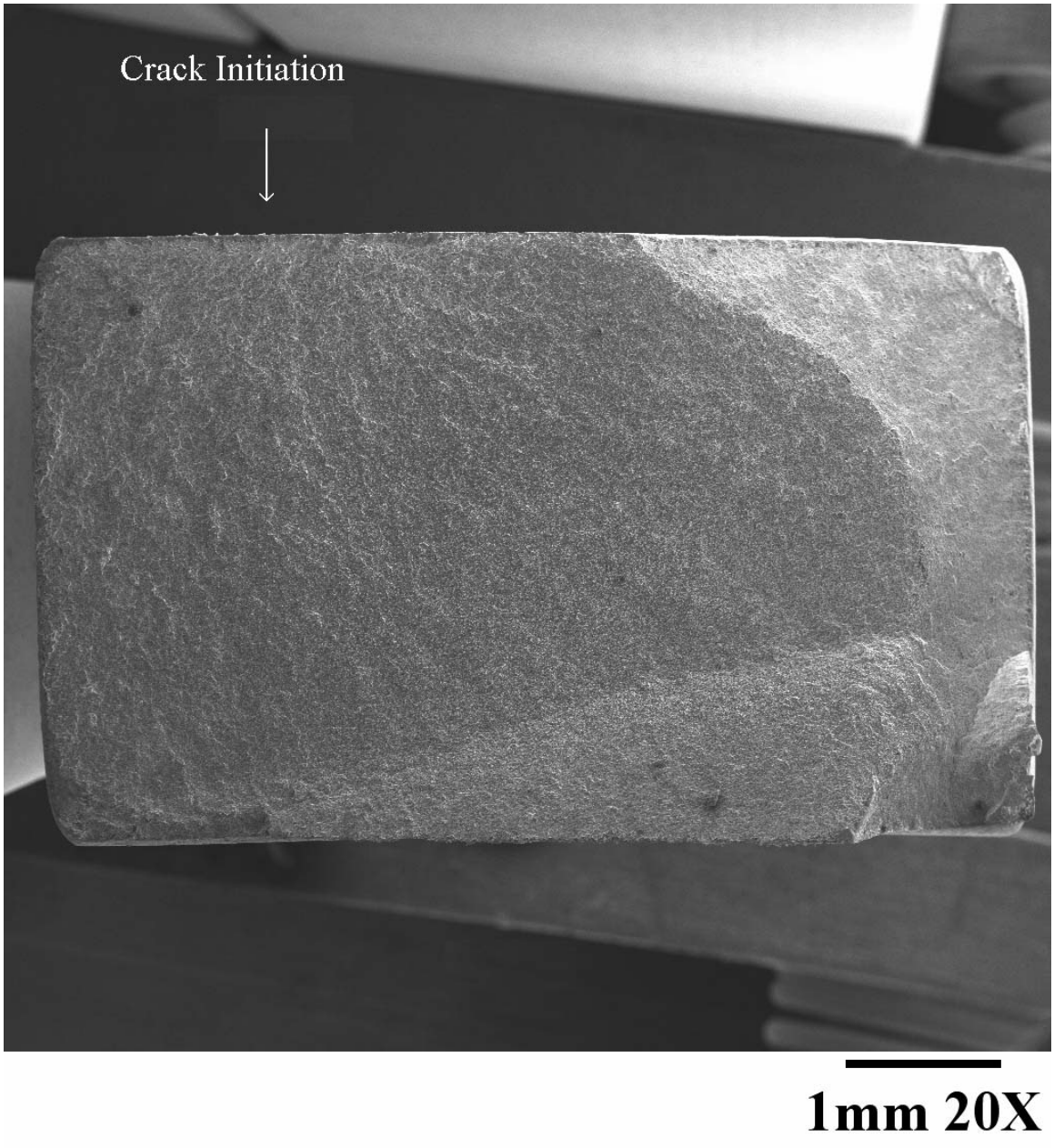

Specimen exposed to seawater conditions at σ_{eff}=377.7 MPa.

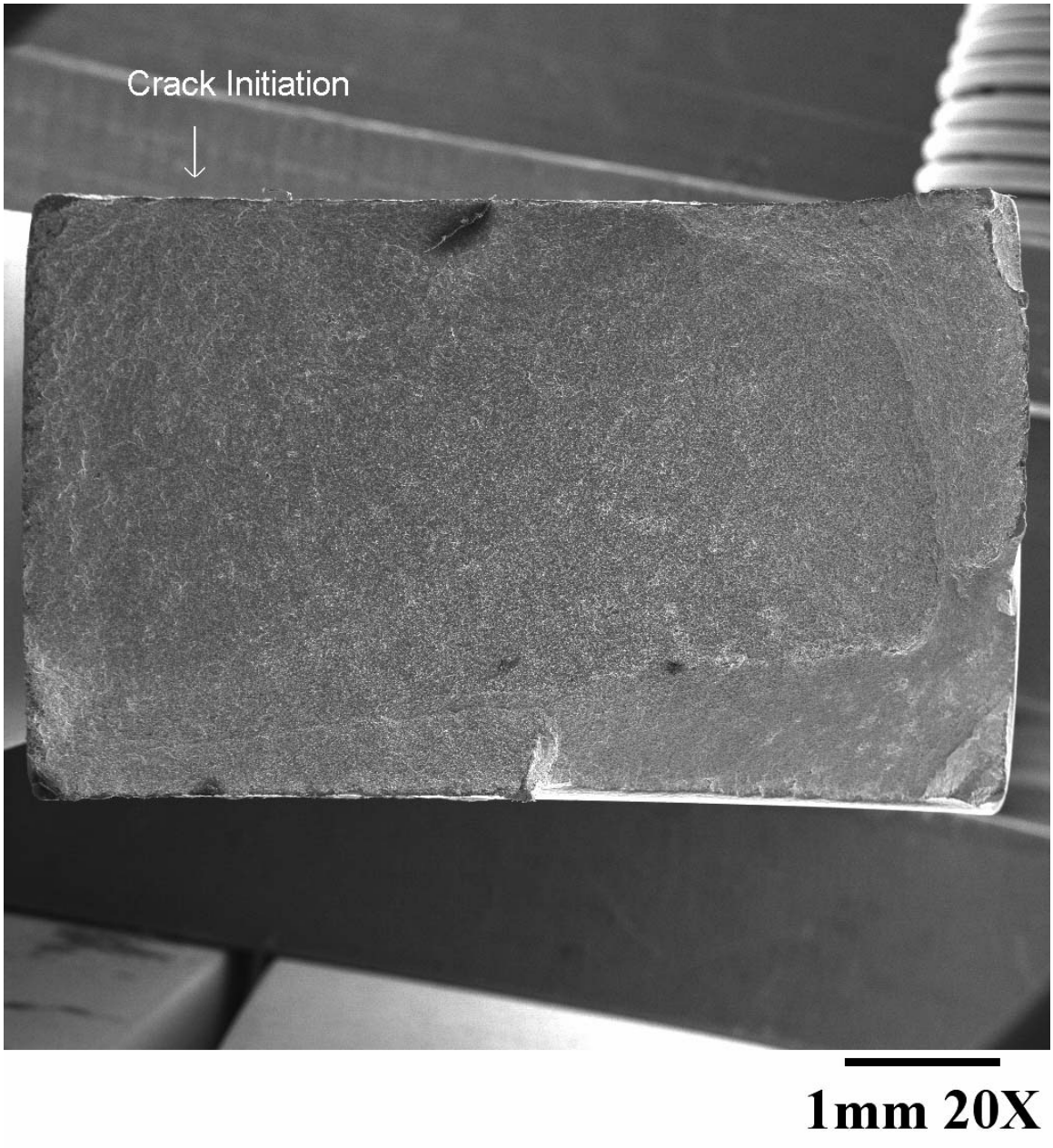

Specimen exposed to seawater conditions at σ_{eff}=418.0 MPa.

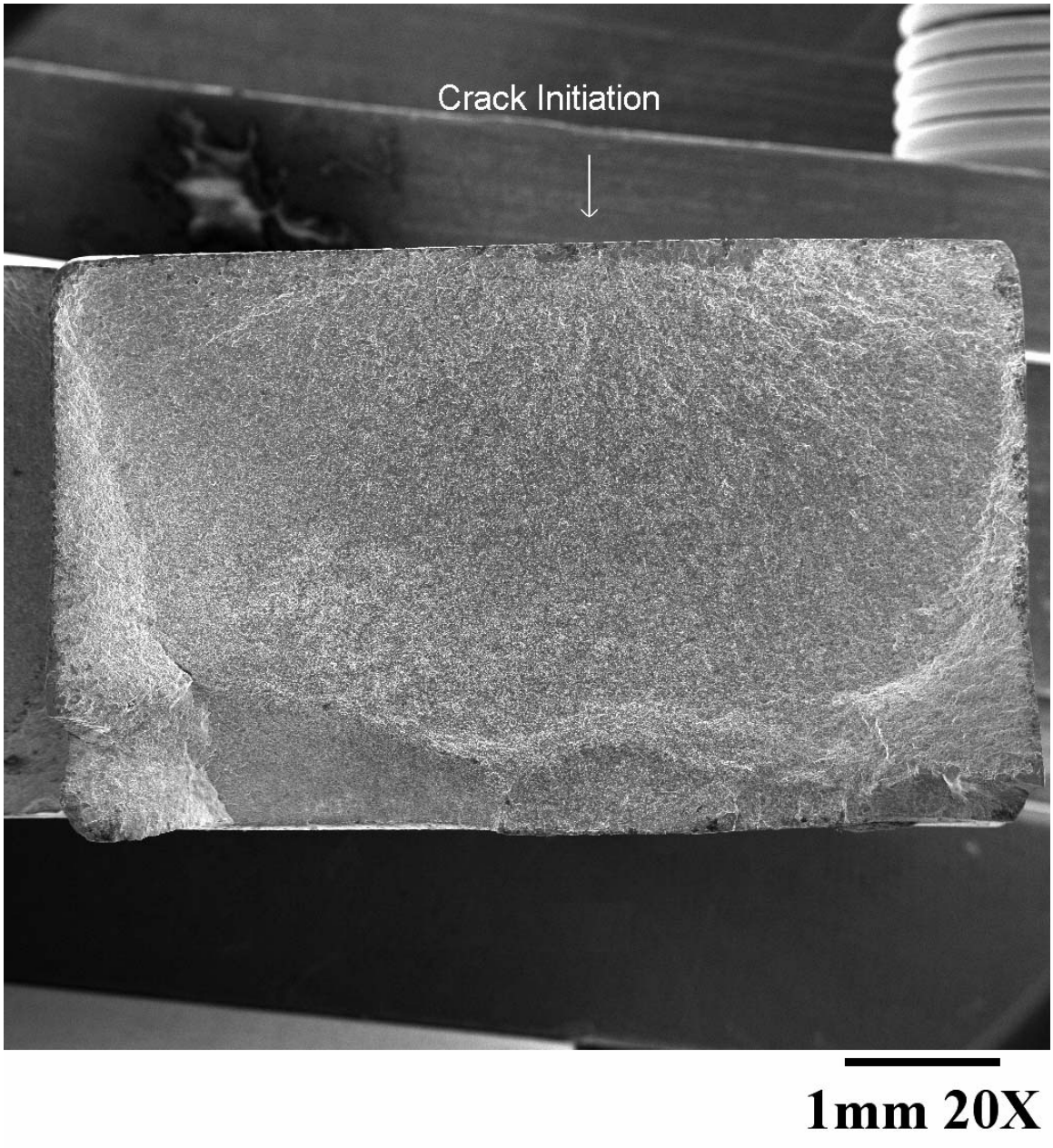

Specimen exposed to seawater conditions at σ_{eff}=449.9 MPa.

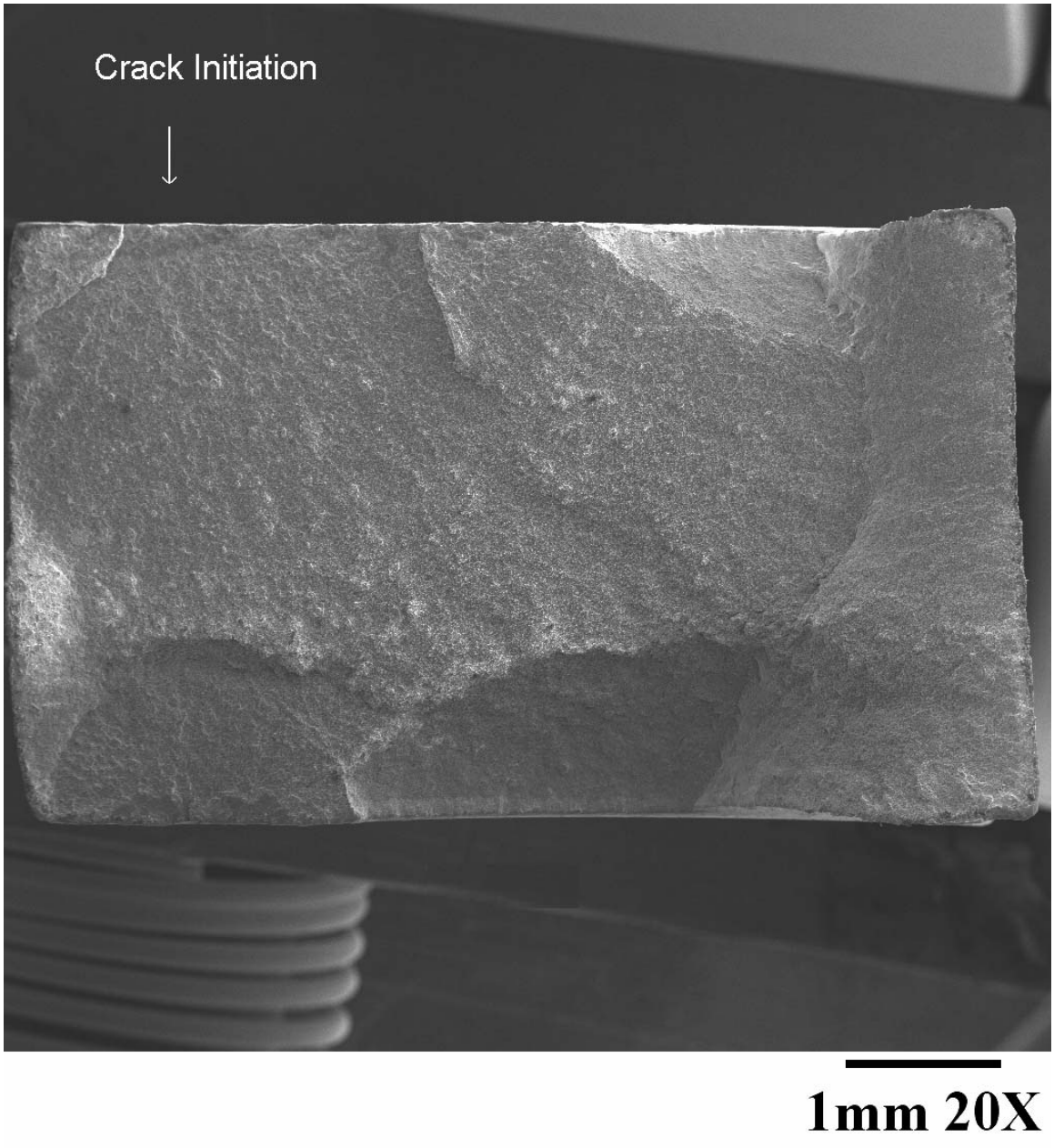

Specimen exposed to seawater conditions at σ_{eff}=534.3 MPa.

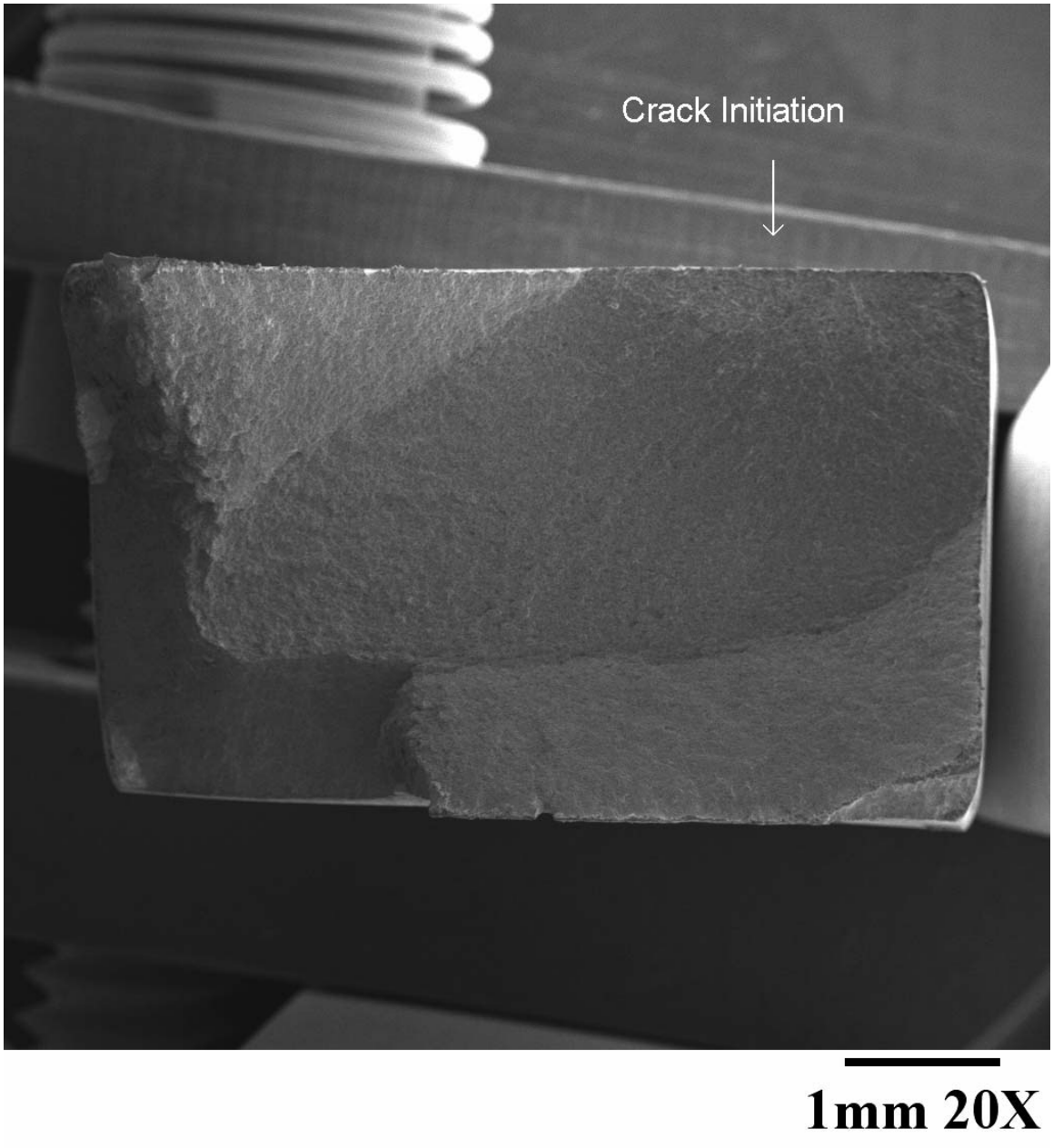

Specimen exposed to seawater conditions at σ_{eff}=568.6 MPa.

Appendix C. Photographs of Fretting Scars at 15,000 cycles.

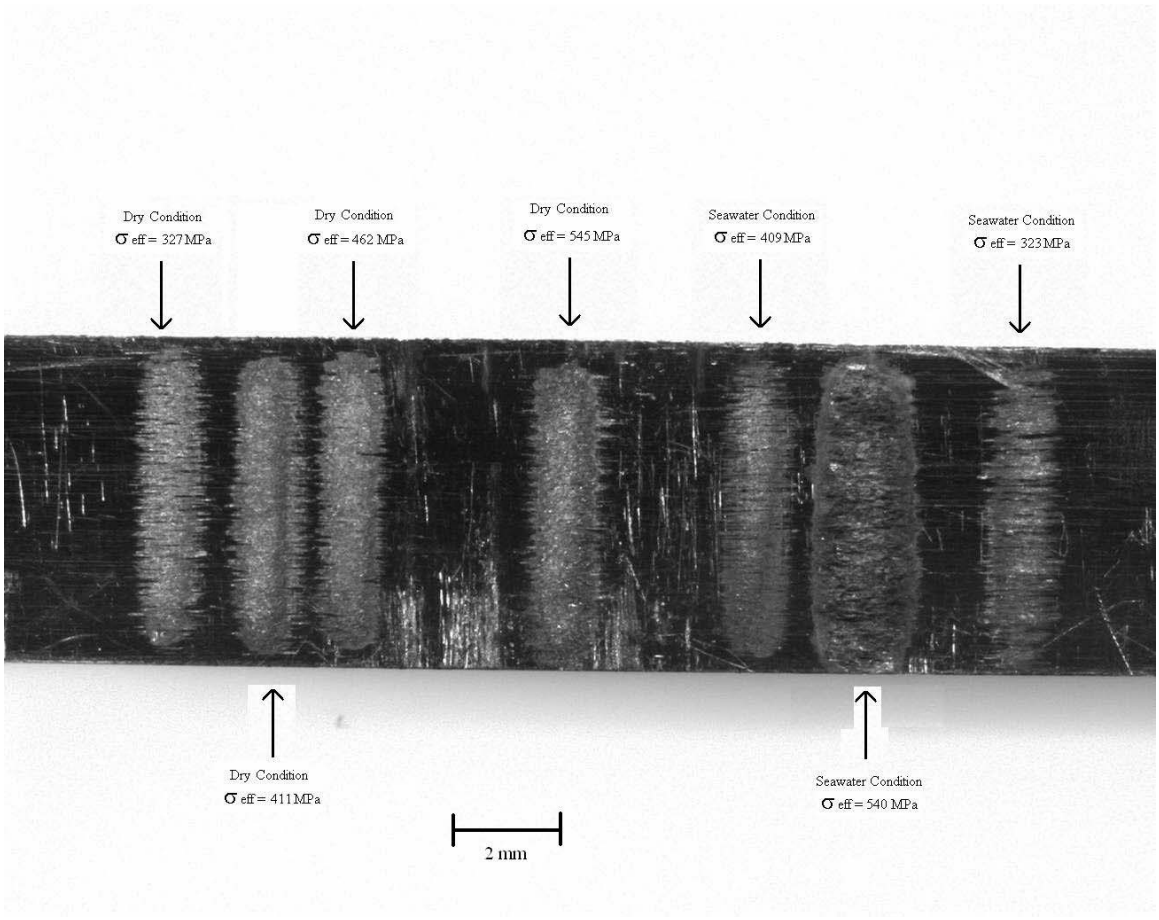

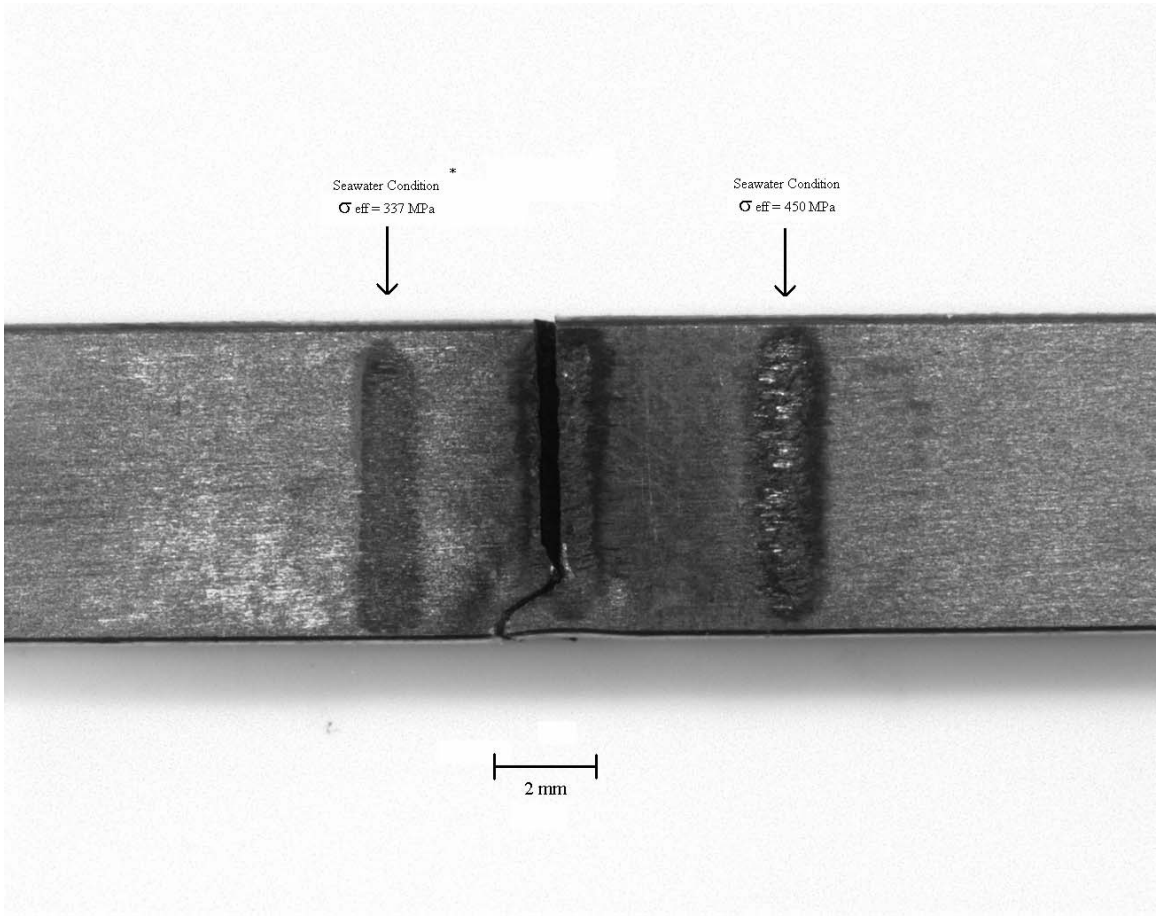

* This scar formed during previous test after more than 2.2M cycles.

Appendix D. Scanning Electron Microscope Photographs of Fatigue Striations.

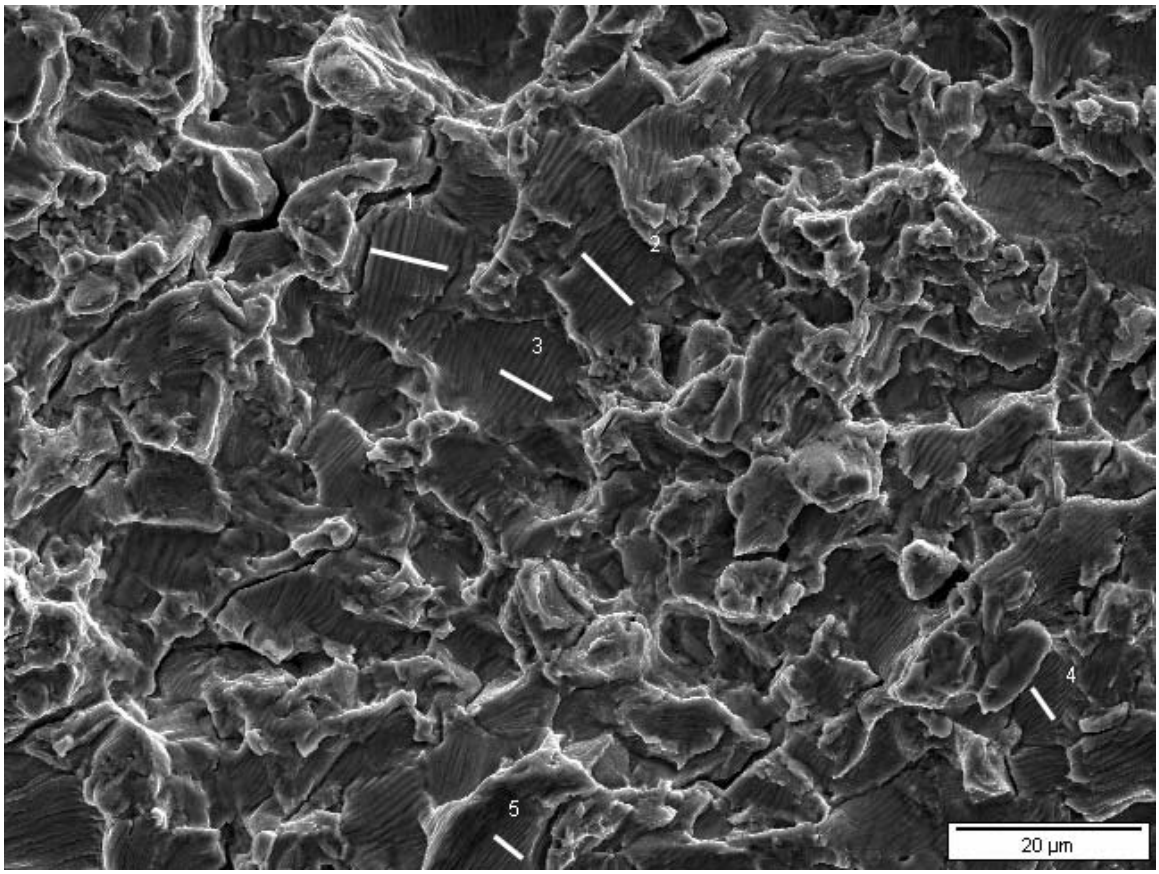

Specimen exposed to dry conditions at σ_{eff}=330.4 MPa.

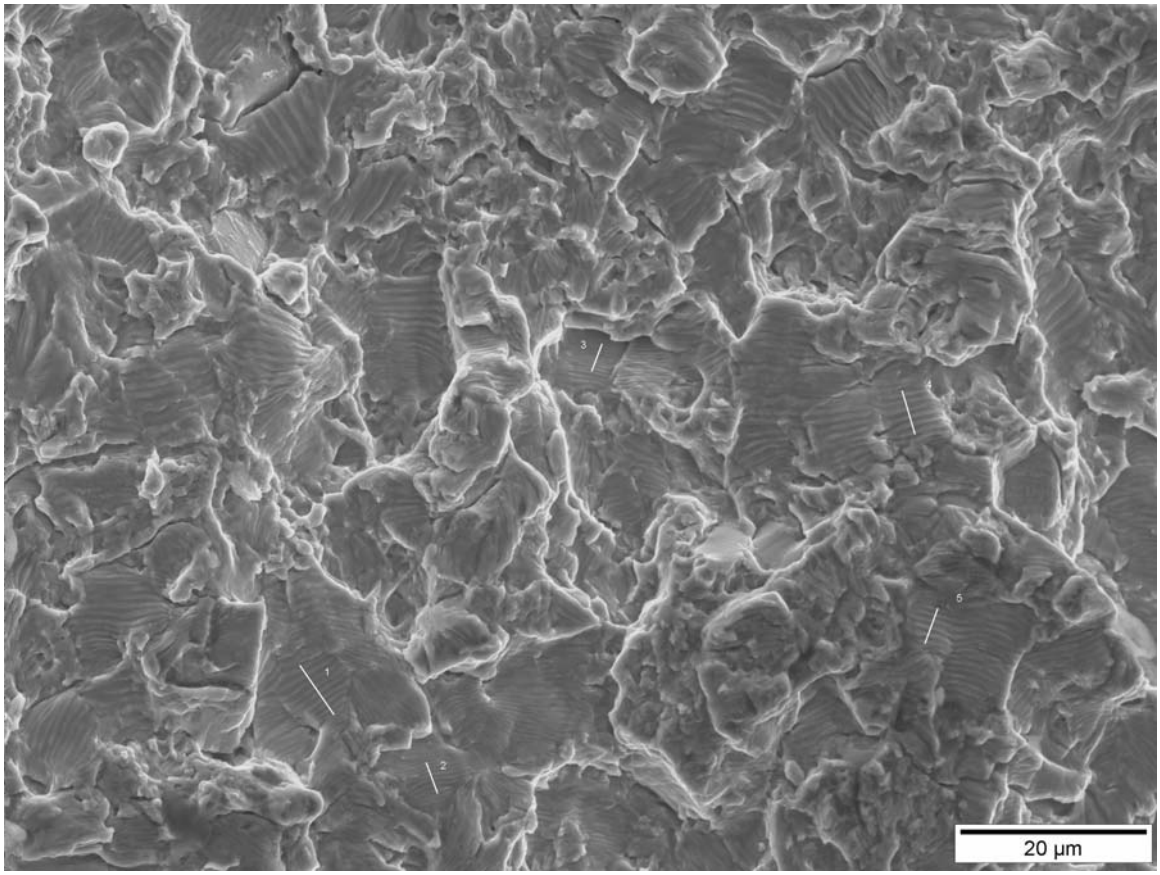

Specimen exposed to dry conditions at σ_{eff}=407 MPa.

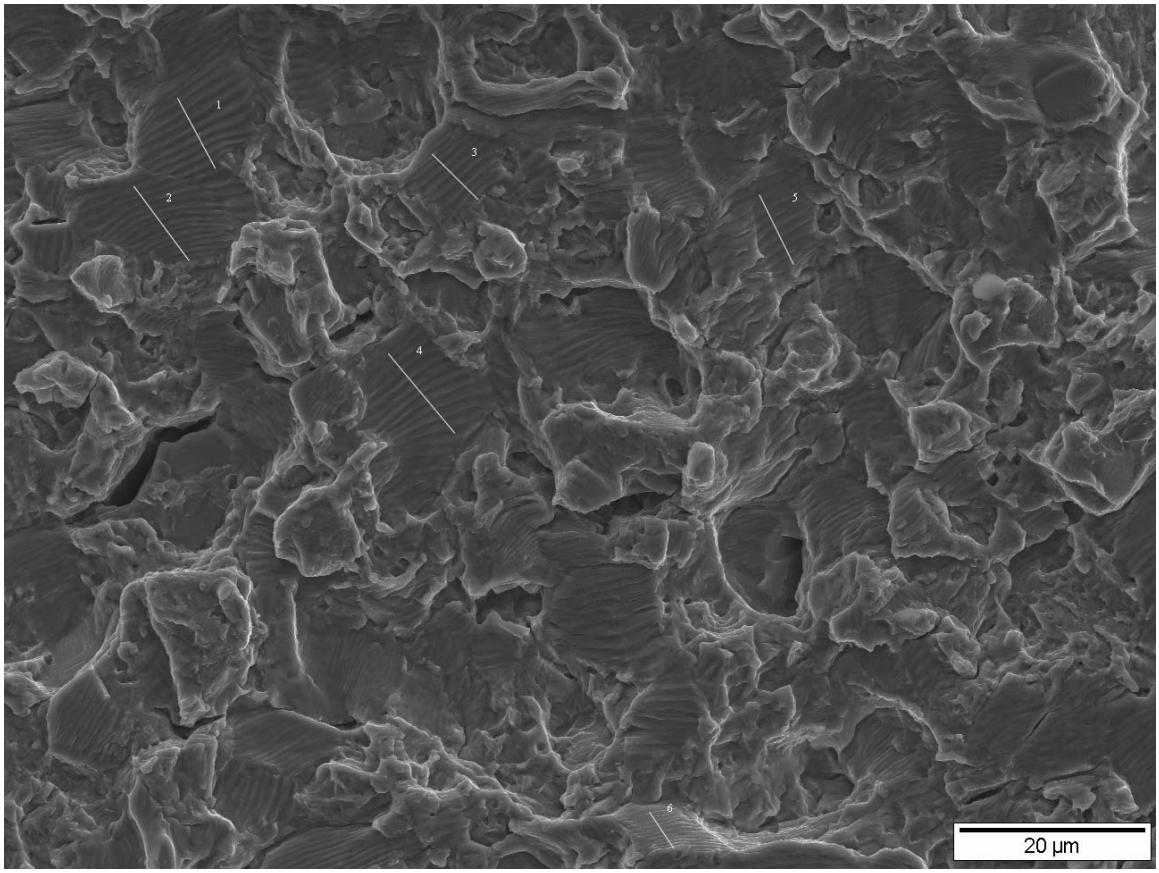

Specimen exposed to dry conditions at σ_{eff}=431.4 MPa.

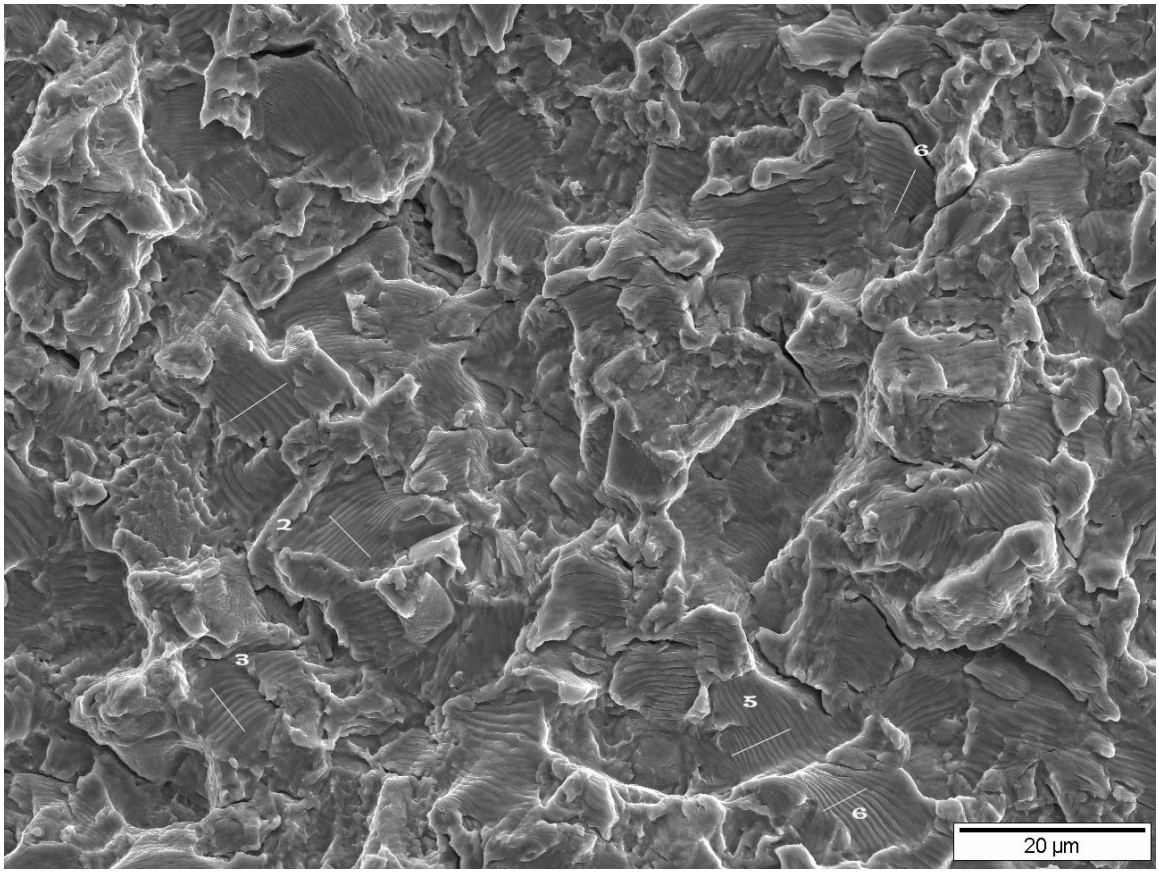

Specimen exposed to dry conditions at σ_{eff}=535.5 MPa.

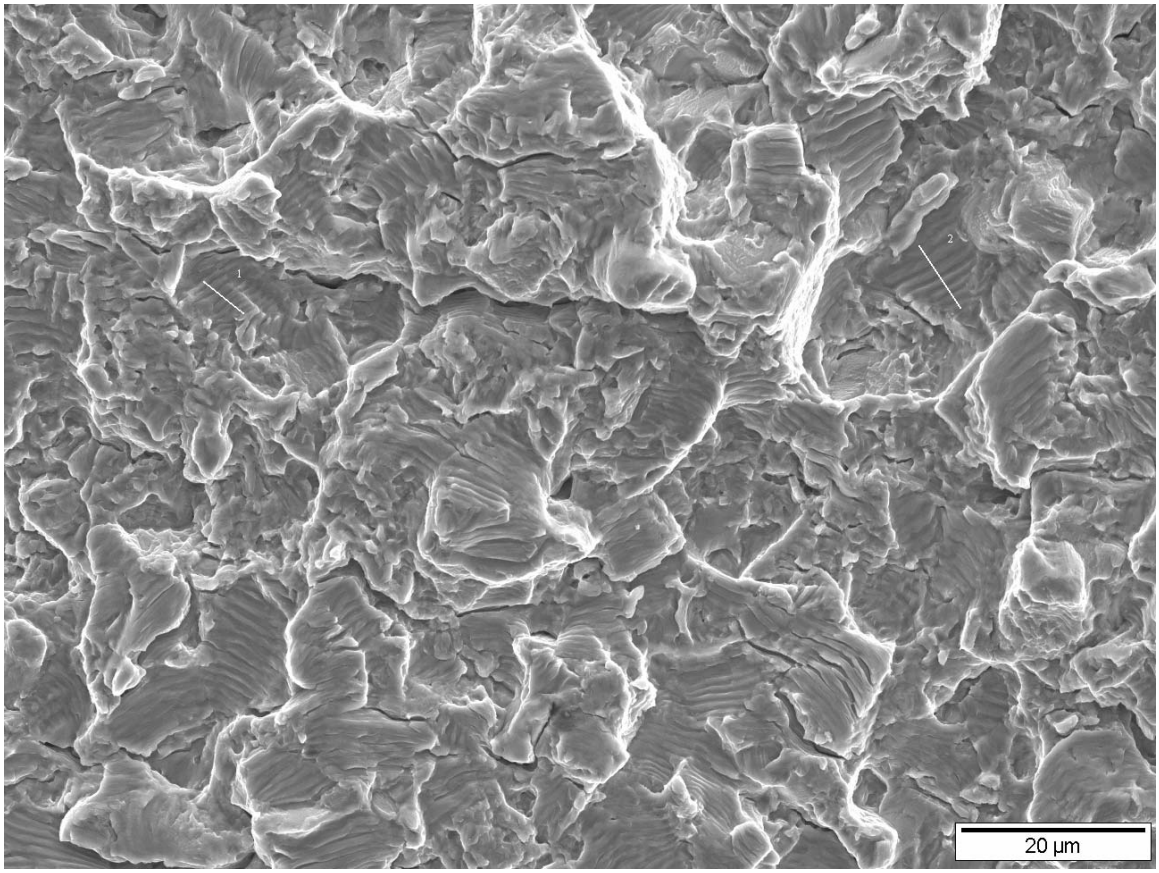

Specimen exposed to dry conditions at σ_{eff}=578.7 MPa.

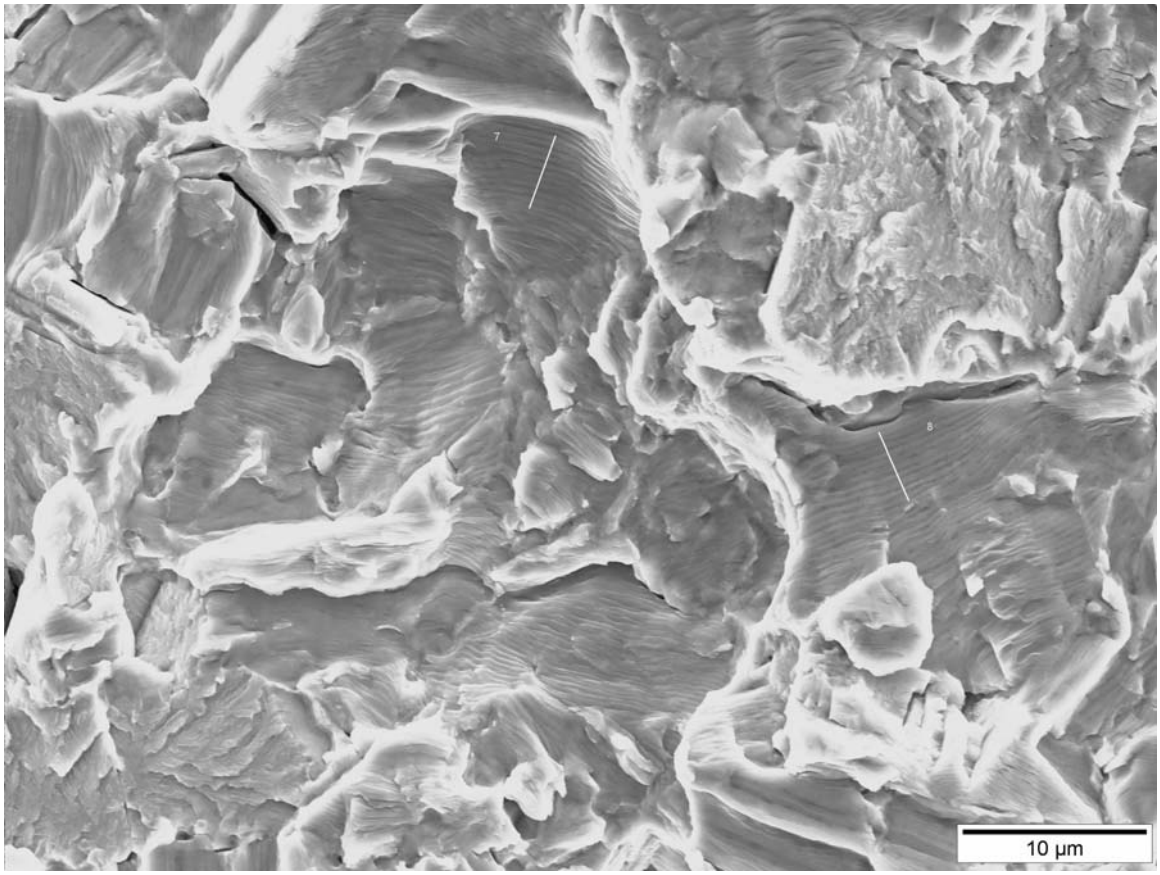

Specimen exposed to seawater conditions at σ_{eff}=377.7 MPa.

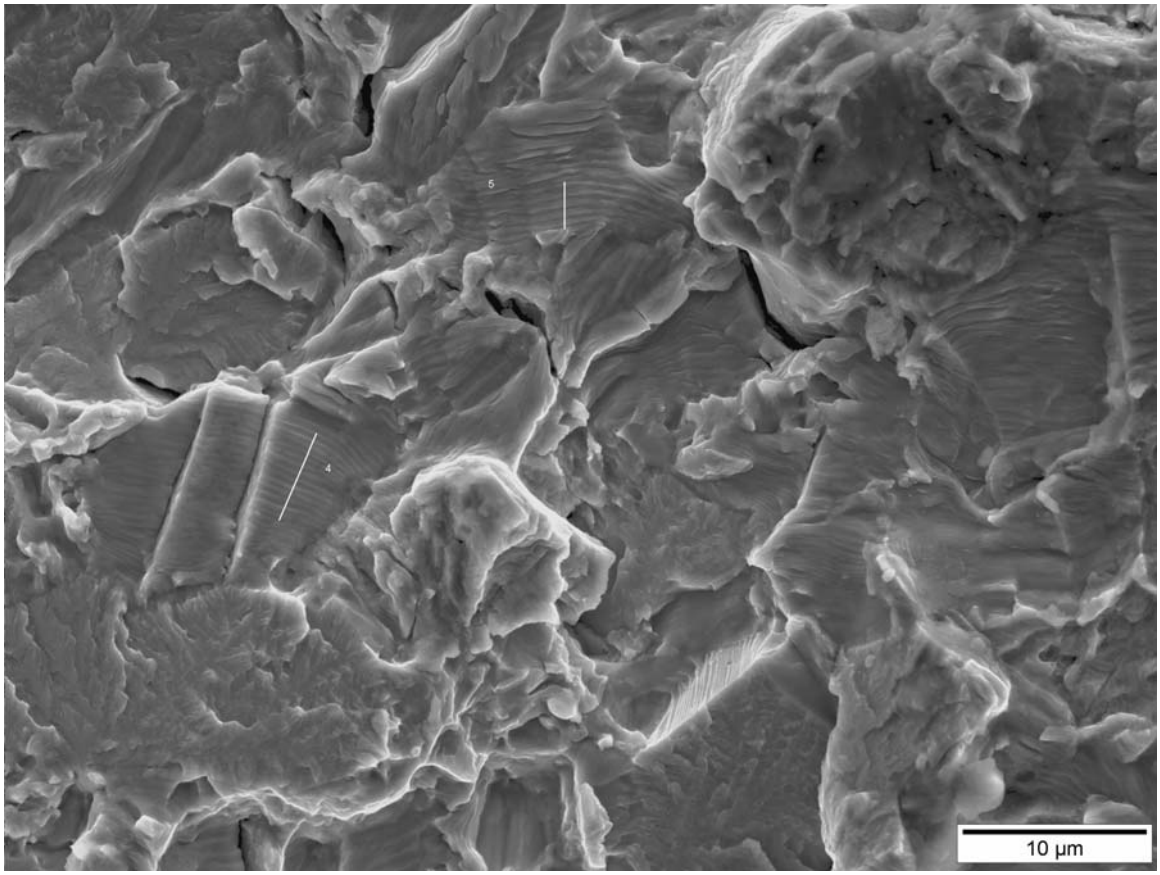

Specimen exposed to seawater conditions at σ_{eff}=418.0 MPa.

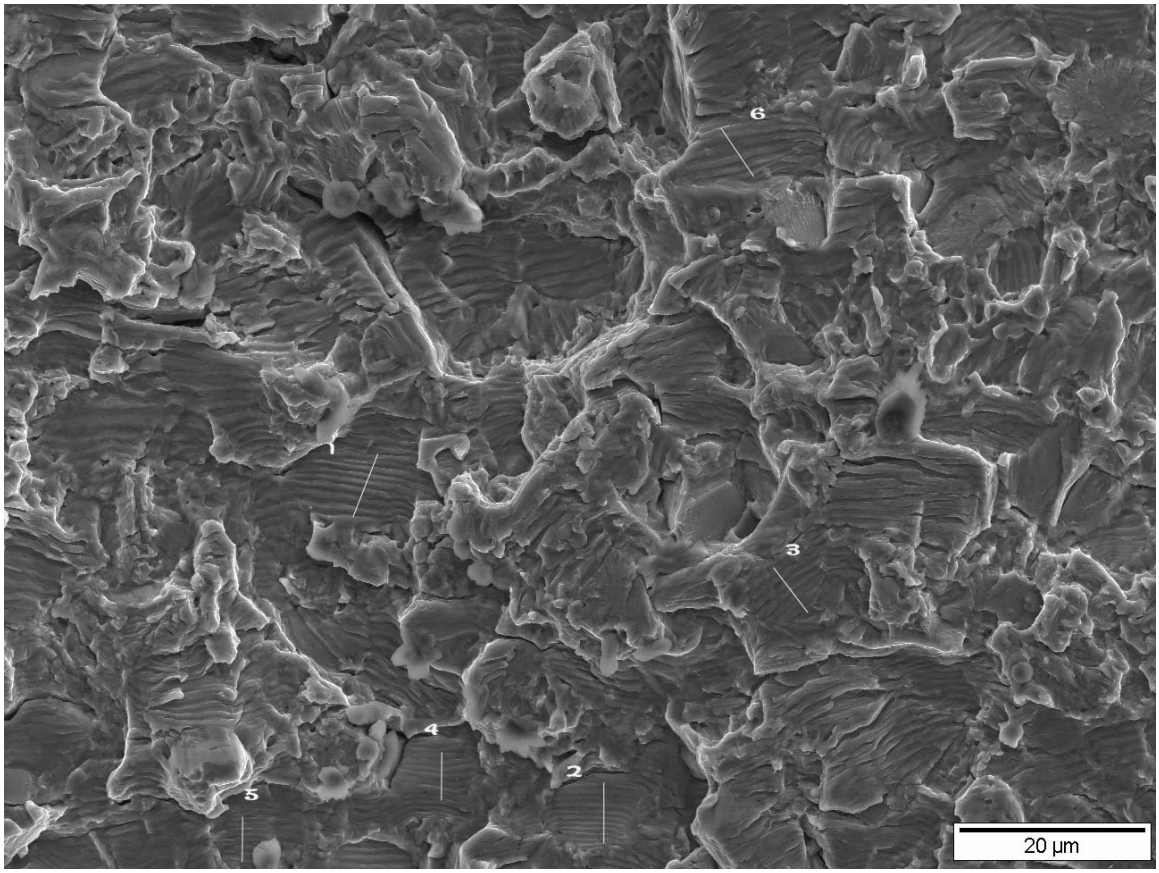

Specimen exposed to seawater conditions at σ_{eff}=449.9 MPa.

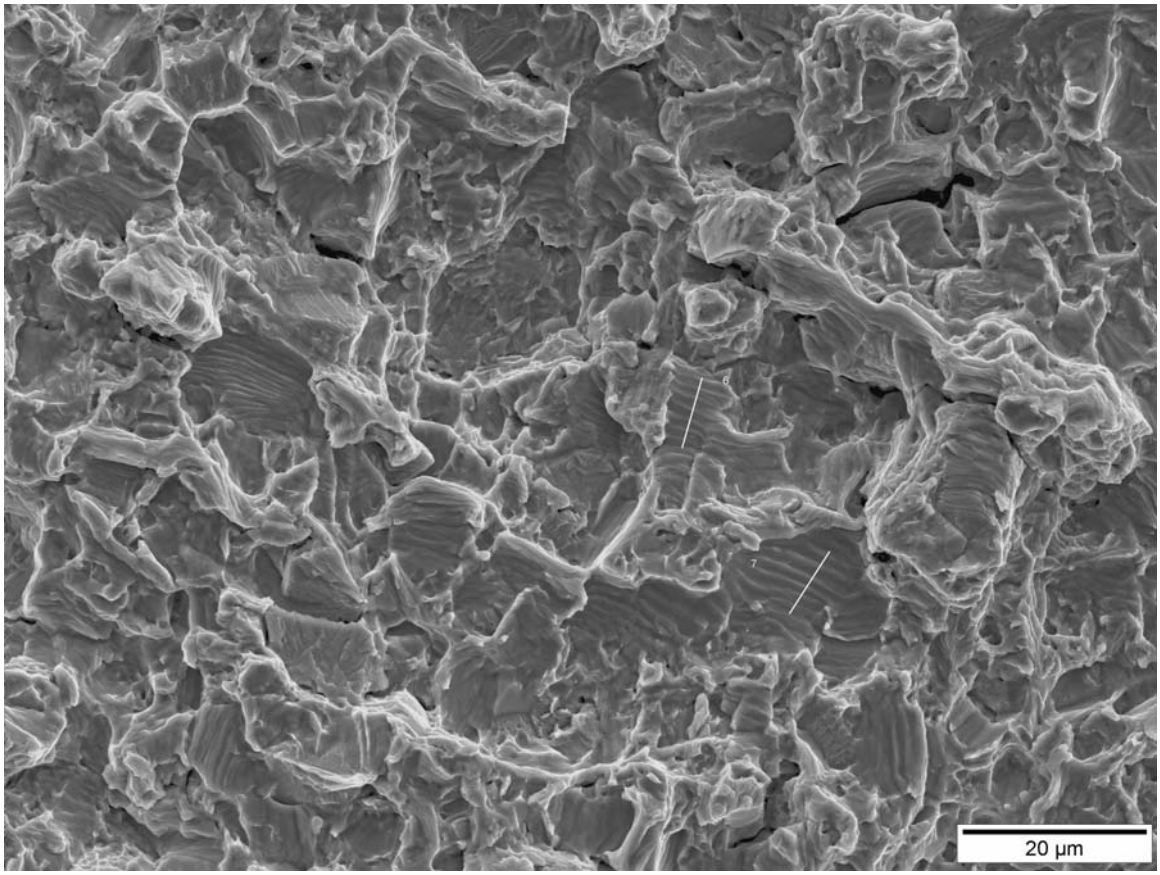

Specimen exposed to seawater conditions at σ_{eff}=534.3 MPa.

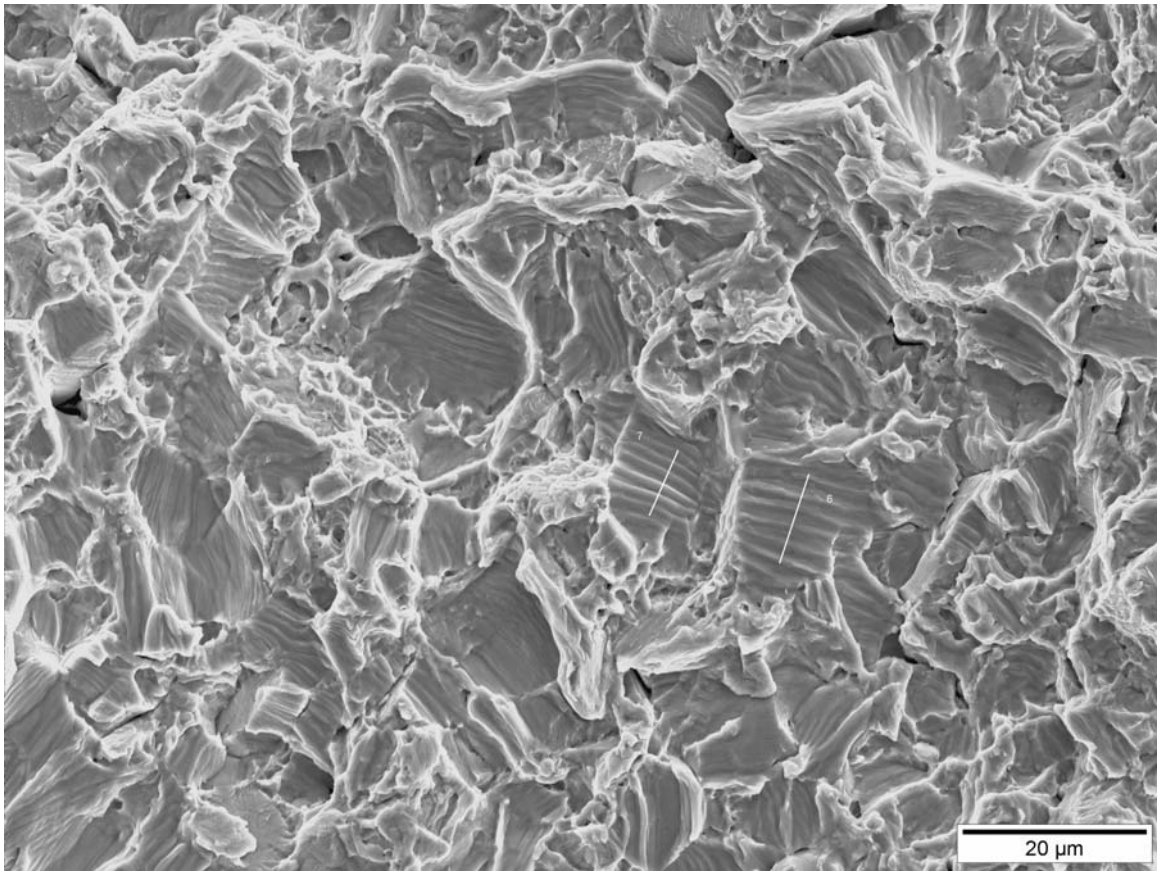

Specimen exposed to seawater conditions at σ_{eff}=568.6 MPa.

Bibliography

1. Conner, B.P., A.L. Hutson, and L. Chambon. "Observations of Fretting Fatigue Micro-Damage of Ti-6Al-4V," *Wear*, 255: 259-268 (2003).

2. Kinzie, R. "Anticipating Damage in the Fleet: Development of a Robust Environmental Severity Index." USAF Corrosion Prevention & Control Office. Report to Aging Aircraft 2001 Conference, Kissimmee FL, September 2001.

3. Cooke, G. and G. Cooke Jr. *Cost of Corrosion*. Prime Contract No. F09603-99-D-0200. NCI Task 9191-011. CDRL A003. Fairborn OH: NCI Information Systems Inc, February 2003.

4. Waterhouse, R.B. and M.K. Dutta. "The Fretting Fatigue of Titanium and Some Titanium Alloys in a Corrosive Environment," *Wear*, 25: 171-175 (1973).

5. Alam, M.O. and A.S.M.A. Haseeb. "Response of Ti-6Al-4V and Ti-24Al-11Nb Alloys to Dry Sliding Wear Against Hardened Steel," *Tribology International*, 35: 357-362 (2002).

6. Hoeppner, D.W., A.M.H.Taylor, and Venkatesan Chandrasekaran. "Fretting Fatigue Behavior of Titanium Alloys," in *Fretting Fatigue: Advances in Basic Understanding and Applications*. Eds. Y. Mutoh, S.E. Kinyon, and D.W. Hoeppner. West Conshohocken PA: ASTM International, 2003.

7. Nicolaou, P.D., E.B. Shell, and T.E. Matikas. "Microstructural and Surface Characterization of Ti-6Al-4V Alloys After Fretting Fatigue," *Materials Science and Engineering*, A269: 98-103 (1999).

8. Namjoshi, S.A., S. Mall, V.K. Jain, and O. Jin. "Fretting Fatigue Crack Initiation Mechanism in Ti-6Al-4V," *Fatigue and Fracture Engineering of Material Structures*, 25: 1-10 (2002).

9. Mall, S., V.K. Jain, S.A. Namjoshi, and C.D. Lykins. "Fretting Fatigue Crack Initiation Behavior of Ti-6Al-4V," *Fretting Fatigue: Advances in Basic Understanding and Applications, ASTM STP 1425*. Eds. A.B. Smith and C.D. Jones. American Society for Testing and Materials, West Conshohocken PA, 199#.

10. Poon, C. and D.W. Hoeppner. "The Effect of Environment on the Mechanism of Fretting Fatigue," *Wear*, 52: 175-191 (1979).

11. Sankaran, K.K., R. Perez, and K.V. Jata. "Effects of Pitting Corrosion on the Fatigue Behavior of Aluminum Alloy 7075-T6: Modeling and Experimental Studies," *Materials Science and Engineering*, A297: 223-229 (2001).

12. Zhou, Z.R. and L. Vincent. "Mixed Fretting Regime," *Wear*, 181-183: 531-536 (1995).

13. Hills, D.A. and A. Mugadu. "An Overview of Progress in the Study of Fretting Fatigue," *Journal of Strain Analysis*, 37: 591-601 (2002).

14. Takeuchi, M., T. Satoh, Y. Mutoh, R.B. Waterhouse, and Y. Kon. "Fretting Fatigue of an Austenitic Stainless Steel in Seawater," *Fatigue and Fracture of Engineering Materials and Structures*, 17: 949-958 (1994).

15. Wharton, M.H. and R.B. Waterhouse. "Environmental Effects in the Fretting Fatigue of Ti-6Al-4V," *Wear*, 62: 287-297 (1980).

16. Moody, N.R. and W.W. Gerberich. "Hydrogen-Induced Slow Crack Growth in Ti-6Al-6V-2Sn," *Metallurgical Transactions*, 11A: 973-981 (1980).

17. -----. *Hydrogen Effects on Material Behavior*. Eds. N. R. Moody and A.W. Thompson. Warrendale PA: The Minerals, Metals and Materials Society, 1990.

18. Bache, M.R., W.J. Evans, and M. McElhone. "The Effects of Environment and Internal Oxygen on Fatigue Crack Propagation in Ti-6Al-4V," *Materials Science and Engineering*, A234-236: 918-922 (1997).

19. Demulsant, X. and J. Mendez. "Influence of Environment on Low Cycle Fatigue Damage in Ti-6Al-4V and Ti 6246 Titanium Alloys," *Materials Science and Engineering*, A219: 202-211 (1996).

20. Yeh, M.S. and J.H. Huang. "Internal Hydrogen-Induced Subcritical Crack Growth in Ti-6Al-4V," *Scripta Materialia*, 36: 1415-1421 (1997).

21. Fullenwider, M.A. *Hydrogen Entry and Action in Metals*. New York: Pergamon Press, 1983.

22. Christ, H.J., A. Senemmar, M. Decker, and K Prübner. "Effects of Hydrogen on Mechanical Properties of β-Titanium Alloys," *Sādhanā*, 28: 453-465 (2003).

23. Moody, N.R. and W.W. Gerberich. "The Effect of Stress State on Internal Hydrogen-Induced Crack Growth in Ti-6Al-6V-2Sn," *Metallugical Transactions*, 13A: 1055-1061, 1982.

24. Moody, N.R., F.A. Greulich, and S.L. Robinson. "The Influence of Hydrogen and the Interface Phase on Fracture in Ti Code 12," *Metallugical Transactions*, 15A: 1955-1958, 1984.

25. Bache, M.R. and W.J. Evans. "The Fatigue Crack Propagation Resistance of Ti-6Al-4V Under Aqueous Saline Environments," *International Journal of Fatigue*, 23: S319-S323 (2001).

26. Waterhouse, R.B. *Fretting Fatigue*. Oxford: Pergamon Press Ltd, 1972.

27. Taylor, D.E. "Environmental Fretting Fatigue," in *Fretting Fatigue*. Eds. R.B. Waterhouse and T.C. Lindley. London: Mechanical Engineering Publications, 1994.

28. Sato, J., M. Shima, and M. Takeuchi. "Fretting Wear in Seawater," *Wear*, 110: 227-237 (1986).

29. Elliott, III, C.B. and D.W. Hoeppner. "The Importance of Wear and Corrosion on the Fretting Fatigue Behavior of Two Aluminum Alloys," *Wear*, 236: 128-133 (1999).

30. Vingsbo, O. and S. Soderberg. "On Fretting Maps," *Wear*, 126: 131-147 (1988).

31. Endo, K. and H. Goto. "Effects of Environment of Fretting Fatigue," *Wear*, 48: 347-367 (1978).

32. Takeuchi, M., R.B. Waterhouse, Y. Mutoh, and T. Satoh. "The Behavior of Fatigue Crack Growth in the Fretting-Corrosion-Fatigue of High Tensile Roping Steel in Air and Seawater," *Fatigue and Fracture of Engineering Materials and Structures*, 14: 69-77 (1991).

33. Price, S. and D.E. Taylor. "The Application of Electrochemical Techniques to Evaluate the Role of Corrosion in Fretting Fatigue of a High Strength Low Alloy Steel," *Standardisation of Fretting Fatigue Test Methods and Equipment*. Eds. H. Attia and R.B. Waterhouse. ASTM, Philadelphia, 1992.

34. Antoniou, R.A. and T.C. Radtke. "Mechanisms of Fretting-Fatigue of Titanium Alloys," *Materials Science and Engineering*, A237: 229-240 (1997).

35. Molinari, A., G. Straffelini, B. Tesi, and T. Bacci. "Dry Sliding Wear Mechanisms of the Ti-6Al-4V Alloy," *Wear*, 208: 105-112 (1997).

36. Saritas, S., R.P.M. Procter, and W.A. Grant. "Effect of Ion Implantation of Fatigue, Fretting and Fretting-Corrosion of Ti-6Al-4V," *Materials Science and Engineering*, A115: 307-314 (1989).

37. Jiang, J., M.M. Stack, and A. Neville. "Modelling the Tribo-corrosion Interaction in Aqueous Sliding Conditions," *Tribology International*, 35: 669-679 (2002).

38. Walker, K. "The Effect of Stress Ratio During Crack Propagation and Fatigue for 2024-T3 and 7075-T6 Aluminum," *Effects of Environment and Complex Load History on Fatigue Life, STP 462*, American Society for Testing and Materials. West Conshohocken, PA, pp. 1-14, 1970.

39. Lykins, C.D., S. Mall, and V.K. Jain. "A Shear Stress Based Parameter for Fretting Fatigue Crack Initiation," *Fatigue and Fracture of Engineering Materials and Structures*, 24: 461-473 (2001).

40. Yuksel, H.I. *Effects of Shot-Peening on High Cycle Fretting Fatigue Behavior of Ti-6Al-4V*. MS thesis, AFIT/GAE/ENY/02-12. School of Engineering and Management, Air Force Institute of Technology (AU), Wright-Patterson AFB OH, March 2002 (ADA401223).

41. Sahan, O. *Fretting Fatigue Behavior of a Titanium Alloy Ti-6Al-4V at Elevated Temperature*. MS thesis, AFIT/GAE/ENY/02-11. School of Engineering and Management, Air Force Institute of Technology (AU), Wright-Patterson AFB OH, March 2002 (ADA401275).

42. Lykins, C.D. *An Investigation of Fretting Fatigue Crack Initiation Behavior of the Titanium Alloy Ti-6Al-4V*. PhD dissertation. University of Dayton, Dayton OH, 1999.

43. Material Test System Model 793.10 MultiPurpose Testware. MTS Systems Corporation, Eden Prairie MN, 2001.

44. Stereoscan 360FE Scanning Electron Microscope Operating Instructions. Leica Cambridge Ltd, Cambridge UK, 1992.

45. Voyager Applications Guide. Noran Instruments, Middleton WI, 1996.

46. Bransonic 200 Ultrasonic Cleaner. Branson Ultrasonics Corporation, Denbury CT.

47. Form Talysurf Series 2. Taylor Hobson Inc, Rolling Meadows IL, 2002.

48. Chapra, S.C. and R.P. Canale. *Numerical Methods for Engineers*. New York: McGraw-Hill Publishing Company, 1988.

49. Hills, D. and D. Nowell. *Mechanics of Fretting Fatigue*. Dordrecht, The Netherlands: Kluwer Academic Publishers, 1994.

50. Fellows, L., D. Nowell, and D. Hills. "Contact Stresses in a Moderately Thin Strip (With Particular Reference to Fretting Experiments)," *Wear*, 185: 235-238 (1995).

51. ABAQUS Standard User's Manual. Vol. 2. Hibbit, Karlsson and Sorensen Inc, Providence RI, 1995.

52. Chan, K. and Y. Lee. *Ruiz Program*. Southwest Research Institute.

Vita

Captain Lewis C. Lietch graduated from Porum High School in Porum, Oklahoma. He attended the University of Oklahoma in Norman, Oklahoma, for undergraduate studies where he graduated with a Bachelor of Science degree in Chemical Engineering in 1994. He was commissioned into the United States Air Force through Officer Training School in 1995.

His first assignment was at Hill AFB, Utah, as a project engineer for munitions. In September 1998, he became an aircraft maintenance officer at Nellis AFB, Nevada, where he served as Flight Commander for the A-10 aircraft. Before being selected to attend the Air Force Institute of Technology, he served as the squadron maintenance officer for the 11th Reconnaissance Squadron Nellis AFB, Nevada. Upon graduating with a Masters of Science degree in Materials Engineering and Science, he will be assigned to the Air Force Research Laboratory, Materials and Manufacturing Directorate, Wright-Patterson AFB, OH.

REPORT DOCUMENTATION PAGE

Form Approved
OMB No. 074-0188

1. REPORT DATE *(DD-MM-YYYY)*	**2. REPORT TYPE**	**3. DATES COVERED** *(From – To)*
23-03-2004	**Master's Thesis**	October 2002 – March 2004

4. TITLE AND SUBTITLE

FRETTING FATIGUE BEHAVIOR OF THE TITANIUM ALLOY TI-6AL-4V UNDER SEAWATER CONDITIONS

5a. CONTRACT NUMBER

5b. GRANT NUMBER

5c. PROGRAM ELEMENT NUMBER

6. AUTHOR(S)

Lietch, Lewis, C., Captain, USAF

5d. PROJECT NUMBER
JON 326

5e. TASK NUMBER

5f. WORK UNIT NUMBER

7. PERFORMING ORGANIZATION NAMES(S) AND ADDRESS(S)
Air Force Institute of Technology
Graduate School of Engineering and Management (AFIT/EN)
2950 Hobson Way, Building 641
WPAFB OH 45433-7765

8. PERFORMING ORGANIZATION REPORT NUMBER

AFIT/GMS/ENY/04-MO2

9. SPONSORING/MONITORING AGENCY NAME(S) AND ADDRESS(ES)
AFRL/MLLMN
Attn: Dr. Jeffrey Calcaterra
2230 Tenth Street Suite 1
WPAFB OH 45433-7817 DSN: 785-1360 e-mail: Jeffery.Calcaterra@wpafb.af.mil

10. SPONSOR/MONITOR'S ACRONYM(S)

11. SPONSOR/MONITOR'S REPORT NUMBER(S)

12. DISTRIBUTION/AVAILABILITY STATEMENT
APPROVED FOR PUBLIC RELEASE; DISTRIBUTION UNLIMITED.

13. SUPPLEMENTARY NOTES

14. ABSTRACT

The fretting fatigue behavior of Ti-6Al-4V was investigated in laboratory air and under a controlled environment consisting of synthetic seawater. Fretting fatigue tests were performed for both low and high cycle fatigue regimes. Finite element analysis was utilized to model and analyze the experimental data. The applied stress range and the Modified Shear Stress Range were evaluated as potential fatigue parameters.

The results found from this study can be summarized as: (1) seawater had a deleterious effect on fretting fatigue life in the low cycle fatigue regime but improved life in the high cycle fatigue regime, (2) although the Q/P ratio for both conditions increased with an increasing applied stress, the difference between the two conditions was negligible, (3) debris from dry samples contained titanium and oxides while the debris from seawater samples contained titanium, oxides, and seawater contaminants, (4) fretting scar volume was larger under seawater conditions than dry conditions, (5) there were more, closely spaced striations on the fracture surface of the dry samples than of the seawater samples, and (6) both the applied (far field) stress range and the Modified Shear Stress Range can potentially be used as conservative fretting fatigue parameters under high cycle fatigue conditions.

15. SUBJECT TERMS
Fretting, Fatigue Life, Titanium Alloys, Corrosion, Seawater Condition

16. SECURITY CLASSIFICATION OF:			**17. LIMITATION OF ABSTRACT**	**18. NUMBER OF PAGES**	**19a. NAME OF RESPONSIBLE PERSON**
REPORT	**ABSTRACT**	**c. THIS PAGE**			Dr. Shankar Mall, AFIT/ENY
U	**U**	**U**	**UU**	129	**19b. TELEPHONE NUMBER** *(Include area code)* (937) 255-3636X4587; e-mail: shankar.mall @afit.edu

Standard Form 298 (Rev: 8-98)
Prescribed by ANSI Std. Z39-18